NTNU – Trondheim
Norwegian University of
Science and Technology

Hydrological Assessment of Water Resources in Bergen

Climate Change Impacts

Erle Kristvik
Birthe Kvale Riisnes

Civil and Environmental Engineering
Submission date: June 2015
Supervisor: Sveinung Sægrov, IVM
Co-supervisor: Knut Alfredsen, IVM
Ånund Killingtveit, IVM
Ivar D. Kalland, Vann- og avløpsetaten, Bergen Kommune

Norwegian University of Science and Technology
Department of Hydraulic and Environmental Engineering

Birthe Riisnes
Erle Kristvik

Hydrological Assessement of Water Resources in Bergen

Master of Science in Civil and Environmental Engineering
Submission date: 10 June 2015
Supervisors: Sveinung Sægrov, Knut Alfredsen and Ånund Killingtveit

Norwegian University of Science and Technology
Department of Hydraulic and Environmental Engineering

Abstract

Bergen Waterworks is reliant on steady loads of precipitation to meet the drinking water demand. Accordingly, the system is vulnerable to drought events and seasonal changes in inflow. Climate change impact analysis, as part of water management design and operation, is advantageous for ensuring a reliable and economic development of the infrastructure. Consequently, adaptation strategies in terms of hydrological assessments ought to keep up with the scientific progress in climate research. This thesis provides a complete framework for evaluating climate change impacts on drinking water resources in Bergen. A comprehensive hydrological assessment is conducted, including inflow data analysis, calibration of regional HBV model, and transferring of calibrated parameters to ungauged catchments. Projected changes in temperature and precipitation are obtained using empirical-statistical downscaling of the global climate model, Nor-ESM1-M, and IPCC AR5 emission scenarios RCP2.6, RCP4.5 and RCP8.5. Climate change impacts are evaluated by comparing historical climate variables for the control period 1981-2010, with future projections for 2011-2040, 2041-2070 and 2071-2100. Changes in water supply capacity in Bergen are estimated using extreme drought event analysis and hydrological routing. The maximum supply capacity, while accounting for 100 % storage reliability, is confronted with projected changes in drinking water demand. The results convey seasonally inflow changes, connected to changes in the snow regime and increased evapotranspiration. More inflow is expected during winter and autumn, while less is expected in spring and summer. Winter drought extremes are therefore likely to disappear, as opposed to summer drought extremes, for which an upturn is predicted. Within the time span of 2011-2100, all emissions scenarios reduce the maximum supply capacity of Bergen Waterworks. However, neither of the scenarios threaten the reliability of the drinking water supply, provided that leakages in the distribution system are reduced to 20 %.

Bergen vannverk er avhengig av jevnlig nedbør for å møte byens drikkevannsbehov. Følgelig er systemet sårbart for tørkehendelser og sesongmessige endringer i tilsig. Som en del av forvaltning og drift av vannressurser, er konsekvensanalyse av klimaendringer fordelaktig for å sikre en pålitelig og økonomisk utvikling av infrastruktur. Tilpasningsstrategier i form av hydrologiske analyser, bør derfor holde tritt med vitenskapelige fremskritt i klimaforskning. Denne masteroppgaven gir et rammeverk for å evaluere effekten av klimaendringene på drikkevannsressursene i Bergen. En omfattende hydrologisk analyse er gjennomført, inkludert tilsigsdataanalyse og kalibrering av regional HBV-modell, samt overføring av kalibrerte parametere til umålte nedbørfelt. Endringer i temperatur og nedbør er predikert ved bruk av empirisk-statistisk nedskalering av den globale klimamodellen, NOR-ESM1-M, og IPCC AR5 utslippsscenarier RCP2.6, RCP4.5 og RCP8.5. Effekten av de predikerte klimaendringene vurderes ved å sammenligne historiske klimavariabler for kontrollperioden 1981-2010 med fremskrivninger for periodene 2011-2040, 2041-2070 og 2071-2100. Forventede endringer i vannforsyning er vurdert ved å analysere ekstreme tørkehendelser og magasinbeholdning. Med forutsetning om 100 % lagringspålitelighet, vurderes maksimal forsyningskapasitet opp mot forventede endringer i drikkevannsforbruk. Resultatene formidler sesongvise tilsigsendringer knyttet til endringer i snøforhold og økt fordampning. Det forventes mer tilsig på vinteren og høsten, og mindre på våren og sommeren. Sannsynligheten for tilfeller av ekstrem vintertørke reduseres, i motsetning til sommertørke, hvor sannsynligheten øker. Samtlige utslippsscenarier vil medføre nedgang i maksimal forsyningskapasitet, men forsyningssikkerheten vil bevares dersom lekkasjer i distribusjonsnettet reduseres til 20 %.

Preface

This thesis is submitted to the Norwegian University of Science and Technology (NTNU) as part of the course *TVM4905 - Water Supply and Wastewater Systems, Master's Thesis*, mandatory for the fulfillment of the degree of Master of Science (Sivilingeniør) at NTNU. The project has been performed at the Department of Hydraulic and Environmental Engineering, and supervised by Professor Sveinung Sægrov, Professor Knut Alfredsen and Professor Ånund Killingtveit.

First and foremost we would like to express our humble gratitude to all those involved in the work culminating this thesis and for taking interest in our project and sharing their knowledge. We would like to acknowledge Professor Sveinung Sægrov for his valuable inputs on Water Supply and Wastewater Systems, and his thoughtful and considerate advices for guiding us through the fulfillment of this thesis. Further, we would like to thank Professor Knut Alfredsen for helping us find the appropriate hydrological literature and methodologies, for organizing workshops on climate change studies vital for the continuation of our work, and finally for his generosity. We are grateful to Professor Ånund Killingtveit for his dedication to helping us overcome difficulties we have encountered, and for persistently challenging us with technical questions and discussion of our results. We would especially like to express are gratitude to Dr. Byman H. Hamududu for uncountable hours of patient and unconditional tutoring on empirical-statistical downscaling. His contribution has been invaluable to the downscaling conducted in this thesis. Lastly, we would like to thank Senior Engineer Ivar D. Kalland at VA-etaten for his resolute support and providing of indispensable information on Bergen Waterworks.

Contents

List of Figures

List of Tables

List of acronyms

ANN	Artificial neural networks
AOGCM	Atmospheric-Ocean Model
AR4	Fourth Assessment report
AR5	Fifth Assessment report
BM	Block maxima
BW	Bergen Waterworks (Bergen vannverk)
CCA	Canonical correlation analysis
DD	Dynamical downscaling
EOF	Empirical orthogonal function
ESD	Empirical-statistical downscaling
ESM	Earth System Model
FDC	Flow duration curve
GCM	Global Climate Model
GEV	Generalized Extreme Value
GHG	Greenhouse gas
HBV	Hydrologiska Byrån för Vattenbalans
IPCC	Intergovernmental Panel on Climate Change
IQR	Interquartile range
NMI	Norwegian Meteorological Institute
NVE	Norwegian Water Resources and Energy Directorate
MA	Moving average
MVR	Multivariate regression analysis
PCA	Principal component analysis
PDS	Partial duration series
RSD	Relative standard deviation
SSB	Statistics Norway
SVP	Singular Vector Decomposition

Chapter 1

Introduction

1.1 Background and motivation

With the augmenting awareness of a changing climate, and evolvement of quantitative techniques for predicting future climate conditions on a global-scale, stakeholders' demand for local-scale projections and impact analysis is accordingly increasing. Climate change convey a panoply of adverse effects, including threatening impacts on vulnerable water resources and associated infrastructure. In 2010, the city of Bergen, renowned for its plentiful rainfall, experienced a severe drought incident causing rising concerns for the city's water resources. The drought incident originated from cold and dry weather in December 2009, followed by poor rainfall in the consecutive months. These unusual precipitation patterns, combined with high consumption, induced water levels to drop dramatically in all reservoirs. In early March, the water utility encouraged the citizens of Bergen to start preserving water. A heavy rainfall event averted the crisis in mid-March 2010.

More frequent occurrences, and droughts of longer durations, are in addition to increased frequency of other extreme-weather phenomena, likely effects of climatic change. The *fifth* assessment report (AR5), published in 2013, is the most recent report from the Intergovernmental Panel on Climate Change (IPCC). This report indicates overall increases of inflow to humid regions with pronounced topography, but this change is not necessarily equally distributed over the seasons. Observations in Bergen region confirm these changes, where the driest winter season in over 100 years occurred in the middle of a cohesive period of the 15 wettest years ever recorded in the region.

Due to the uniqueness of this event in a historical perspective, drought has become vast concern in terms of water resource availability in Bergen. Generally, water supply storage in areas of wet climate tends to refill annually, and functions principally to smooth out seasonal fluctuations in flows [Dingman, 2015]. As

Bergen is located within the most humid region of Norway, where longer periods of precipitation deficits have been rare, the small reservoir storage capacity has so far been sufficient to supply the citizens with drinking water. However, with changes in the seasonal distribution of precipitation, the length of the growing season, and increased evapotranspiration, the future storage capacity may not be adequate [Stahl et al., 2008; Tallaksen and van Lanen, 2007].

In order to evaluate future availability of water resources in Bergen, an impact study bridging historical patterns of inflow with local-scale projections of climate change is wanted. We have initiated such studies by the work of *TVM4510 specialization project* conducted in fall 2014, at the Norwegian University of Science and Technology (NTNU). In this thesis, we continue the studies by devising the sequence of procedures requisite for translating historical records into future projections, and present a comprehensive drought analysis and review of the climate in Bergen. The work is conducted with regards to the commencement of the BINGO-project in summer 2015, a project where methods for predicting water resources in Bergen on short, medium and long term is requested.

1.2 Research context

1.2.1 Climate change in Norway

A key contributor to climate change studies, is the NOU climate adaptation, which engaged the major climate change research community in Norway to make a complete report on the climate in the past, today and in the future [Hanssen-Bauer, 2009]. The projected climate data are based on the results from the *fourth* assessment report, IPCC 2007, but also relies upon more recent research. An updated report is currently in progress and will be released in the end of 2015. For historical climate, the report covers the development of meteorology in terms of temperature, precipitation and evapotranspiration, and hydrology in terms of snow storage, flood and drought. The climate alteration in Western Norway with respect to 1979-2008, is found to be a 0.47 °C increase in temperature, 7 % increase in precipitation and 5 % increase in runoff. Projected changes for 2071-2100 in temperature, precipitation and runoff where estimated to 3.1 °C, 22 % and 20-30 %, for the moderate emission scenario [Hanssen-Bauer, 2009]. Hitherto, there exist little research on climate change in Norway based on AR5 output, particularly for specific locations such as Bergen. There is however ongoing research within the field of downscaled climate prediction, including activity at the Bjerknes Centre for Climate Research in Bergen, for which results have not yet been published by the termination of this thesis.

1.2.2 Extreme drought analysis

Extreme drought analysis is common practice among hydrologists, however, little work has been done related to drinking water management in Norway. Most studies concern hydrological droughts on a regional scale [Hisdal et al., 2001; Wong et al., 2011]. Hisdal et al. [2001] analyzed summer droughts in Europe for historical climate (1962-1990), and revealed that drought deficit volume and duration have a decreasing trend for the west coast of Norway. Climate change impacts on summer drought duration and spatial extent in Norway were examined by Wong et al. [2011]. The change in meteorological and hydrological drought characteristics were investigated, and gave that temperature changes are expected to lead to more severe hydrological droughts, even for regions where climate is predicted to become wetter. Further they concluded that considerable increases in summer drought duration is expected in Southern Norway, where the major contributor was reduced summer precipitation [Wong et al., 2011]. Chernet et al. [2013] studied climate change impact on basin-scale droughts, analyzing a single hydropower system in Aurland, located in Western Norway. Their study included a brief summer drought analysis, which yielded a future increase by 30 % in drought deficit volume, but little change in drought duration.

Winter droughts were studied in two catchments representing Europe, of which the cold climate region was located in Southeastern Norway and the mild climate catchment in Slovakia[Van Loon et al., 2010]. The authors found that winter droughts with lack of precipitation and no snow cover are likely to become more frequent in the future, as it may continue into summer. On the contrary, snow cover droughts, typically altered by snowmelt at the end of the season, are expected to decrease [Van Loon et al., 2010].

1.2.3 Water supply capacity

Killingtveit and Hamududu [2012] contributed with climate change studies for Oslo municipality in a project on future design of the water supply system. The results indicate a regime shift of the inflow to Maridalen catchment, where the scenarios predict a decrease in frost days and earlier snow melt. For the remote future, snow storage is expected to disappear almost completely, causing higher discharges during winter, and lower discharges during spring and summer. Climate change impacts on water supply capacity revealed a slight decrease in the maximum capacity for near projected scenarios, and a return to its original level by the end of the century.

1.2.4 Previous work

As mentioned, this thesis is a continuation of the pre-studies carried out in *TVM4510 specialization project* fall 2014. The work performed in this project covered; (1) a literature review on global and local climate change modeling, and a review of hydrological modeling approaches; (2) a comprehensive acquisition and assessment of available data requisite to perform climate change impact studies, including a careful quality control; and (3) the construction of a calibrated hydrological model for Dyrdalsvatnet, which was considered representative for Bergen region. Additionally, water balance calculations, based on systematic measurements by Bergen Water Utility (VA-etaten), revealed that the collected data was inadequate for modeling purposes.

1.3 Research goals and questions

The main objective of the research conducted in this thesis is to encapsulate a system, or sequence of modeling procedures, such that the impacts of altered climatic conditions in Bergen can be predicted, evaluated, and accounted for by VA-etaten, in the design, operation and management of the water supply system and the resources. By establishing such a system, we aim to be able to quantitatively assess the local impacts of climate change on the supply capacity in Bergen, and be able to answer the following research questions:

RQ1 Is it feasible to conduct a hydrological assessment incorporating climate change impacts for VA-etaten?

RQ2 What are the expected impacts of climatic change on runoff and drought in Bergen, with respect to historical inflow pattern and drought incidents, such as the one in 2010?

RQ3 Is there sufficient supply capacity to account for climate change, population growth, and altered leakage conditions in the supply network?

RQ4 Which precautionary measures can be made to withstand significant impacts on water resources, and ensure reliable drinking water supply?

1.4 Approach

The research questions listed in the previous section are approached by conducting a routine based on the flow chart presented in Figure 1.1. We have chosen an

approach that gives us the ability to evaluate projected changes with regards to historical conditions. This is achieved by; (1) processing historical data records for meteorological parameters (precipitation and temperature) in terms of detailed climate studies of historical conditions and detected changes. The parameters are further fed into a hydrological model creating historical runoff series, which in turn is subject to a drought analysis of the region; (2) observations of precipitation and temperature are utilized for simulating future time-series of the same parameter. These time-series are, similarly to historical data, embedded in a hydrological model, such that future projections of inflow are produced; (3) the results of the hydrological modeling are further processed in a storage routing model, and future supply capacity determined in context of population growth, and altered leakage conditions; and (4) the historical review from (1) and future projections from (2) and (3) form a basis for comparison such that projected *changes* can be evaluated.

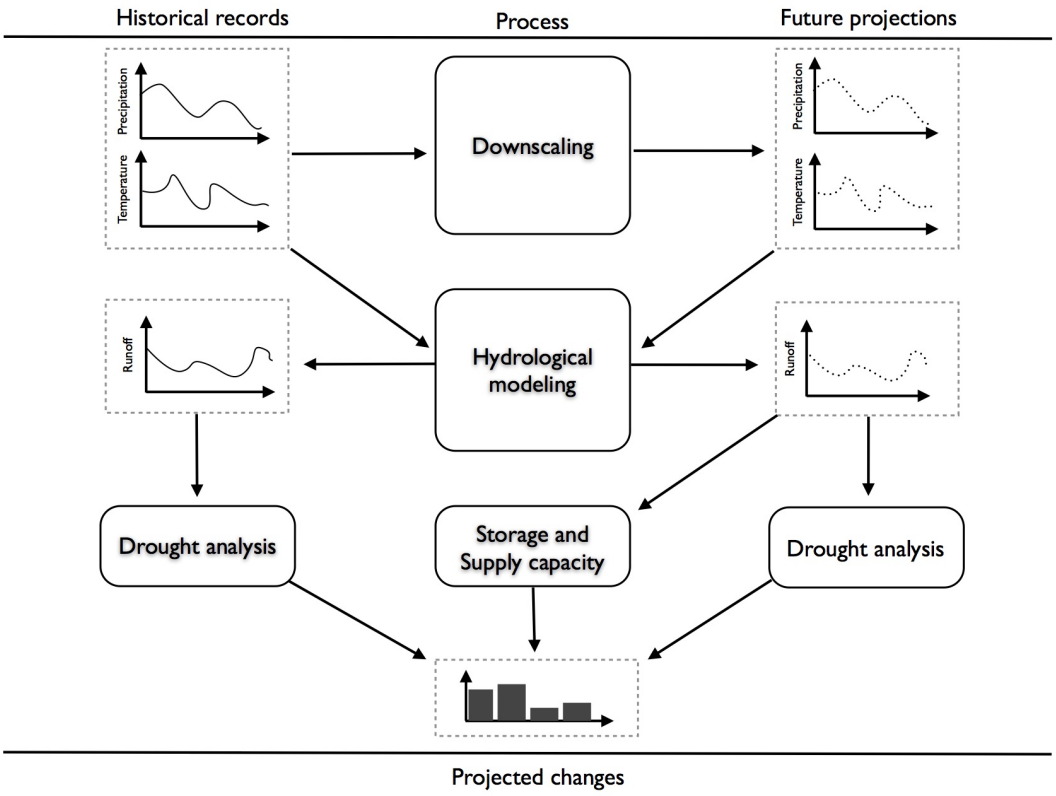

Figure 1.1: High-level description of the quantitative work of water resource availability prediction, and evaluation of such, conducted in this thesis

1.5 Thesis structure

Chapter 1 - This chapter present the background and motivation for the project, what we aim to accomplish, and how we approach the research problem.

Chapter 2 - In this chapter we describe the water resources, associated catchments, and water supply reliability of our study site, Bergen.

Chapter 3 - This chapter contains a theoretical overview of the methods utilized in climate change impact studies. It includes a literature review comprising downscaling of global climate models, hydrological modeling, and extreme drought event analysis.

Chapter 4 - Here, we present the selected approach and modeling sequence conducted in this thesis.

Chapter 5 - A description of the data acquisition and quality control of the data requisite in each step of our modeling approach, including meteorological, climatic, and hydrological data, in addition to population projections that influence the drinking water consumption in Bergen.

Chapter 6 - This chapter contains an analysis of the historical climate in Bergen and detected changes.

Chapter 7 - In this chapter we present the results from an empirical-statistical downscaling, hydrological modeling of catchment inflow under altered climate conditions and obtained estimates of future water resource availability.

Chapter 8 - Lastly, we conclude our thesis, discuss the main findings and present our suggestions for further work

Chapter 2

Study site

The study site of this thesis, Bergen region, is presented in the following chapter. Vann- og avløpsetaten (VA-etaten) is the water utility of Bergen, for whom we will perform our analysis. They control the complete system of Bergen Vannverk, from hereon referred to as Bergen Waterworks (BW). Herein, we aim to illustrate the system structure and the availability of water resources. The contents of this chapter is partly based on Specialization project [2014], and has been modified for this thesis. They include; (1) a description of BW; (2) the catchments within Bergen region; and (3) the water supply reliability.

2.1 Bergen Waterworks (BW)

In Bergen, 97 percent of the total 270 000 citizens are connected to the municipal water supply. Five major water treatment plants produce drinking water for the customers; Jordalsvatnet, Svartediket, Sædalen, Kismul and Espeland. While providing drinking water to a common distribution system, all the plants serve as backup for each other with a total regulated storage capacity of 26.5 mill. m3. Furthermore, the structure of the system allows for a non-fixed distribution pattern, where the plant operation may be optimized according to the water availability in the respective reservoirs, and the demand.

The structure of the water resources of BW is indicated in Figure 2.1. Reservoirs associated with the water treatment plants are presented in terms of main and minor reservoirs, connected by either weirs or regulated transfer mains. The minor reservoirs are located upstream of the main reservoir (although not the case for Espeland), which are directly connected to the corresponding treatment plants. Korlatjørn, the minor downstream reservoir at Espeland treatment plant, is not considered in the analysis due to its small storage capacity compared to Svartavatnet (1:340). From 1 April to 30 September the minimum flow at Svartavatnet

is restricted to 0.12 m3/s. Kismul treatment plant constitutes the main reservoir, Ulvvatnet, into which, there are several minor stream intakes connected through pipes and tunnels, and where Joravatnet is the largest minor reservoir.

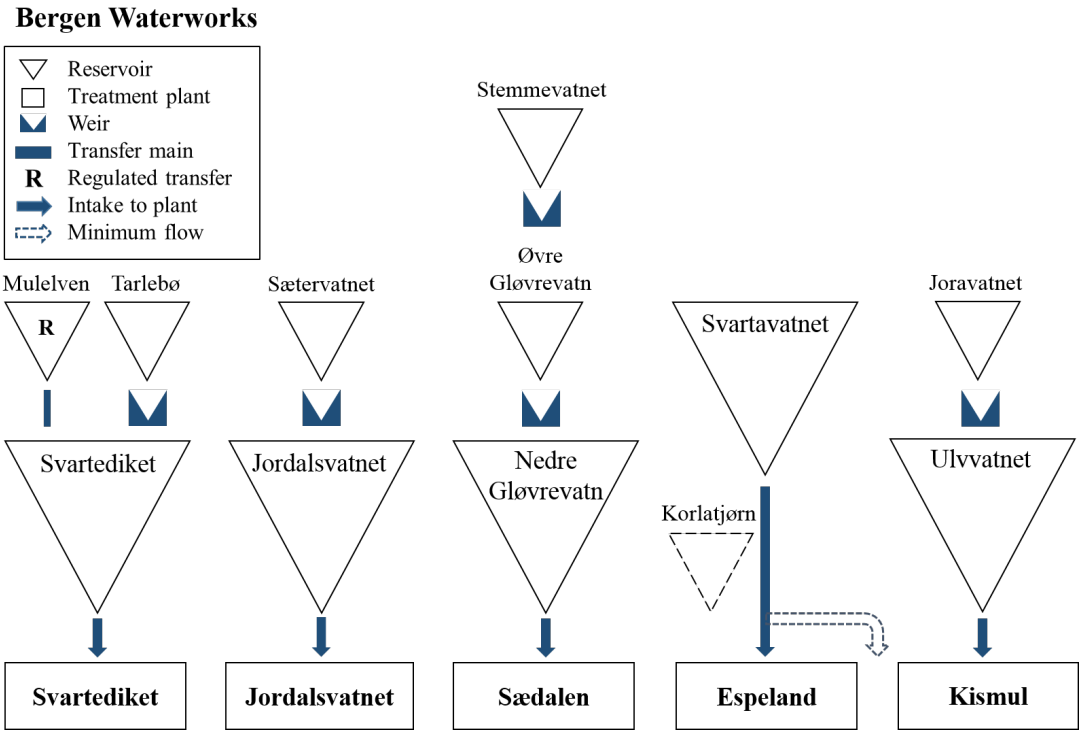

Figure 2.1: The structure of Bergen Waterworks

2.2 Catchments

In addition the the catchments constituting BW, there are two more catchments to be included in the analysis, monitored by the Norwegian Water Resources and Energy Directorate (NVE). Røykenes and Haukåselva are gauged catchments situated adjacently within Bergen region. Locations of the relevant catchments are presented on the map in Figure 2.2. The five BW catchment areas range from 1.8 to 14.3 km^2, where Svartediket, Espeland and Jordalsvatnet represent the largest. Røykenes (50.5 km^2) has borders to Espeland in the northwest and Kismul in the south, whereas Haukåselva (7.6 km^2) is situated in the northeast of Jordalsvatnet. Dyrdalsvatnet, which was modeled in Specialization project [2014], is located within Røykenes. Additionally, an overview of the land use in the region is presented in Figure 2.3. While indicating the vegetational conditions in the

catchment areas, the map simultaneously disclose the particularly dispersed urban settlement in Bergen. In general, all catchments are located in non-urban areas with a combination of wetlands, open-land and forested areas. Despite for Kismul and Jordalsvatnet, the majority of the catchment areas are located in open-land, mountainous zones.

2.3 Water supply reliability

The water distribution network contains 900 km of water mains, 62 dams and 30 balancing reservoirs constituting a total capacity of 223 000 m^3, equal to 2 days demand. The total replacement price is estimated to 10 billion NOK. Recently, VA-etaten improved their resource storage availability, by increasing storage capacity. This was obtained by dam renewal at Svartavatnet within Espeland treatment plant, and an increase of the reserve capacity at Kismul. In 2014 the estimated leakages were measured as 33 %. BW function as a safety water resource for Os municipality. Under any circumstances, Bergen should therefore be able to supply Os municipality with 0.1 m^3/s, for 3 months duration.

In the Master plan (2014-2023), VA-etaten argue that their current actions on leakage detection and water main renewal is likely to decrease the leakages to minimum 20 % by 2040 [VA-etaten, 2014]. Moreover, they emphasize the current facilities' ability to deliver adequate amounts of drinking water for several decades ahead. At the same time, the population in Bergen is estimated to grow steadily until 2040 [SSB, 2014], and the connection degree is assumed to increase to 98 % by 2020. VA-etaten strives towards achieving a decrease in demand until 2020, before a stagnation at the same level. While acknowledging that predicting future water consumption involves many uncertainties, water reserve transfer from Samnanger municipality (east of Bergen) is considered on a long-term basis [VA-etaten, 2014].

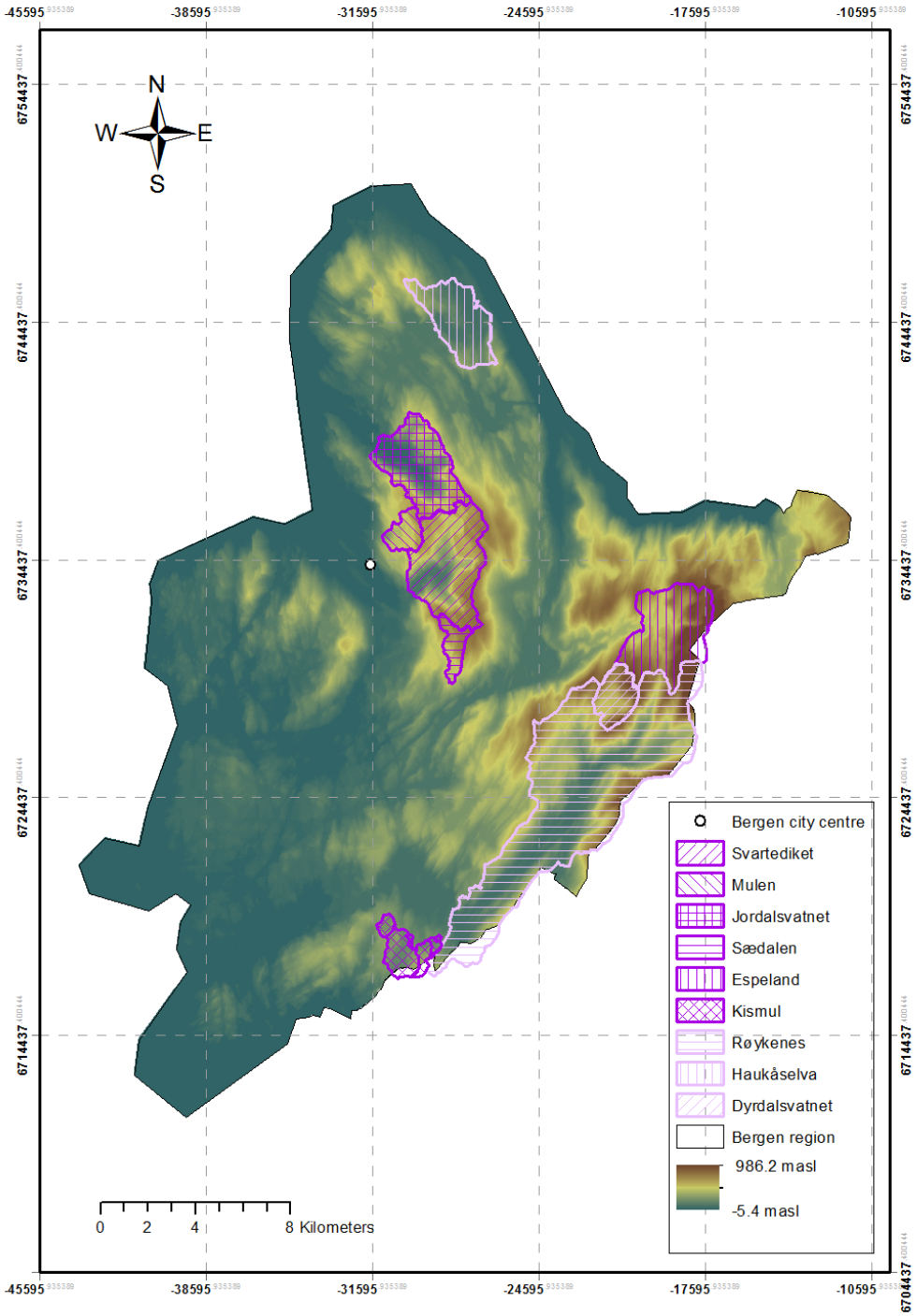

Figure 2.2: Catchments in Bergen controlled by VA-etaten and NVE [NVE Lavvann, 2014; Norwegian Mapping Authority, 2014].

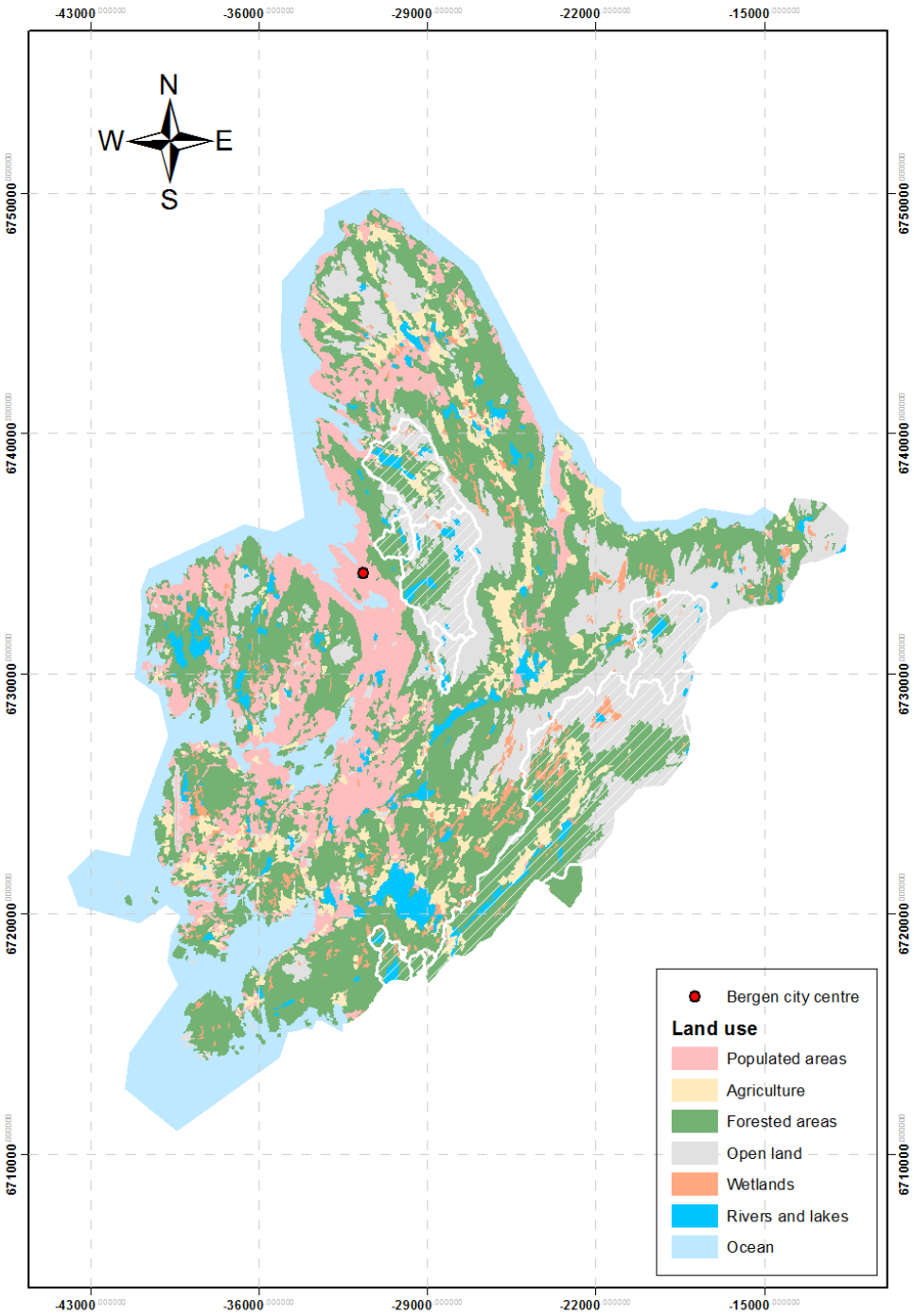

Figure 2.3: Geographical presentation of the land use in Bergen [Skog og Landskap, 2014]

Chapter 3

Theoretical overview

This chapter embraces an array of theory regarding climate change impact studies and hydrological assessments. Methods and theory from previous and current research have been evaluated with the aim of constructing a convenient sequence of approaches for climate change impact studies in Bergen. Four main scientific fields are included; (1) Modeling and quantification of climate change on a global and local scale; (2) hydrological modeling, inflow scaling methods, and hydrological routing; (3) extreme drought analysis; and (4) water supply reliability.

(1) embrace the background for climate change studies in terms of detected changes, globale climate models, and emission scenarios utilized in prediction of future climate. Furthermore, a review of downscaling techniques for translating large-scale predictions to local-scale is presented. (2) presents the elementary principals of hydrological modeling, a review of different approaches, the basics of the chosen modeling strategy, HBV. Further, we discuss methods for estimating inflow. For the purpose of investigating the drought incident in 2010, and detecting drought in runoff projections for the future, (3) provides the theoretical background necessary to understand the drought phenomenon, and the procedures included in drought analysis. Finally, (4) covers a brief review of water supply capacity, and defines commonly accepted design requirements.

3.1 Climate Change

The fifth assessment report from the Intergovernmental Panel on Climate Change, AR5, defines climate changes as changes of a climatic parameter over an extended time period, such as alterations of the parameter mean or variability in its properties [IPCC, 2013]. Temperature is a climatic parameter, in which these phenomena are distinct. Amongst the records of temperature, which reaches back to 1850, the linear trend over the time-span 1880-2012 is a global warming of 0.85^{o}C. Since

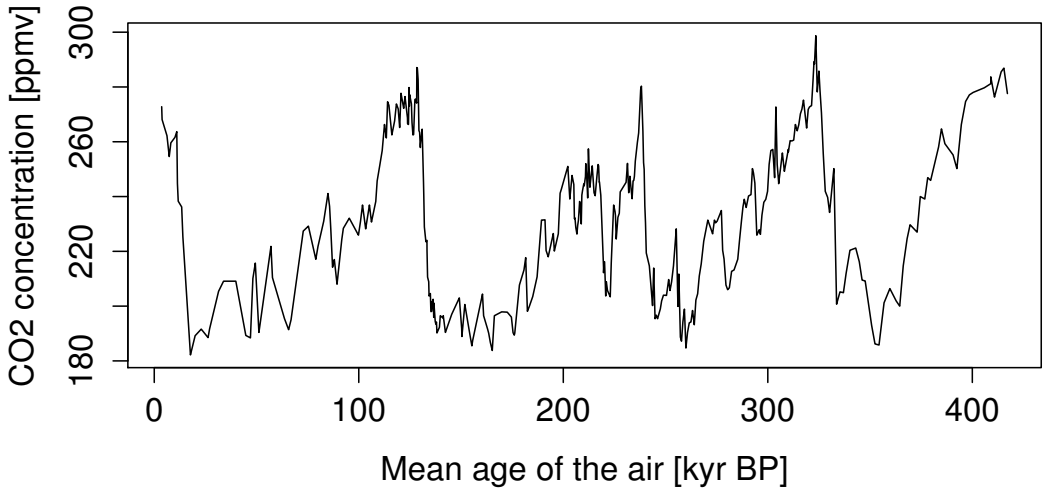

Figure 3.1: Historical CO_2 record from the Vostok ice core [Barnola et al., 1999]. Concentration is given in parts per million by volume (ppmv) and the historical axis in thousand years before present (kyr BP).

pre-industrial times, the CO_2 concentration in our atmosphere has increased by 40% [IPCC, 2013]. Additionally, drilling of the Vostok ice core, Antarctica, sets the current CO_2 concentration in a historical perspective by its reconstruction of CO_2, reaching back 800,000 years. Figure 3.1 shows a 420,000 year long record of the $C0_2$ concentration. Concentration varies from approximately 180 ppmv to 300 ppmv in a cyclic manner throughout the entire time-span. For comparison, today's CO_2 level is about 400 ppmv. Petit et al. [1999] concluded from 420,000 years of historical CO_2 concentrations that the climate has always been in the state of change (within a stable maximum and minimum), and that greenhouse gases such as CO_2 and CH_4 have markedly contributed to the glacial-interglacial change. The link between temperature and CO_2 concentration was detected already in 1861 when John Tyndall measured how CO_2 captures infrared radiation, and thereby retaines heat. More than 100 years later, in 1988, the World Meteorological Organization (WMO) and United Nations Environment Program (UNEP) established IPCC, a neutral organ with respect to politics and scientifically objective, to assess, review and recommend the requisite information on human-induced climate change, and its consequences. Regularly, IPCC publishes reports summarizing state-of-the-art research, herein, results from the most recent techniques in predicting impacts from future emission scenarios of greenhouse gases.

3.1.1 Global Climate Models (GCMs)

GCMs are models that are investigative of fundamental processes in our climaticsystem [Mote and O'Neill, 2000], and the climatic responses to various forcings [IPCC, 2013]. In IPCCs fourth assessment report, the main tools for investigating the likely changes due to emission scenarios were coupled atmospheric-ocean models (AOGCMs), more specifically, numerical models simulating interaction between atmospheric and oceanic processes. They are advanced dynamical cored models with physical parametrization of processes that connot be explicity resolved [IPCC, 2013], including atmospheric processes such as atmospheric convection and clouds, oceanic components, land surface properties that influence surface albedo and evapotranspiration, and finally, thermodynamic and dynamic processes of sea ice. The newest state-of-the-art-models (AR5) are Earth System Models (ESMs). ESMs include bio-geochemical cycles in addition to atmospheric and oceanic processes, and take into account emissions of CO_2, and goals for climate stabilization.

The Coupled Model Intercomparison Project phase 5 (CMIP5) comprises a set of coordinated climate model experiments to provide a better understanding of model differences and predictability [Taylor et al., 2012]. Figure 3.2 renders an overview of all models contributing in CMIP5. All experiments with corresponding descriptions, and an overview of the major purposes of each experiment, are summarized by Taylor et al. [2012]. Experiments include both long-term (century time-scale) and near-term (decadal) simulations with AOGCMs and ESMs. They are also classified based on the major purpose of the experiment, and divided into historical and future projections. For the long-term experiments historical integrations usually start 1850, while future projections start 2006-01. Experiments for future projections are based on different scenarios for emission. Emission scenarios cause radiative forcings in the atmosphere, and the experiments investigate the alterations of the climatic conditions these forcings cause.

3.1.2 Radiative forcing

Solar radiation is the fundamental driving force for the Earth's climate system and energy budget. Anthropogenic climate change is caused by alterations in the *outgoing* energy of the Earth's energy budget. Hansen et al. [1997] defines a radiative forcing as a "*change imposed on the planetary radiation balance*", and the aforementioned alteration of outgoing energy, net radiative flux change (Wm^{-2}), is the measure. The compounds that cause radiative forcing are usually grouped into well-mixed greenhouse gases (WMGHGs) and near-term climate forcers (NTCFs), where the latter is a set of compounds with short lifetimes, such that their impact on climate is restricted to the first decade after being emitted. WMGHGs have longer lifetimes and are mixed in the troposphere so that forcings caused

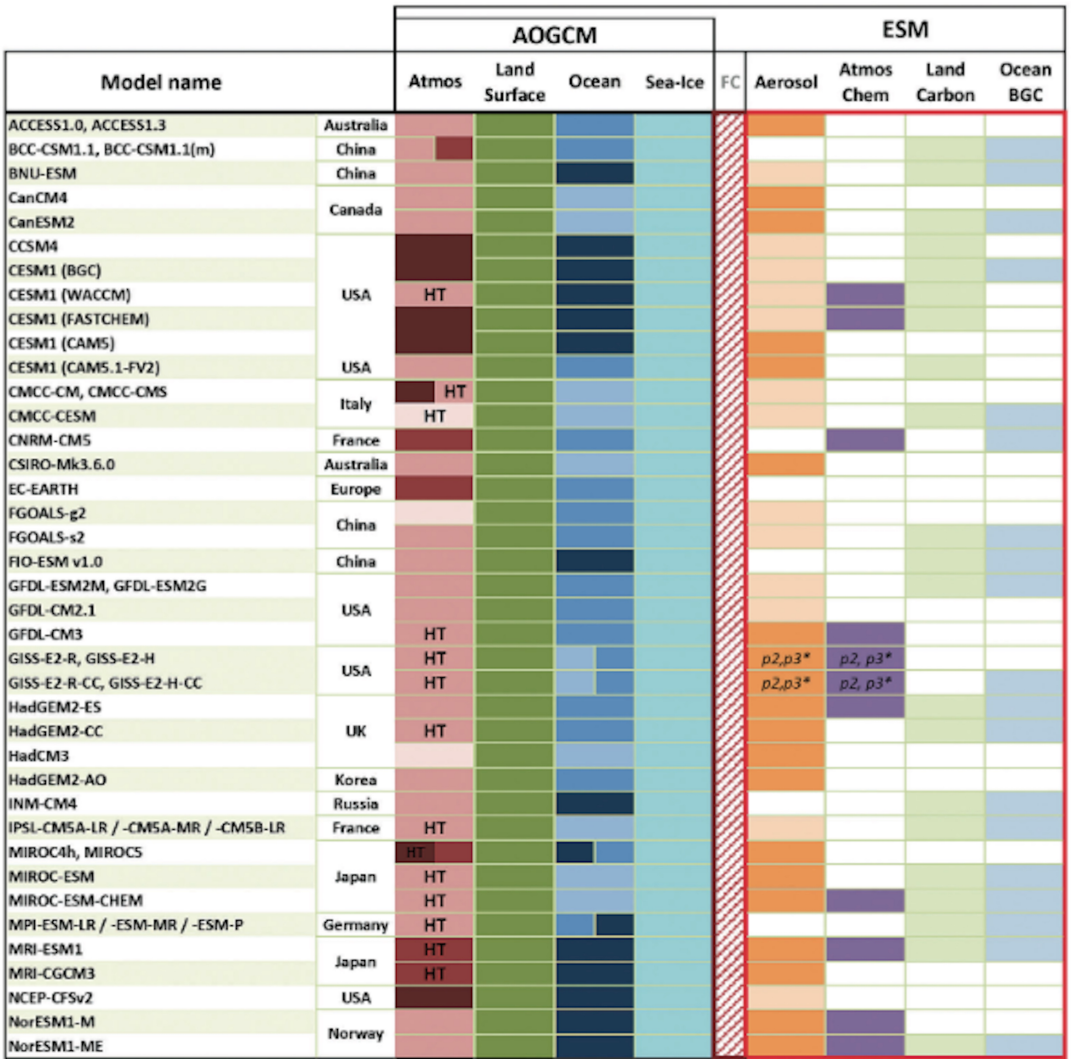

Figure 3.2: AOGCMs and ESMs contributing to CMIP5, and evaluated in AR5, including complexity of model components, such as atmosphere, land surface, ocean, sea-ice (AOGCM), and bio-geochemical cycles (ESM). For AOGCM components, colored boxes indicate that the component contains at least one physically-based predictive equation, and a coupling to another component. Darker shades reflect higher complexity. For ESM components the shades reflect 'semi-interactive' (light shades) and 'fully-interactive' (dark shades) IPCC [2013].

by these gases are global, and independent of the geographic location of their emission. Commonly known WMGHGs are CO2, N2O, CH4 and SF6. Water vapor is also a large contributor to the natural greenhouse effect, but considered a feedback agent, rather than a forcing agent, because the amount of water vapor in the air is controlled by air temperature. Observations of forcing agents issue a better understanding of the various agents' contribution to historical climate change. Scenarios for radiative forcing, causing future climate change, are developed based on assumptions about socioeconomic trends and choices leading to changing emissions.

3.1.3 Representative concentration pathways (RCPs)

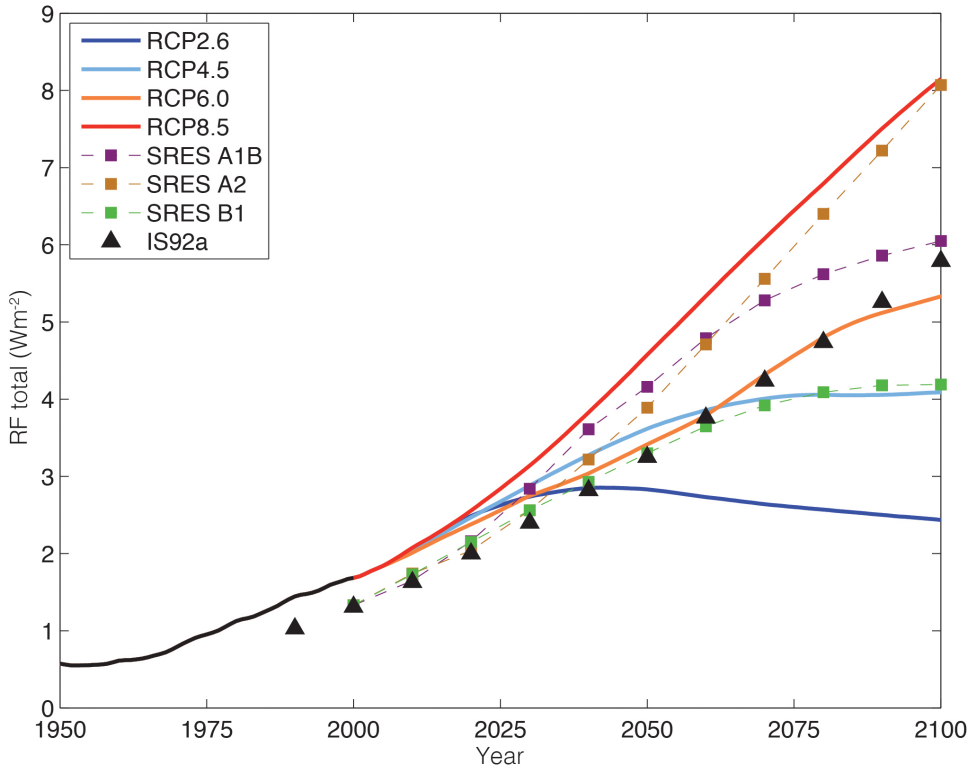

Figure 3.3: Total radiative forcing for AR4 and AR5 representative concentration pathways, [IPCC, 2013].

Emissions scenarios describe the potential discharge of greenhouse gases (GHGs) and future land use changes on a global scale. Until recently, the emissions scenarios that dominated the field of climatic change are those found in the Special Report on Emissions Scenarios (SRES) [Nakicenovic and Swart, 2000]. SRES de-

fines four storylines describing the main characteristics of the world development, referring to social, economic, demographic and technological changes. Developing the scenarios involves a linear chain process, assuming that future GHG emissions are influenced by a range of socio-economic factors. They are used to project climate variables, followed by searching for mitigation possibilities, and further implemented in new scenarios.

Since SRES scenarios are run in a sequence, new observations and advances in research, combined with more sophisticated models cause a prolonged development [Moss et al., 2008]. The submission of IPCC-AR5 emphasizes the need for new scenarios that are able to incorporate data on recent historical emissions, climate change mitigation and impacts, and adaptation and vulnerability [Field et al., 2014]. Rather than starting with socio-economic "storylines" from which emissions trajectories and climate impacts are projected, the new approach coordinates a parallel process describing radiative forcings and concentrations. Referred to as Representative Concentration Pathways (RCPs), each scenario reflects specific plausible future emissions, and may be a basis for trial of different combinations of socio-economic factors [Moss et al., 2010]. Table 3.1 presents the set of scenarios chosen by IPCC, on the basis of contributions from several Integrated Assessment Modeling (IAM) groups.

Scenario	**Description**	**IA Model**	**References**
RCP8.5	Rising radiative forcing pathway leading to 8.5 W/m^2 in 2100	MESSAGE	Riahi et al. [2007]
RCP6	Stabilization without overshoot pathway to 6 W/m^2 at stabilization after 2100	AIM	Fujino et al. [2006] HIJIOKA et al. [2008]
RCP4.5	Stabilization without overshoot pathway to 4.5 W/m^2 at stabilization after 2100	GCAM (MiniCAM)	Clarke et al. [2007] Smith and Wigley [2006] Wise et al. [2009]
RCP2.6	Peak in radiative forcing at ~ 3 W/m^2 before 2100 and decline	IMAGE	van Vuuren et al. [2007] van Vuuren et al. [2006]

Table 3.1: RCP descriptions, model group responsible and publications [Van Vuuren et al., 2011], modified in Specialization project [2014].

3.1.4 The Change factor method

There are different approaches to link the future projections calculated with GCMs and RCP scenarios to local scale, in order to assess further impact analysis of climate change. The 'delta approach', or delta change method, is a common and convenient transfer method for capturing the change signal (delta) of GCM projections and creating local predictions based on historical observations [Hamududu, 2012; Graham et al., 2007]). Delta change factors may be computed directly from GCM output or from downscaled GCM output, and thereafter projected onto historical records. Variations and extremes tend to be smoothed out in GCMs due to their coarse spatial resolution. Applying change factors to historical records ensures preserving of variations within each parameter. State-of-the-art practice is to add averaged delta change factors to a 30 year historical control period, producing 30 year future predictions.

3.1.5 Downscaling

Local parameters can be obtained from global circulation models by the process of downscaling. Benestad et al. [2008] defines downscaling as "the process of making the link between the state of some variable representing a large space and the state of some variable representing a much smaller space". In other words, downscaling is about finding a fundamental link between a large-scale and small-scale variable. As the name implies, the method of empirical-statistical downscaling (ESD) detects this link as a statistical relationship between the local climate variable and the large-scale spatial climate patterns (GCM results). Another approach, dynamical downscaling (DD) is a computer-intensive numerical downscaling technique to fit coarse gridded GCM output to finer resolution regional weather models. Although dynamical downscaling have successfully been implemented to a number of regions around the world [Benestad et al., 2008], there are drawbacks related to capability and accuracy. The main drawbacks, and advantages, of dynamical downscaling are listed in Table 3.2 [Wilby et al., 2002] along with the same attributes of statistical downscaling. Statistical and dynamical downscaling share some merits, but differ in the requisite computer power for computations. Additionally, the expected errors from the two approaches are divergent and Benestad et al. [2008] argues that a combination of the two might be a reasonable approach. Furthermore, Imbert and Benestad [2005] emphasize that no method can be universally considered superior to another, due to the variability in strengths and drawbacks of each model.

	Statistical downscaling	**Dynamical downscaling**
Strengths	• Station scale climate information from GCMs-scale output	• 10−15 km resolution climate information from GCM-scale output
	• Cheap, computationally undemanding and readily transferable	• Respond in physically consistent ways to different external forcings
	• Ensembles of climate scenarios permit risk/uncertainty analyses	• Resolve atmospheric processes such as orographic precipitation
	• Flexibility	• Consistency with GCM
Weaknesses	• Dependent on the realism of GCM boundary forcing	• Dependent on the realism of GCM boundary forcing
	• Choice of domain size and location affects results	• Choice of domain size and location affects results
	• Requires high quality data for model calibration	• Requires significant computing resources
	• Predictor-predictand relationships are often non-stationary	• Ensembles of climate scenarios seldom produced
	• Choice of predictor variables affects results	• Initial boundary conditions affects results
	• Choice of empirical transfer scheme affects results	• Choice of cloud/convection scheme affects (precipitation) results
	• Low frequency climate variability problematic	• Not readily transferred to new regions

Table 3.2: Comparison of statistical and dynamical downscaling by main strengths and weaknesses [Wilby et al., 2002]

3.1.6 Empirical-statistical downscaling

Empirical-statistical downscaling employs statistical relationships between the large-scale variable, from here on referred to as the *predictor*, and the small-scale, local variable, the *predictand*. Being a GCM output, the predictor variable is spatially distributed, while the predictand is single-point variables such as weather station records. Thus, methods utilized in ESD encompass multivariate techniques for processing field objects, station objects and interactions between them.

The principal assumption behind empirical-statistical downscaling is that the link between the predictor and predictand has a strong physical analogy. When choosing predictor, this must be accounted for in order to circumvent coincidental correlations between predictor and predictand [Benestad et al., 2008]. Additionally, a criteria for ESD is stationarity in the link between predictor and predictor. As indicated in table 3.2 [Wilby et al., 2002] this is not necessarily the case, and Wilby [1997] presented evidential findings of non-stationarity. In ESD, this issue may be addressed by considering a *regional-scale* predictor.

Contrarily to dynamical downscaling, ESD is inexpensive computational-wise and thereby more adaptable and flexible. ESD is a predictive model, which mathematically is possible to build on a variety of approaches. The statistical techniques employed in ESD are often classified into linear or non-linear models (sec. 3.1.6 and 3.1.6). Benestad et al. [2008] mentions linear techniques like multivariate regression (MVR), canonical correlation analysis (CCA) and singular vector decomposition (SVD) as suitable methods. Contrarily, non-linear approaches are provided by the analog model, or classification methods, such as cluster analysis or artificial neural networks. However, the complete downscaling procedure involves not only the choice of statistical approach, but also a pre-processing of the data to diminish the impact of data skewness or reduce data size such that model performance is improved [Kuhn and Johnson, 2013]. A common approach is to apply empirical orthogonal function (EOF) analysis (also referred to as principal component analysis, Sect. 3.1.6) to the predictor data prior to downscaling, in order to train the model [Benestad, 2001].

Principal component analysis (PCA)

Any data that consist of lists of measurements, made on a collection of objects or individuals, may be subject to principal component analysis [Lay, 2012]. According to Wilks [2005], is possibly the most commonly multivariate statistical technique utilized in atmospheric sciences nowadays. Gridded climate data normally consist of collinear time series, varying in both time and space. Due to spatial interdependence within these data fields, redundant information is stored. In addition to dimensional reduction of large data sets, PCA is a technique to analyze multi-

variate data and minimize redundancy therein. In ESD, PCA is a pre-processing of the data aiming to identify which information is important, redundant or noise [Shlens, 2014].

The idea of PCA is that if a variable can be expressed *by* another variable, the data matrix containing these variables can be reduced through linear combinations. PCA search for the linear combinations which reflect the largest variances within the data set for one variable [Härdle and Simar, 2012]. To do so, the variance-covariance matrix is evaluated. Variances in the observations appear along the diagonal in this matrix, whilst the covariance between two variables is found in the off-diagonal terms. Hence, optimization of this matrix in terms of PCA is to maximize the diagonal and minimize the off-diagonal terms.

The obtained linear combinations are called principal components, PCs, and they are weighted with respect to their ability to preserve variance. The first component represents the largest variance, i.e. the largest eigenvalue of the matrix. Corresponding eigenvectors (EOFs) to the PCs represent the coherent spatial structures yielding the highest variance.

Linear techniques

Multivariate regression is based on minimizing the root-mean square error, while canonical correlation analysis and singular vector decomposition are focused on maximizing correlations and covariance [Benestad et al., 2008]. In MVR, regression coefficients, representing predictor patterns, between a station record and a predictor field are calculated. The method depends on eliminating collinearity within the predictor to ensure the beneficial interpretability of calculated regression coefficients [Kuhn and Johnson, 2013]. This is the main reason to perform PCA in advance and thereafter utilizing the PCs as input to the regression model.

CCA was presented by Hotelling [1936] as a two-variable problem of finding one optimal set of bases for each of the variables, with respect to correlations [Borga, 2001]. In other words, CCA is a method for correlating linear relationships between two multidimensional variables [Hardoon et al., 2004], such as *field objects* (in the case of ESD). It is performed such that the diagonal entries of the correlation matrix of the two bases are maximized. CCA yields a pattern between two variables, which is optimized with respect to temporal correlation.

Singular vector decomposition is intimately related to PCA [Shlens, 2014], being a generalization of the PCA diagonalization procedure [Bretherton et al., 1992]. In linear algebra, the factorization of a symmetric matrix is a well known procedure, but when working with multivariate climate data, the matrices are not always symmetric. Within applied linear algebra, SVD is a powerful tool for factorizing a rectangular (m x n) matrix A, into U and V orthogonal matrices, and a diagonal matrix Σ.

$$A = U\Sigma V^T \tag{3.1}$$

The *singular values* of A are equal to the square root of the eigenvalues of $A^T A$. If for A, there exist r singular values, then the diogonal terms of Σ are the r singular values of A [Lay, 2012].The columns of U and V are called the left and right singular vectors of A, respectively.

SVD is also simular to CCA, but where CCA finds patterns with maximum correlation, SVD finds patterns with maximum covariance [Benestad et al., 2008]. Bretherton et al. [1992] compared methods for finding coupled patterns in climate data, including CCA and SVD. They rank SVD superior to CCA, due to its general good performance, easy interpretation and lack of systematic biases.

Non-linear techniques

The commonly applied linear approach, linear regression, yield lower variance in a variable than its observed data [Imbert and Benestad, 2005]. An alternative approach to linear techniques is the more simple analog model; a method for downscaling which conserves variance in the data. Imbert [2003] applied both an analog model and linear regression in the prediction of precipitation, and found that the analog model described close to 100% of the observed variance, whereas the linear regression underestimated variance. The idea of this method consists of searching through historical records and associating the local parameter most similar to the large-scale output to the simulated large-scale pattern [Zorita and Von Storch, 1999]. In practice, the local parameter that is most similar to the large-scale output is found by employing the principal components phase space, in which the analog search is performed [Benestad et al., 2008]. The main drawback of the model is its inability to predict values which are not present in the historical records, and accordingly large training samples are requisite for modeling. Consequently, the analog model is better suited for predictions on a daily time-step than a monthly, due to the difference in record lengths.

Another approach, cluster analysis, is a classification method to distribute the historical data into classes associated to recurrent and significant patterns observed in large-scale climate. The objective is to generate clusters in which data can be grouped based on their internal degree of "natural association" [Anderberg, 2014]. Finally, artificial neural networks (ANN) is a commonly applied method in predictive modeling. The method includes a system of neurons, inspired by the human brain, which are interconnected such that output is calculated when input values are propagated through the network of neurons [Jain et al., 1996]. Schoof and Pryor [2001] downscaled maximum and minimum air temperature on a daily basis and total precipitation with both daily and monthly time-step, using cluster

analysis and ANN. The model performed well in downscaling of temperature, but rendered the recurrent incidence of underestimated variability in precipitation.

3.2 Hydrological modeling

For analyzing climate change impacts on water resource availability, a hydrological model is useful for its ability to generate runoff series of a catchment based on inputs of air temperature and precipitation. However, a complete inflow data series corresponding to the catchment in question is necessary in order to calibrate the model. This section embraces applications of hydrological modeling, in addition to procedures for achieving representative inflow series of ungauged catchments. The procedures included are inspired by common Norwegian practice as well as recent research recommendations.

3.2.1 Catchment definition

According to Dingman [2015] a catchment, (also called drainage basin, watershed or river basin) is the area that appears based on topography to generate all the water that passes through a given cross section of a stream. The hydrological response of any catchment, over a time step Δt, may be estimated through the general water balance equation:

$$\Delta S = P + G_{in} - (Q + ET + G_{out}), \tag{3.2}$$

where all variables are measured in volume (m^3 , mm/m^2). P is precipitation, G is groundwater, Q is the stream outflow, ET is evapotranspiration, and ΔS is the change in storage (solid or liquid) over the time period [Dingman, 2015]. Based on the components of the water balance equation, the inflow to a catchment can be calculated. Gauging all the components flowing out from the reservoir, Q, in addition to the volumetric change in the reservoir within a time step, ΔS will yield the associated inflow.

3.2.2 Hydrological models

Hydrological models are sets of mathematical descriptions of dominant hydrological processes aiming at resembling a real system behavior. There exist simple empirical "black box"-models, for which the rational method and the unit hydrograph model are typical examples. Due to their simplicity, these models are not suited for modeling flow variation in a catchment, and may therefore not be used to estimate inflow to ungauged catchments.

Conceptual hydrological models take into account principle physical elements, and reasonable a priori relationships between them in the simulation of catchment response to external forcing. Model structures are generally homogeneous, semi-distributed or physically distributed. By example, the latter is useful when studying the effect of land use changes on the basin hydrology. The shared feature of the models is the inclusion of parameters, which subsequently to calibration represent the characteristics of watershed's hydrological response. Further, the calibrated parameters are assumed to apply also for runoff simulations in the future. Generally, the more detailed the model, the higher the data demand and number of parameters, resulting in a major increase in uncertainty. After 40 years of development and application of the common HBV-model, Bergstrom and Lindström [2015] pose some key requirements for hydrological modeling application. While emphasizing the need for a model that is complex enough to describe the principle physics of a catchment, the data demand should not exceed the standard climatological and hydrological networks' data availability. Additionally, the number of free model parameters (used for calibration) shall be kept to a minimum [Bergstrom and Lindström, 2015]. This is the foundation for using the conceptual lumped and semi-distributed HBV-model for application in our thesis.

3.2.3 HBV model

The HBV model, (Hydrologiska Byrån för Vattenbalans) is a common conceptually based lumped hydrological model [Bergström, 2002; Stanev, 2004]. The model simulates daily inflow from input data in terms of daily precipitation, temperature, and monthly estimates of potential evapotranspiration. It takes into account the catchment area, elevation distribution and lake percentage in the calculations. The model consists of four routines as depicted in Figure 3.4. The first is the snow routine computing snow accumulation and melt in ten different elevation zones, from inputs of precipitation and air temperature. In the following soil-moisture routine, water storage in upper soil is computed based on soil evapotranspiration and net precipitation. A response routine consisting of two linear reservoirs of quick and slow response, generates the runoff from the catchment. In the four stages of the model, there are internal processes and fluxes controlled by the parameters estimated during calibration. These parameters represent the characteristics of the local basin. Additional reading is documented in Killingtveit and Sælthun [1995].

Model calibration and efficiency coefficient

Calibration of HBV-model parameters is necessary to obtain sufficient runoff simulation. Hydrological model performance is commonly assessed using the Nash-Sutcliffe model efficiency coefficient [Nash and Sutcliffe, 1970].

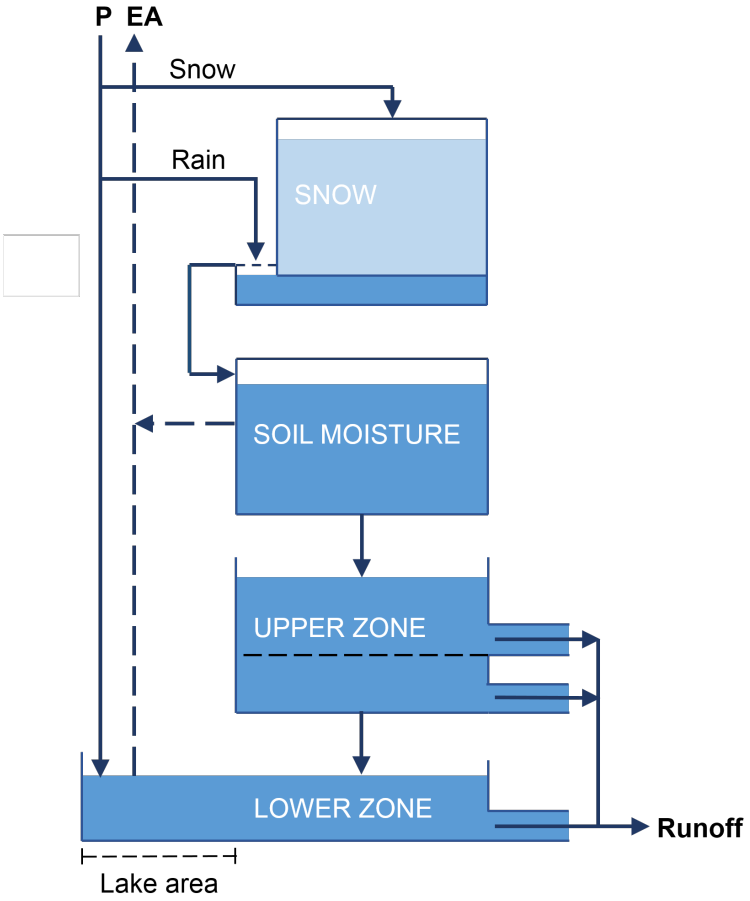

Figure 3.4: Schematic representation of the HBV model

$$R^2 = \frac{\sum(Q_O - \bar{Q_O}^2) - \sum(Q_S - Q_O)^2}{\sum(Q_O - \bar{Q_O})^2} \tag{3.3}$$

where:

R^2 = model efficiency coefficient
Q_O = observed runoff
$\bar{Q_O}$ = average observed runoff
Q_S = simulated runoff

Being defined identically to the coefficient of determination used in linear regression, R^2 yields a value from $-\infty$ to 1. $R^2 = 1$ is equivalent to best achievable model fit. Moreover, R^2=0 indicates that simulated prediction accuracy is similar to the accuracy of the mean observed runoff. Nash-Sutcliffe efficiencies can also be used for estimating accuracy of model outputs other than discharge, i.e. storage volume, or water quality constituents [Nash and Sutcliffe, 1970].

Model calibration, namely adjustment of parameters, is commonly executed using a combination of the R^2-criteria, and the conformity between the simulated and observed mean value. Manual calibration involves a sequence of trial and error, repeated until a reasonable *goodness of fit* is obtained. Automatic calibration implies using methods that seek for the best parameter combinations. So-called *error function topography*, combines parameters two by two in a systematical manner, obtaining an error "topography map" [Killingtveit and Sælthun, 1995]. PEST is an algorithm for model-independent parameter optimization using a non-linear technique [Doherty et al., 1994]. The method is commonly used for automatic calibration of the HBV-model. What should be remarked for the nature of conceptual hydrological models, is the fact that no parameter set uniquely produces a certain goodness of fit. Consequently, the same R^2 value may be obtained for several combinations of parameters.

3.2.4 Estimation of inflow at ungauged catchments

Not all catchments are equipped with gauging stations, and thus, the inflow needs to be estimated. One can assume that catchments within the same "climate region" and with similar characteristics share the same hydrological behavior [Bárdossy, 2007]. Based on this assumption, inflow from a gauged catchment can be transferred to adjacent ungauged catchments. There are several methodologies for transferring inflow series to ungauged catchments, ranging from the simpler scaling-method, to transfer of calibrated parameter sets from hydrological models, to more advanced kriging and map-correlation methods [Archfield and Vogel, 2010]. In the following, the first two methods are discussed.

Traditional scaling

In Norway, scaling of inflow series is a widely used method for achieving inflow series to ungauged catchments. NVE uses the method for creating nationwide maps showing specific runoff [Beldring et al., 2002]. The method will from hereon be referred to as traditional scaling. When scaling from a gauged (proxy) watershed the inflow series to the ungauged (target) watershed is calculated by Equation 3.4:

$$Q_{Target} = \frac{A_{Target} * q_{Target}}{A_{Proxy} * q_{Proxy}} * Q_{Proxy}, \tag{3.4}$$

where A is the catchment area (km^2), and q is the specific runoff, typically given in (mm/yr) or ($l/s \cdot km^2$). Generally, the method is applicable when the proxy watershed is reasonably close to the target watershed. Challenges related to traditional scaling are associated with the different behavior of large catchments, as opposed to small catchments. A large catchment have slower response to precipitation events than smaller catchments, causing the timing and duration of events to differ considerably between such catchments. Additionally, traditional scaling may involve major inaccuracies, as it ignores elevation differences between proxy and target catchments, which for cold climate regions imply different conditions in snow accumulation and release. Neither is the lake percentage of the catchment considered in the procedure, which influences the runoff response.

Transfer of calibrated hydrological model parameters

The calibration process in hydrological modeling produces a parameter set representing the hydrological response of the catchment in question. Parameter sets are considered transferable if the associated model performance on the proxy catchment is good, and annual climate statistics for the target catchment are well reproduced by the model [Bárdossy, 2007]. By transposing the parameter set from the proxy catchment into an individual hydrological model for the target catchment, while specifying corresponding characteristics (i.e. elevation zones, area and lake percentage), inflow series to the target catchment can be simulated. The methodology is commonly applied among hydrologists [Merz and Blöschl, 2004; Beven, 2011], and takes into account aforementioned features neglected in traditional scaling.

3.2.5 Hydrological routing

Hydrological routing is a simple procedure to estimate components of a reservoir water balance or a river reach, based on the continuity equation for hydrology

(Equ. 3.2). In its simplest form, inflow to the reservoir is equal to the outflow of the reservoir plus the change of storage:

$$Q_{in} = Q_{out} + \frac{dV}{dt}, \tag{3.5}$$

where Q_{in} is average inflow during dt, Q_{out} is average outflow during dt; and V is the storage volume at time t. The procedure can be used to evaluate model simulation efficiency, or to calculate expected water resource availability given an estimated inflow series.

3.3 Extreme drought event analysis

In this section, the necessary theory to understand the drought phenomenon and procedures in drought analysis is documented.

3.3.1 Drought definition and seasonality

Hisdal et al. [2001] defines droughts as normal, recurrent climatic circumstances. Meteorological droughts arise from lack of precipitation, whereas hydrological droughts are possible consequences, where prolonged precipitation deficits induce stream flow shortfalls. The phenomena are relative in volume and duration and therefore applicable to any region.

When analyzing hydrological droughts, seasonality plays an important role [Tallaksen and Van Lanen, 2004; Tallaksen et al., 1997]. In regions of cold climate, one distinguishes between summer and winter droughts. While summer droughts are caused by precipitation deficits over a period of time in combination with high evaporation losses, winter droughts are related to temperatures below zero, where precipitation is being stored as snow [Tallaksen and Van Lanen, 2004]. Van Loon et al. [2010] classified winter droughts into two categories; cold climate winter droughts, caused by late summer droughts continuing into winter droughts, and mild climate winter droughts, which evolve when snow cover disappears and precipitation is lower than normal. The latter category may be more suitable to define winter droughts in Bergen, due to its typical mild climate.

According to Hisdal et al. [2001] the start of the summer season is indicated as the first month of the year with a mean temperature above 0° C. Moreover, the regional drought study in Europe, conducted by the same authors, defined the summer season, representing Central Europe and the coastal zone of Norway, as 15 April - 30 November [Hisdal et al., 2001]. The authors argued that a summer drought terminates at the start of the winter season, even though the flow is still below the threshold level. Winter season is more difficult to select for catchments

of a large altitude range, for which the lower parts of the catchment experience continuous frost periods only for a few days, while the mountainous areas can have prolonged periods of frost days for several months [Fleig et al., 2006]. Further, Fleig et al. [2006] recommend analyzing the flow regime prior to selecting the seasons.

3.3.2 Threshold level method

The threshold level method is a common quantitative way of defining droughts. A sequence of drought events emerges for situations where the stream flow fall short of a selected threshold level. This implies that series from different sites within a region experience the same number of days with flow below the threshold level, although the distribution of drought duration and deficit volume may vary [Tallaksen et al., 1997]. The method is common for reservoir storage design and operation purposes in both hydropower and drinking water management.

Tallaksen and Van Lanen [2004] recommend to choose the truncation level between the 70^{th} and 90^{th} percentile from the flow duration curve (FDC) i.e. the flow exceeded 70 to 90 % of the time. According to Hisdal et al. [2000], selecting a high threshold level may introduce problems in terms of too many zero-drought years (reduced information content for statistical analysis), while a low threshold level can impose challenges where long drought durations become unrealistically normal. Fleig et al. [2006] emphasize that threshold level selection is a compromise between the two aforementioned outcomes, and remains a subjective decision based on the data in question. In recent literature, regional analyzes involving high spatial inflow variability tend to require high truncation levels, such as Q70 [Hisdal et al., 2001; Stahl et al., 2008]. Meanwhile, Q80 is used in Norwegian regional drought studies [Wong et al., 2011; Hisdal and Tallaksen, 2003; Tallaksen et al., 2009; Van Loon et al., 2010]. In the catchment scale analysis in Aurland, Q90 is applied although few arguments for the choice are documented [Chernet et al., 2013].

The threshold level can be constant for the whole year or fluctuating to reflect monthly or seasonal inflow variability. Events defined with the varying threshold are referred to as stream flow deficiencies or stream flow anomalies rather than stream flow droughts [Hisdal et al., 2000]. According to Fleig et al. [2006] it is important to derive separate threshold levels if two distinct seasons are present, since an FDC based on the summer period may differ considerably from the FDC based on the winter season.

3.3.3 Mutually dependent and minor droughts

There are two major challenges related to drought identification, namely minor droughts and mutually dependent droughts. As indicated in Figure 3.5, the flow

sometimes exceeds the threshold level for a short period, partitioning a long dry period into a number of minor droughts that are mutually dependent. This problem could undoubtedly disturb extreme value analysis. A solution is to apply a pooling procedure in advance of the analysis. The moving average (MA) procedure is a common method where daily flows are averaged over a consecutive period, which smooths the time series. While reducing the problem of minor droughts, mutually dependent droughts are simultaneously pooled together [Hisdal et al., 2000]. The duration of pooled droughts, is the sum of the drought durations and inter-event time. A moving window of 7 days has been recommended by Fleig et al. [2006], based on a test study of several different lengths. This method is frequently applied in preceding drought studies [Stahl et al., 2008; Wong et al., 2011; Chernet et al., 2013].

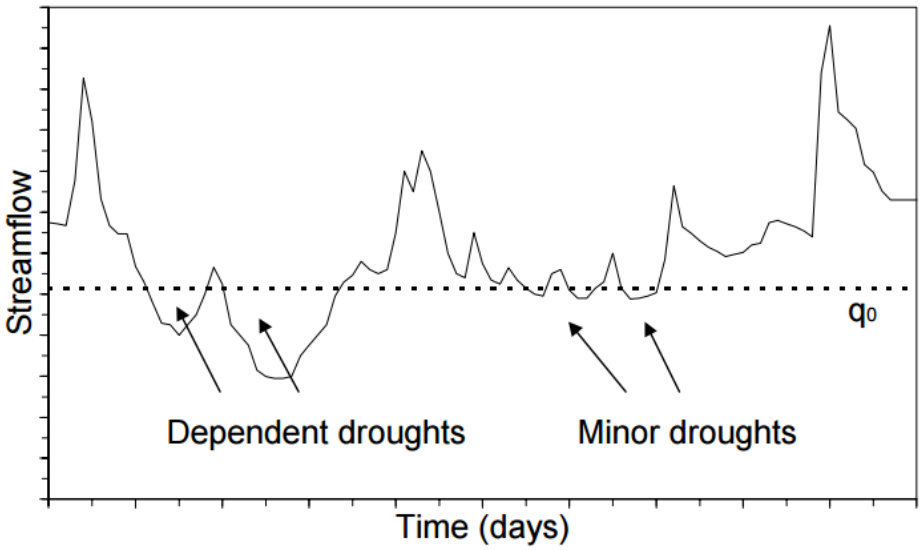

Figure 3.5: A daily time-step flow regime and appearances of minor droughts and mutual dependent droughts for threshold level, q_0 [Hisdal et al., 2000; Tallaksen and Van Lanen, 2004].

3.3.4 Drought event identification

Subsequent to selecting the threshold level, the drought events can be identified according to their duration and deficit volume [Tallaksen and Van Lanen, 2004; Fleig et al., 2006]. Accordingly, a times series of drought sequences can be obtained.

The deficit volume, $w(t)$ is defined as the sum of the excess volume, for all days in a sequence, of discharge $q(t)$ below the threshold level q_0 (Equ. 3.6). When $w(t)$ equals zero, volumes are not subtracted and the drought sequence is finished.

$$w(t) = \begin{cases} w(t-1) + q_0 - q(t) & \text{if } w(t-1) + q_0 - q(t) > 0 \\ 0 & \text{if } w(t-1) + q_0 - q(t) \leq 0 \end{cases} \tag{3.6}$$

Similarly, a duration sequence, $d(t)$ is obtained by summing up the days of which there is a deficit between the discharge, $q(t)$, and the threshold level, q_0, until $w(t)$ returns to zero. The derivation emerges from Equation 3.7:

$$d(t) = \begin{cases} d(t-1) + d(t) & \text{if } w(t-1) + q_0 - q(t) > 0 \\ 0 & \text{if } w(t-1) + q_0 - q(t) \leq 0 \end{cases} \tag{3.7}$$

Extreme value statistics

In drought analysis extreme events are of main interest. For statistical interpretation of drought extremes, there are two common procedures for selecting the extreme events from a time series; (1) block maxima (BM), often in terms of annual maxima; and (2) partial duration series (PDS). PDS is less applied in hydrological analyses which is mainly due to difficulties in its definition [Madsen et al., 1997]. The objective of frequency analysis of hydrological data is to relate the magnitude of extreme events to their frequency of occurrence. Assuming that droughts are independent and identically distributed measures, data processing and selection is important to assure the validity of these conditions. When using BM, the assumption of independence is valid, since the sequential observations from year to year are autonomous [Dingman, 2015]. Hence, in drought analysis, the annual maximum deficit volume, w_{max}, and annual maximum duration, d_{max}, are commonly applied to describe extreme drought events [Tallaksen and Van Lanen, 2004].

The available observed data series are often too short to extract reliable frequency estimates from extreme events. Different distribution models are able to generate return levels beyond the series of historical events. The approach comprises of defining the hydrological measure of interest and from there select a suitable distribution. A common method for modeling annual maximum series is the Generalized Extreme Value (GEV) distribution [Coles et al., 2001]. The method is explained in detail in Appendix B.

3.4 Water supply reliability

Water supply, as defined by Dingman [2015], is the maximum sustainable rate at which water can be withdrawn from existing sources without causing undesirable ecological, human-health, economic, legal or other consequences. Water supply reliability depends upon hydrological factors, as well as the system regulation capacity and the drinking water demand.

For water supply systems depending on surface-water, the sustainable withdrawal must account for a variable flow regime [Dingman, 2015]. River flow pattern fluctuates seasonally, and from year to year. Designing water supply systems involves a deliverance reliability at 100 %. This implies accounting for all variations in stream flow in the design. This is different from hydropower, where rationing is accepted at a certain level. General practice in reservoir design has been based upon historical observations of hydrological variables. If inflow variations were to change, this would have direct effect on the supply.

Chapter 4

Methodology

In this chapter, the methods to be applied in our thesis are presented. Based on the theoretical background reviewed in Chapter 3, selected procedures of drought analysis, climate downscaling, hydrological modeling, and techniques to evaluate impacts of climate change will be briefly described.

The approach for predicting temperature and precipitation is rendered in Section 4.1, and the procedure for constructing a functioning HBV-model representative for BW catchments, and suitable for prediction of future inflow, is found in Section 4.2. Both models are based on the fundamental assumption of stationary relationships between the model input parameters and output values, i.e. it is assumed that the relationships found between historical variables are apply for the future. In order to evaluate projeced changes, observed historical climate and hydrology in Bergen are examined. The analysis comes in two parts; (1) general climate variable trend analysis, and (2) extreme drought event analysis (Sec. 4.3). These analyses yield a solid background for evaluating the projected changes predicted in downscaling of precipitation and temperature, and hydrological simulation of future inflows. Finally, Section 4.4 summarizes the methods we utilize to evaluate the projected changes found with the aforementioned modeling approaches.

A majority of the calculations are executed in Excel, including HBV-modeling. Statistical operations, such as drought analysis and downscaling is performed in R. R is an open source software environment and programming language for statistical analysis. In addition to its built-in functions, collections of functions, and scripts for various applications, are available through packages developed by contributors in the R community.

4.1 Downscaling of climate data

Prediction of temperature and precipitation at the Florida weather station in Bergen is executed according to the described procedure in the following section. Global- and regional-scale predictors, from selected GCMs and RCP scenarios, and reanalysis projects for gridded observations, are downscaled with a linear statistical approach. The output is applied to historical records of data by the delta change method for downscaled data.

4.1.1 Delta change method

Predictions of climate conditions for the 21st century in Bergen are embedded in the full water resource availability analysis by the delta change method. On the basis of downscaled GCM output, monthly change factors for three future reference periods are calculated on a 30-year average. To create scenarios for future temperature and precipitation, the change factors are added to a 30-year historical normal period for each variable respectively. Preferably, the historical normal period should be as close to present as possible in order to best represent today's climate. However, the division of GCM historical and future output is 2005/2006, as addressed in Section 3.1.1. Consequently, 1975-2005 is instituted as historical normal period for the three future reference periods, 2011-2041, 2041-2070 and 2071-2100, referred to as first-decades, mid-decades and late-decades from hereon.

4.1.2 Statistical approach

An approach where local-scale precipitation is predicted by large-scale precipitation, and likewise for temperature, is selected in an attempt to capture a physical, rather than purely statistical, relation between predictor and predictand. The predictive model employed in this thesis is build with functions from the R package, 'clim.pact'. The 'clim.pact' package comprise functions useful to climate change impact studies and empirical-statistical downscaling on monthly and daily data, involving functions for the methods discussed in Section 3.1.6. 'clim.pact' has been successfully utilized in previous studies, and scripts ready for downscaling are accessible. The selected procedure involves selection of region by correlation analysis, where the border is set where the correlation with the station object becomes zero. Principal component analysis (EOF) is applied for pre-processing the data and combining regional-scale predictor (reanalysis project) and global-scale predictor (GCM). Finally, the actual downscaling is performed by a linear multiple regression. The script utilized to perform these calculations is presented in Appendix G.

4.2 Hydrological modeling

In this section the procedure for achieving a complete inflow series to all catchments of BW is presented. Hydrological modeling of inflow requires calibration data in terms of historical runoff series. The necessary steps of retrieving such a series are specified, followed by calibration of parameters, and transferring to ungauged catchments.

4.2.1 Reservoir inflow analysis

In BW catchments, inflow is implicitly measured through records of water levels and water flow components of the reservoirs. Therefore, an attempt to create inflow series is carried out. Due to the central location, calculations are performed for Svartediket catchment. In accordance with Equation 3.5, the volumetric change in a reservoir must equal all components flowing into a reservoir, Q_{in}, subtracted with every component flowing out, Q_{out}. For Svartediket, the components flowing into the reservoir comprise runoff from the associated watershed and controlled transfers from proxy watersheds, while the outgoing flows include drinking water consumption, other consumes and overflow at weirs. Figure 4.1 renders a flowchart of the Svartediket reservoir, and the components of the respective water balance in Svartediket are the following flows:

- Inflowing, Q_{in}
  - Runoff from Svartediket watershed, Q_R
  - Transfer from Skredderdiket, Mulen, Q_{skredd}
  - Return water from treatment plant, $Q_{ret.TP}$
- Outflowing, Q_{out}
  - Overflow at weir when water level exceeds 77 m.a.s.l., Q_{weir}
  - Transfer to HiB, Q_{HiB}
  - Transfer to treatment plant Q_{TP}

Based on this information, and by assuming that all measurable components are indeed measured and known, the inflow to Svartediket reservoir can be calculated with equation 4.1.

$$Q_R = dV + Q_{weir} + Q_{HiB} + Q_{TP} - Q_{skredd} - Q_{ret.TP} \tag{4.1}$$

However, Q_{weir} does not have to be explicitly given. It may be calculated from the water level in the reservoir and characteristics of the weir by equation 4.2

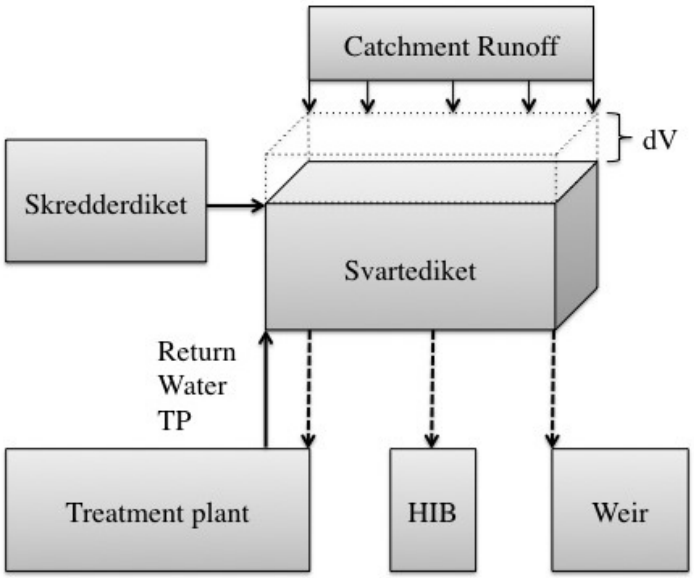

Figure 4.1: Illustrated reservoir balance, Specialization project [2014].

$$Q_{weir} = C * b * H^{1.5} \tag{4.2}$$

Where C is a weir-specific constant, b is the width of the weir and H is the water level.

4.2.2 HBV calibration

A regional set of hydrological model parameters is established for Bergen using the HBV model. Røykenes catchment is representative for the region. Herein, the HBV model version described by Killingtveit and Sælthun [1995] will be used, which is implemented in Excel.

Parameters are calibrated to fit the observed runoff data from Røykenes for the period 1980-2009 (hydrological years). Precipitation data from five stations and air temperature from one station are input to the model. This is due to significant local variations in precipitation, while temperature is more continuous. Potential evapotranspiration (PET) is computed on the basis of average monthly temperature, and the average elevation of Røykenes catchment. The procedure for calculating PET is disclosed in Appendix A.

Model performance is assessed based on two quantitative criteria, namely the Nash-Sutcliffe efficiency coefficient R^2 (Eq. 3.3), and the conformity between the average simulated and observed runoff. Calibration of parameters is conducted through a combination of manual and automatic calibration. Automatic calibration is executed through the PEST-algorithm incorporated in HBV-Excel. The best combination of station weighting is determined after parameter adjustment.

4.2.3 Inflow transferring

The HBV model output is a time series of daily inflow to Røykenes and a calibrated parameter set assumed to represent the regional hydrological behavior in Bergen. In order to create inflow series to the ungauged BW catchments, there are two procedures for inflow transferring considered in this thesis; (1) traditional scaling of inflow series to Røykenes (Eq. 3.4), and (2) transfer of Røykenes hydrological model parameters. The latter method implies employing individual HBV models with locked regional parameters, and catchment-specific parameters representing Svartediket, Jordalsvatnet, Sædalen, Espeland and Kismul, respectively. Kismul constitutes five minor catchments, which for simplicity are treated as one equivalent catchment.

Evaluation of inflow transferring methods

In order to verify the transferred inflow series, a hydrological routing procedure is constructed (Eq. 3.5), to calculate the daily reservoir storage relevant for each treatment plant of BW:

$$S_t = \begin{cases} S_{t-1} + (Q_t + Q_{t-1})/2 - W & \text{if } S_{t-1} + (Q_t + Q_{t-1})/2 - W < 0 \\ S_{max} & \text{if } S_{t-1} + (Q_t + Q_{t-1})/2 - W \geq 0 \end{cases} \tag{4.3}$$

Equation 4.3 takes into account variables at the treatment plant level, in terms of daily inflow, Q, total storage, S, and withdrawal, W at time step, t (day). For simplicity, no transfers between reservoirs are considered in the model. Additionally, the model ignores the amount of water passing as flood-spill, through simply saying that the reservoir is full when the storage exceeds the maximum reservoir volume. All reservoirs contribute to the total storage. The simulation starts 1 September, a time where the reservoirs in Bergen generally are full. The input to the model constitutes transferred inflow series to respective catchments, in the period 2001-2013. Annual withdrawal data from each treatment plant is constructed from available records, considering the withdrawal to be even over the year.

Observed storage is computed in each main reservoir based on associated reservoir volume curves and water level records (Cha. 5). The correlation between

simulated and observed storage is calculated by the Nash-Sutcliffe correlation coefficient (Eq. 3.3). Consequently, the two transfer procedures are compared to conclude which is preferable to employ throughout the assessment.

4.3 Extreme drought event analysis

Extreme drought event analysis is conducted in accordance with the threshold level method. The analysis is performed on Røykenes, which is considered representative for Bergen region. The procedure is divided into three parts; (1) selecting drought seasons and threshold level; (2) extracting drought event characteristics; (3) evaluation of trends and frequencies.

Initially, temperature and inflow data are examined in order to select the drought seasons and threshold level suitable for the site in study. The start and end date for the seasons are selected as 15 April-30 November for summer, and 1 December-14 April for winter. Further, in order to avoid splitting up the years in the middle of a drought period, the time series are presented in terms of the calendar year for summer drought analysis, and the hydrological year for winter droughts. MA pooling procedure with 7-day-window for hydrological years and calendar years respectively, is applied on the data prior to the analyses to reduce the effect of minor droughts. Determination of the threshold levels are based on data from the season of interest, and chosen as Q70 for historical climate analysis and Q80 for the climate change impact study. It needs to be noted that Q80 is taken from the HBV-simulated inflow for the control period, and consistently applied for the control and projected periods. In this way, model errors are excluded from the impact analysis, and the relative change in drought characteristics can be studied. Drought characteristics extracted in this thesis are annual maxima series (BM), in terms of d_{max} (days) and w_{max} (mill. m^3).

Extreme value statistics are performed on observed data to identify return periods and return levels for historical drought characteristics. The Generalized Extreme value distribution model is used for this purpose, for which detailed theory is implemented in Appendix B. GEV-modeling is performed in R, using the package 'fExtremes'. Statistical analyses on maximum series, are disturbed by zero-values in the data. Therefore deficit volume less than 0.5 % and durations smaller than d=1 are excluded from the analyses.

4.4 Climate change impact study

In this section the methods for evaluating the climate change impacts on water resources are outlined.

4.4.1 Projected changes in inflow

To evaluate whether the flow regime will change in character for future scenarios, the downscaled climate data are driven into the HBV-models for each catchment, and simulated inflow series are produced. Inputs to the model are delta change factors calculated from downscaled air temperature and precipitation, in addition to calculated changes in evapotranspiration at the catchment level. The values are given as monthly delta changes in °C, % and mm/day, respectively.

4.4.2 Projected changes in drought characteristics

Drought analysis is conducted for assessing whether the characteristics of droughts are changing for future downscaled scenario data relative to the historic control period. The methodology is similar to the one presented in Section 4.3. Q80 was found as an appropriate threshold level when studying the FDC for the control period. For simplicity, this value is consistently applied in both control and projection periods, to ensure a constant threshold when analyzing the impacts of climate change.

4.4.3 Projected changes in supply capacity

The climate change impacts on water supply reliability in BW are identified using hydrological routing (Eq. 3.5). The objective is to determine the maximum amount of water that can be withdrawn from the reservoirs of BW when all restrictions such as minimum flows and storage reserves are accounted for. Subsequently, this tapping is compared to the projections of water demand, on the basis of population projections and leakage reduction goals set by VA-etaten (Sec. 4.4.4). A simplified hydrological routing procedure is constructed, assessing the reservoirs of BW as one equivalent reservoir. The procedure is similar to Equation 4.3, although the one-reservoir model accounts for the total inflow to the catchments, Q_{tot}, the total storage capacity, S_{tot}, and the total withdrawal, W_{tot} at time, t. The input to the model is hydrological simulations of inflow to all BW catchments for the control and projection periods. Inflow to Mulelven, an adjacent catchment to Svartediket, is created from traditional scaling by the HBV-simulated inflow to Svartediket. A threshold level for minimum storage reserves is defined by VA-etaten as 50 days of consumption. The threshold level is assumed constant, and determined as the volume equal 50 days of demand for the population projection in 2040, considering the highest growth rate (Table 5.8), and leakage percentage of 33 %, representing 2014. The estimated volume is thereby 5.5 mill. m^3. The minimum flow at Svartavatnet is accounted for by adding the discharge of of 0.12 m^3/s to the withdrawal in the model, for 1 April to 30 September. Consequently, the

maximum supply capacity, that can be withdrawn while restraining the minimum reserves, is considered the capacity of the system as a whole.

4.4.4 Projected changes in drinking water demand

Projected changes in demand for the scenario periods are estimated on the basis of population projections from SSB, and intended leakage reduction actions employed by VA-etaten. Projections of the population in Bergen for 2070 and 2100 are calculated with an assumption that the regional growth follows the national growth. In addition, the population ratio between Bergen and Norway is assumed to change by the same rate as between 2014 and 2040.

Population growth rate is regarded as constant from one projection year to another, i.e. from 2014 to 2040, 2040 to 2070, and 2070 to 2100. Thereby, the representative population of each projection period is estimated as the mean of the start and end point of that particular period. Demand is further calculated for each period based on the projected population, using the specific consumption values indicated by VA-etaten, and assuming that they stay unchanged. Moreover, the corresponding demand is calculated for the scenarios. Four scenarios are estimated on the basis of leakage and population combinations:

- MOD20: Moderate population growth and 20 % leakage.
- MOD40: Moderate population growth and 40 % leakage.
- HIGH20: High population growth and 20 % leakage.
- HIGH40: High population growth and 40 % leakage.

Chapter 5

Data Aquisition and Quality Control

In the following chapter we perform an acquisition and quality control of requisite data for the aforementioned methodology. Meteorological and hydrological data are selected for calibrating an HBV model representative for the region. Available hydrological data from VA-etaten are processed with an aim of constructing a one-reservoir model of the water resources. Global-scale GCM outputs and gridded observations are collected and evaluated.

5.1 Meteorological data

Meteorological data in terms of precipitation and air temperature are required inputs to the HBV model. The data are retrieved from eKlima, a web portal managed by the Norwegian Meteorological Institute (NMI). The database covers all national gauging stations, and provides data on temperature, precipitation, air pressure, and relative humidity.

5.1.1 Air Temperature

Air temperature data are studied for Florida, the official NMI station in Bergen. Systematic errors may be detected using accumulation plots, and thereby control the variation pattern at the station. Figure 5.1, shows an accumulation plot depicted for the period 1904-2015. A virtually constant gradient stipulates good data quality.

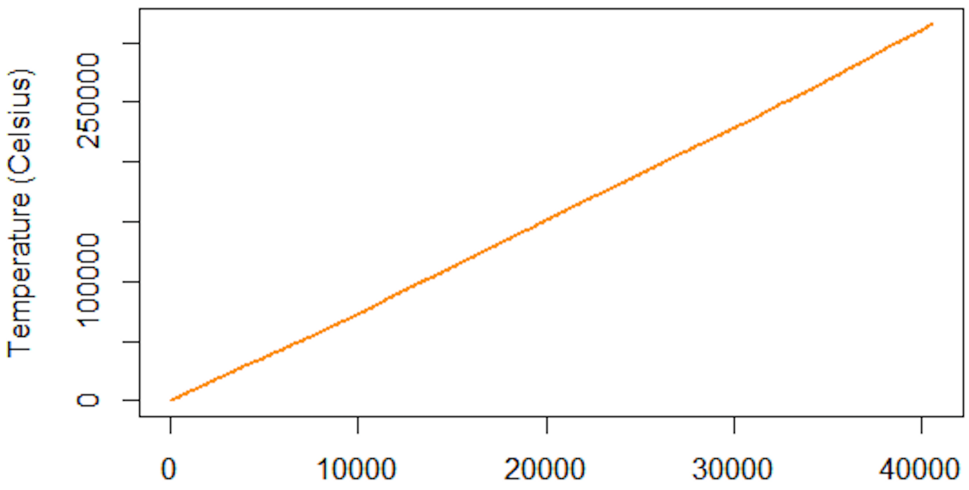

Figure 5.1: Temperature data accumulation plot

5.1.2 Potential evapotranspiration

Potential evapotranspiration (PET) is acquired input to the HBV model in terms of monthly averages. In this thesis, PET is computed using the Thornthwaite method. The approach is disclosed in Appendix A. Average monthly temperatures from Florida are corrected to fit each catchment using the elevation factor of -0.6^0C/100m. Finally, PET is computed for monthly temperature averages above 0 °C, and expressed as mm/day.

5.1.3 Precipitation

In the following, precipitation data series from year 1900 to 2014 is evaluated. The gauging stations to be analyzed are selected based on distance from catchments and geographical location, in order to reflect the associated climatic conditions. Consequently, gauging stations are picked out from Bergen and adjacent municipalities (Vaksdal, Samnanger, Kvinnherad and Lindås). Operating time lengths are displayed in Figure 5.3, and locations in Figure 5.2.

Quality control

For scaling between stations and filling in gaps of detected errors in the precipitation data series, the annual average method is used, as demonstrated in Equation 5.1.

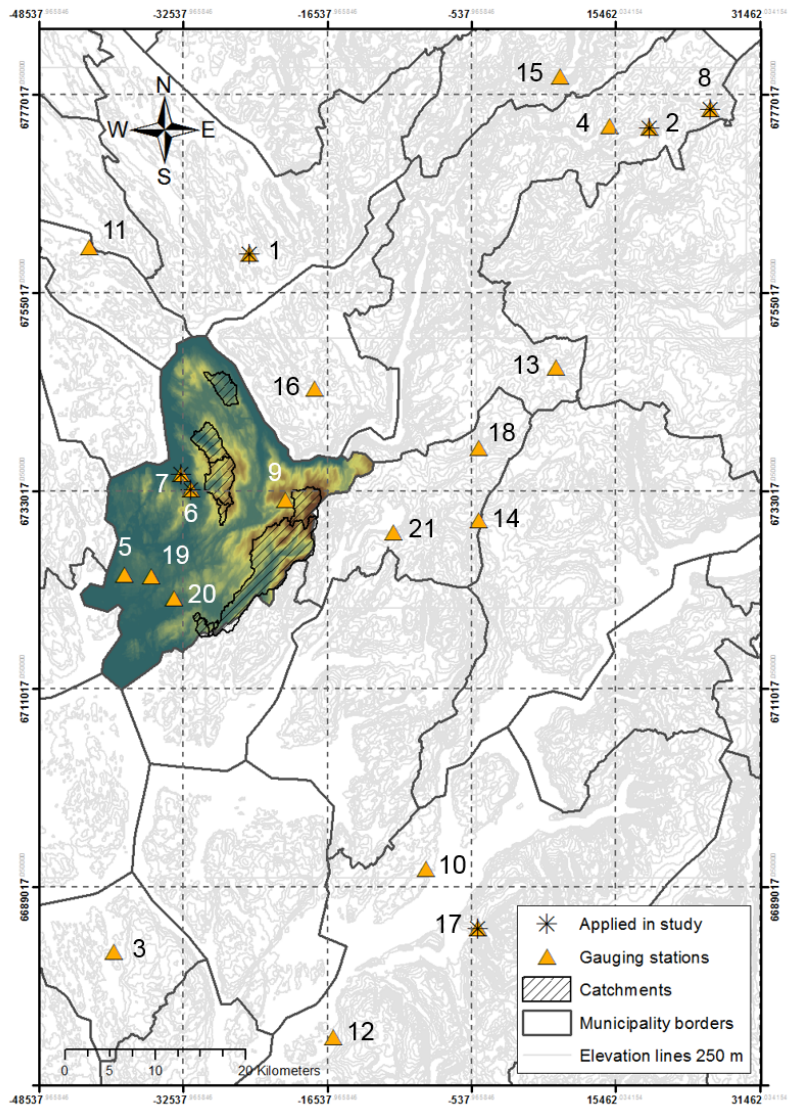

1 EIKANGER
2 EKSINGEDAL
3 FITJAR
4 FJELLANGER
5 FLESLAND
6 FLORIDA
7 FREDRIKSBERG
8 GULLBRÅ
9 GULLFJELL
10 HATLESTRAND
11 HOLSNØY
12 HUSNES
13 KALDESTAD
14 KVAMSKOGEN
15 MODALEN
16 OSTERØY
17 ROSENDAL
18 SAMNANGER
19 SANDSLI
20 STEND
21 TYSSE

Figure 5.2: Precipitation gauging stations in Bergen and adjacent municipalities

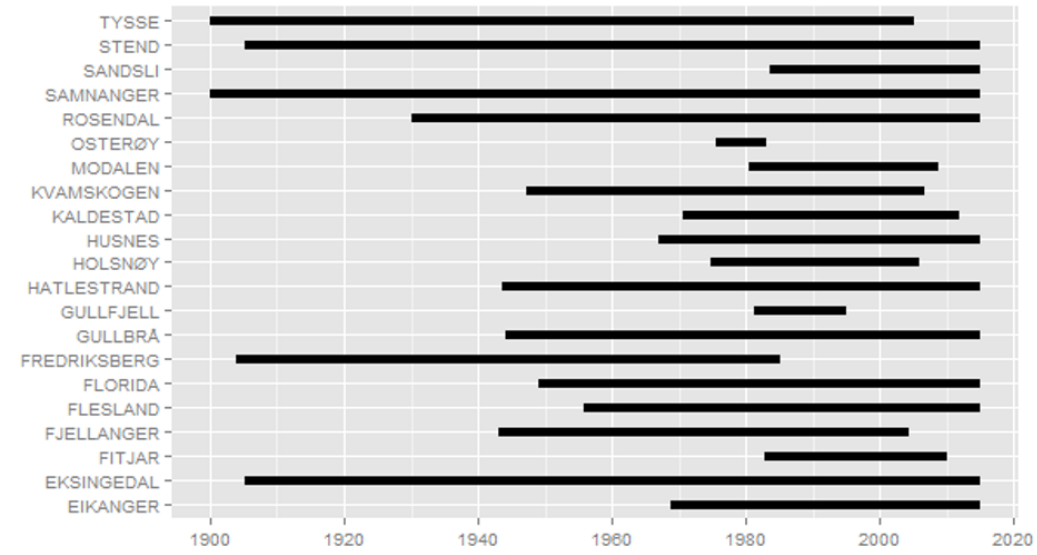

Figure 5.3: Gantt chart showing operating time lenghts for precipitation gauging stations near Bergen

$$P_1 = \frac{P_{1,avg}}{P_{2,avg}} \cdot P_2 \tag{5.1}$$

Similarly to air temperature, systematic errors in precipitation may be detected by using double mass plots, and thereby controlling the variation patterns of the stations against each other. The plots are shown in Figure 5.4, where stations are plotted against Florida, due to its convenient location in the center of Bergen, and error free data records. Consistent linearity in the plots stipulates good data quality for all stations.

While being the official NMI station, and additionally containing the longest data series free from errors, Florida is chosen to be used in hydrological modeling. HBV-Excel allows for five stations to be included in the input file. Based on record length, validity, and number of errors, the four accompanying stations are chosen; Rosendal, Gullbrå, Eikanger and Eksingedal (Fig. 5.2). The conformity in monthly variation for Eikanger and Florida is captured in Figure 5.5, and indicates that delta changes for Florida are applicable also for adjacent stations.

Station	**Latitude** (m.a.s.l.)	**Municipality** (mm)	**Annual precip.**	**Errors**
Florida	12	Bergen	2416	0
Fredriksberg	41	Bergen	2291	0
Rosendal	51	Kvinnherad	1896	0
Eksingedal	450	Vaksdal	2548	13
Gullbrå	579	Vaksdal	2108	0
Eikanger	72	Lindås	2312	1

Table 5.1: Precipitation gauging stations that fulfill the requirements to be used in HBV modeling

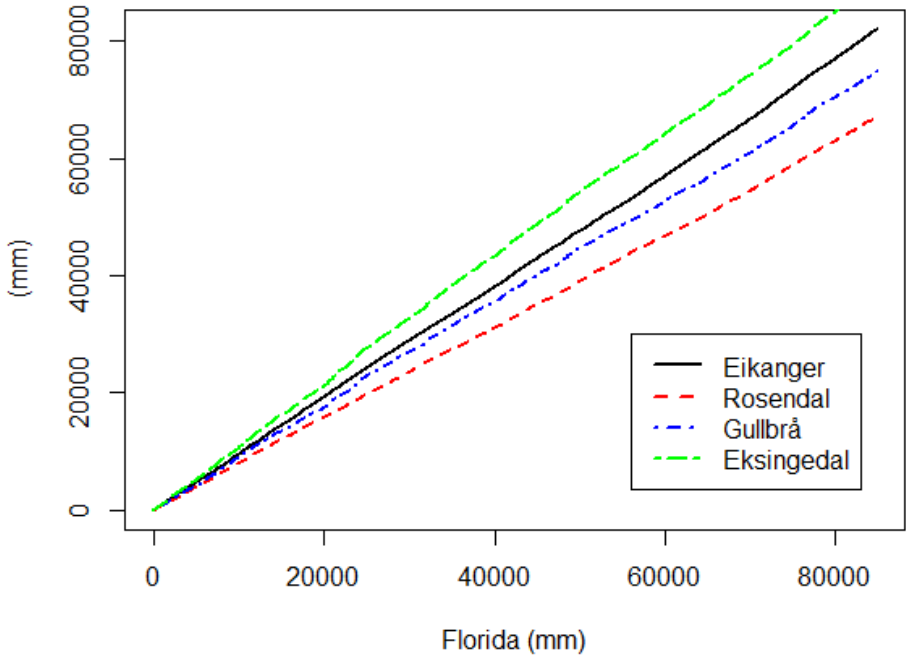

Figure 5.4: Precipitation double mass plots for Eikanger, Eksingedal, Gullbrå and Rosendal against Florida for the period 1980-2014.

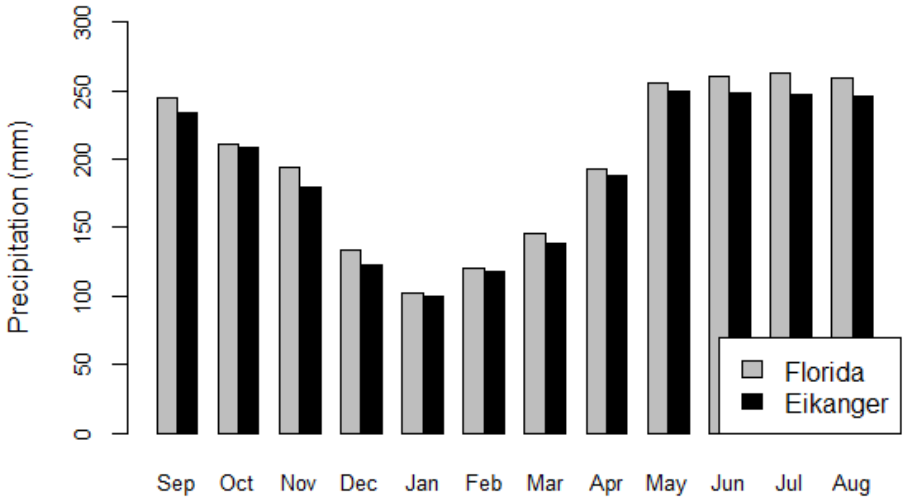

Figure 5.5: Average monthly precipitation for Florida and Eikanger. As illustrated, the observations vary in line with each other.

Data type	**Description**	**Time-series**	**Source**
Point observations	Precipitation and temperature from the Florida weather station	1904-2015	Eklima
Gridded observations	Convective precipitation rate and temperature	1947-2015	NCEP/NCAR
Global climate models	AR5 model output from selected models for pr and tas	1850(1900)-2005 2006-2100	ESGF portal

Table 5.2: Key information on the three major groups of data collected for precipitation (pr) and temperature (tas).

	Jan	Feb	Mar	Apr	May	Jun	Jul	Aug	Sep	Oct	Nov	Dec
tas	2.1	2.0	3.5	6.3	10.4	13.1	14.8	14.8	11.9	8.7	5.1	2.7
pr	243	189	187	125	105	126	140	191	270	262	261	268

Table 5.3: Climatology 1975-2005 for Florida: monthly mean precipitation (pr) [mm] and temperature (tas) [degC]

5.2 Climate data for downscaling

For each ESD model run, the requisite data to perform downscaling according to the method elaborated in section 4.1 is one set of point-scale historical records and two sets of gridded climate data; one for gridded observations and one for future projections. Table 5.2 renders key information about each data group utilized in the prediction of precipitation and temperature at Florida.

5.2.1 Point-observations

Records for the predictand of the downscaling, Florida, is evaluated in section 5.1. For downscaling purpose, the time-series with the longest possible records, and which are reliable and quality controlled, are selected. The series last from 1904 to 2015, giving a reasonable representation of the Bergen climate. Downscaling is performed on a monthly time-step, and due to specifications in 'clim.pact', variables must be stored in a *station object*. A station object stores the monthly values in a data frame, rather than a vector, where values are ordered by year and month. The station location, observation units, and start and end date of the observations, etc., are also specified in this object. The 1904-2015 series from Florida is processed by the script attached in Appendix F for creating station objects, for both temperature and precipitation. The results of this pre-processing are shown in Figure 5.6, where anomalies of the the monthly precipitation and temperature are plotted for the entire time-span, 1904-2015, along with a fitted trend line. The anomalies are calculated with respect to the normal period 1975-2005. The associated climatology, in terms of monthly averages over the time-span 1975-2005, is presented in Table 5.3

5.2.2 Gridded observations

Gridded observations of mean monthly precipitation rate and 2 meter surface air temperature from the NCEP/NCAR 40-year Reanalysis Project are retrieved from the Physical Science Division at the ESRL, Earth System Research Laboratory. Output variables from this project are classified into four classes; A, B, C and

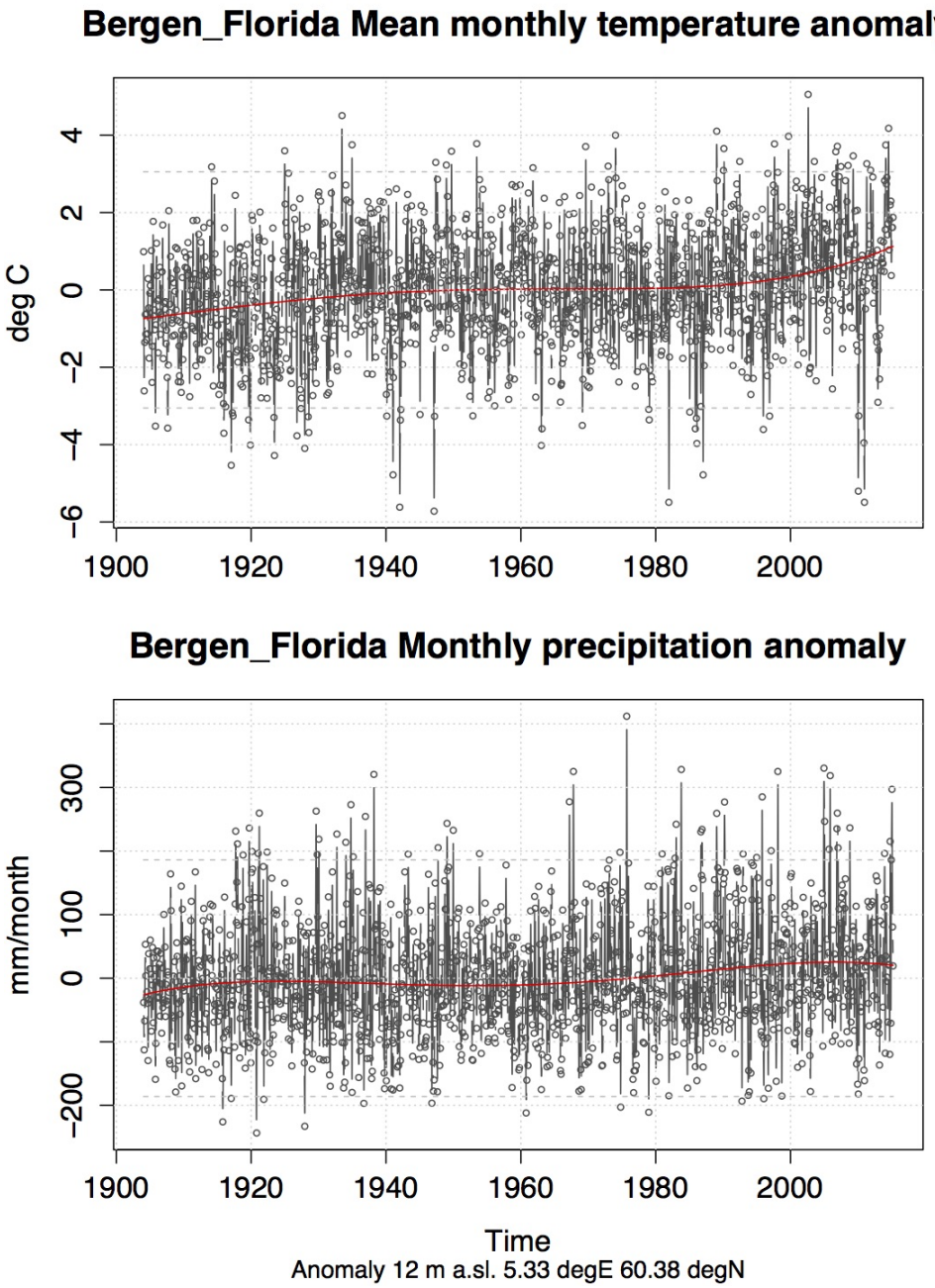

Figure 5.6: Anomalies of mean monthly temperature and monthly precipitation for climatology of 1975-2005, and (5th order) trend line

D. Class A is the most reliable class, where observations strongly influence the analysis variable, whilst class D variables are derived from climatological values and represents the counterpart to class A. Temperature belongs to class B variables, and precipitation to class C variables. Class C variables are derived solely from the model, i.e. they are not affected by any observations. Although caution should be exercised while handling such data, comparison with observations shows satisfactory resemblance [Kalnay et al., 1996]. Additionally, the fit between gridded observations and point observations is addressed in the downscaling routine.

5.2.3 AR5 GCM output

AR5 GCM outputs of temperature and precipitation from three GCMs are assembled from the CMIP5 archive of coupled model simulations. GCM simulations of historical climate for the years 1850-2005 and future climate projections from 2006-2100 are collected for one high (RCP8.5), one intermediate (RCP4.5) and one low (RCP2.6) scenario. Main features and findings of the selected models are summarized in the successive sections, while it is referred to Figure 3.2 for an overview of the model components.

CNRM-CM5

CNRM-CM5, developed by Centre Nationale de Recherches Météorologiques - Groupe d'études de l'Atmosphère Météorologique(CNRM-GAME) and Centre Européen de Recherche et de Formation Avancée (Cerfacs) is part of the collection of CNRM-CM AOGCMs and is an extention of the previous version CNRM-CM3. Compared to CNRM-CM3, the CNRN-CM5 has a more realistic representation of the mean recent climate, and is more successful in simulating atmospheric large-scale circulation [Voldoire et al., 2013]. Additionally, surface mean temperature biases are reduced.

MPI-ESM-MR

The main conceptual difference betweeen MPI-ESM and its forerunner, ECHAM5, is that the atmospheric-ocean circulation model is coupled with subsystems for land, vegetation, and marine biogeochemistry such that the model system includes the carbon cycle [Giorgetta et al., 2013]. MPI-ESM exists in various configurations, where resolution is differing.The MPI-ESM-MR is the mixed-resolution version. MPI-ESM models have contributed to CMIP5 with both historical projections of the climate, as well as future projections for RCP2.6, RCP4.5, and RCP8.5. Historical simulations of temperature are considered reasonable compared to gridded records compiled by the Hadley centre.

NorESM1-M

The Norwegian Earth System Model is based on the Community Climate System Model version 4 (CCSM4) and the research project RegClim [Bentsen et al., 2012]; a research project for the development of Bergen Climate Model (BCM) at the Bjerknes Centre for Climate Research [Furevik et al., 2003]. Bentsen et al. [2012] and Iversen et al. [2012] present basic decriptions and evaluations of the model and climate response to scenario projections, respectively. The main findings of the aforementioned articles, relevant for the impact studies in this thesis, are; (1) simulated response to GHGs is dampened by clouds in the model; (2) the model is underestimating global mean near surface air temperatures; (3) climate evolution simulations for the 20th century correspond satisfactorily with observed surface temperature; (4) global temperature increase due to RCPs is generally lower than those simulated by most of the other contributors to CMIP5; and (5) projections for precipitation yield increase in extra-tropics and high latitudes, and intensification of both drought and heavy precipitation over land.

5.3 Hydrological data

In this section the objective is to process the available hydrological data from VA-etaten and NVE.

5.3.1 Measurements from VA-etaten

VA-etaten collects data records of major flows and water levels in the resources within BW. Relevant data records are retrieved from the monitoring software, 'Cactus', for the time-span 2001-2014. Water level observations exist for different periods and various durations for all treatment plants, except for Sædalen (Tab. 5.4). For series containing obvious errors the data are corrected through either interpolation or reservoir routing simulation.

Treatment plant	Reservoir	Period	Errors
Svartediket	Svartediket	12.06.2007-31.08.2014	149
Jordalsvatnet	Jordalsvatnet	11.05.2006-31.08.2014	0
Sædalen	Nedre Gløvrevatn	-	-
Espeland	Svartavatnet	11.11.2002-09.04.2012	0
Kismul	Ulvvatnet	17.11.2004-31.08.2014	151

Table 5.4: Available data series for reservoir water level and associated point errors.

Withdrawal data are available on a 66 weekly basis for all treatment plants. Figure 5.7 shows the weekly distributed total tapping (2001-2014), illustrating a deviation from the average of maximum 20 %. Thereby, withdrawal can be considered even in the calculations.

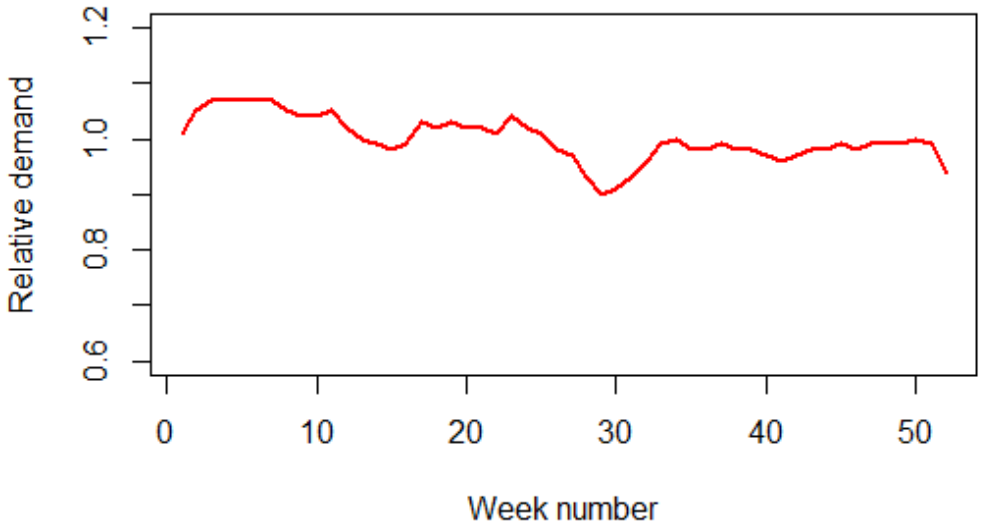

Figure 5.7: Relative total withdrawal of BW on weekly basis (2001-2014), indicating low discrepancy from even withdrawal over the year.

Reservoir volume curves are developed for all treatment plant reservoirs, both regulated and unregulated [VA-etaten, 2014]. The standard volume equation is:

$$V = A \cdot H^2 + B \cdot H \tag{5.2}$$

where V is the storage volume, H is the water level, and A and B are constants given in Table 5.5.

Components for water balance calculations in Svartediket

Daily times series are accessible for all relevant components for Svartediket. Complete series of all components requisite for water balance calculations are retrieved for the time-span 2010-2014. Ingoing and outgoing flows are sufficiently descriptive on a daily basis, while the water level component is needed on both daily and hourly resolution. Outgoing flow over the weir is sensitive to variations in

Treatment plant	**Reservoir**	**A**	**B**	**HRL** (masl)	**LRL** (masl)	**Volume** (mill m^3)
Svartediket	Svartediket	9620	154752	77.00	60.00	5.41
	Tarlebø	4443	52275	378.80	363.50	1.84
	Mulelven	2464	32063	377.00	366.60	0.60
Jordalsvatnet	Jordalsvatnet	32500	395000	16.00	12.00	2.10
	Sætervatnet	3041	24795	253.60	244.10	0.51
Sædalen	Nedre Gløvrevatn	2164	22683	362.72	352.22	0.48
	Øvre Gløvrevatn	4270	25626	371.55	363.50	0.48
	Stemmevatnet	2922	18628	385.00	381.80	0.10
Espeland	Svartavatnet (2014)	6021	157762	408.00	381.31	8.50
	Svartavatnet	5938	158749	393.10	381.30	2.70
Kismul	Ulvvatnet	3337	327696	146.70	132.40	5.37
	Joravatnet	2600	83000	195.40	185.40	1.09

Table 5.5: Reservoir volume equation parameters for all relevant reservoirs of BW.

water level, thus it is evaluated on a hourly time-step to reduce lag errors in the calculations of runoff. The weir constants, C and b, introduced in equation 4.2 are specified to C=2, and b=40.8m, by VA-etaten.

5.3.2 Measurements from NVE

From the Hydra II database provided by NVE, observed inflow data series are obtained for two catchments within Bergen region; Røykenes and Haukåselva. Daily time series are currently recorded for the catchments, and goes back to 01.01.1934 for Røykenes and 24.03.2007 for Haukåselva. The two catchments are included to ensure high data quality for the hydrological modeling process to be conducted in this report, for which their adjacent location to the BW catchments is essential (Fig. 2.2). Hydra II provides adequate data quality due to continuously control and processing [NVE, 2011]. In the quality control performed in this study, no errors are detected, implying that the series are sufficient to base a model upon.

5.3.3 Catchment parameters

Catchment field parameters are retrieved from NVEs geographic database application, Lavvann [NVE Lavvann, 2014]. Table 5.6 presents the characteristics for the target catchments of BW and for the proxy catchments controlled by NVE. Kismul consists of five minor catchments, based upon which, the characteristics representing the entire catchment are calculated.

Parameter	**Svarted.**	**Jord.**	**Sædalen**	**Espel.**	**Kismul**	**Røyk.**	**Haukås.**
H_{min} (masl)	60	16	355	390	139	53	41
H_{10} (masl)	147	29	372	448	144	77	57
H_{20} (masl)	260	67	392	514	148	123	65
H_{30} (masl)	338	136	437	561	167	186	73
H_{40} (masl)	406	185	499	612	201	256	86
H_{50} (masl)	459	248	542	666	201	305	103
H_{60} (masl)	495	285	560	721	213	362	127
H_{70} (masl)	532	342	585	756	224	451	153
H_{80} (masl)	570	414	610	790	244	551	193
H_{90} (masl)	608	487	628	852	286	664	244
H_{100} (masl)	670	586	658	984	400	959	462
Catchm. area (km^2)	12.3	9.7	1.9	9.0	3.8	50.5	7.6
Lake area (%)	4.1	5.9	8.4	2.3	15.8	3.9	2.6
Spec. runoff (l/skm^2)	105	85	112	157	72	101	71

Table 5.6: Lavvann generated field parameters for catchments of BW (Svartediket, Jordalsvatnet, Sædalen, Espeland and Kismul) and NVE (Røykenes and Haukåselva)

5.4 Drinking water demand

Drinking water demand is a highly uncertain measure, owing to the fact that no systematic gauging is feasible in most distribution systems. Demand constitutes of consumption in terms of private, public and industrial consumption, in addition to leakages in the system. In Norway, most municipalities operate with private specific demand of 160 l/p·d when designing infrastructure components, including Bergen. Additional specific demands are defined in Table 5.7. By comparing the specific demands with the registered tapping from the treatment plants, the leakage percentage may be estimated.

Specific demand	Value	Unit
Private	160	l/p·d
Public	10	l/p·d
Industrial	7.5	mill m^3/yr

Table 5.7: Specific demand values used in water management design in VA-etaten [VA-etaten, 2014].

5.4.1 Population projections

Statistics Norway (SSB) has projected the population growth both nationally (BEFINN) and regionally (BEFREG), extending to 2100 and 2040, respectively. The models take into account the fertility rate, immigration versus emigration, death rate, and relocation [SSB, 2014]. Population growth is highly uncertain, and should be taken into careful consideration especially for projections on remote future. This is also the reason for why SSB do not practice regional projections for periods exceeding year 2040 [SSB, 2014]. Available data on current and future population in Bergen emerges from Table 5.8. In the moderate growth alternative, the population growth is computed to continue to grow, although with a decreasing rate. In the high growth alternative, the population is estimated to escalate until the end of the century [SSB, 2014].

	Moderate		High	
Year	Bergen	Norway	Bergen	Norway
2014	271949	5109056	271949	5109056
2040	331571	6323563	380054	7229156
2070	-	7106298	-	10252545
2100	-	7711156	-	14048699

Table 5.8: Population projections based on moderate and high growth alternatives, generated by the regional model, BEFREG, and national model, BEFINN [SSB, 2014].

Chapter 6

Climate and hydrology in Bergen

In the following chapter, the historical data representing Bergen region, in terms of climate and hydrology, are analyzed aiming at detecting the changes and variations during the preceding century. A trend analysis of temperature, precipitation and runoff will indicate how much and in what way the climate is changing on annual, seasonal and the daily basis. Extreme drought event analysis is conducted to evaluate the return periods and levels corresponding to historical runoff.

6.1 Present climate in Bergen

Bergen is a city known for its wet climate. The location in Western Norway (60N,5E), indicates coastal climate and pronounced topography. For the normal period of 1961-1990, statistical reports render an annual precipitation of 2250 mm (Florida weather station) and typically precipitation occurs 243 days every year (i.e. days with 0.1 mm or more precipitation) [NMI, 1999]. The mean temperature is between 4-8 degrees, whereas the daily temperature stays higher or equal to 0 °C for 337 days every year [NMI, 1999]. Late autumn is the wettest period of the year in this region, and low flows can occur both in summer and winter [Wong et al., 2011]. The region is mostly affected by orographic precipitation, which is produced when humid air from the Northern Sea is lifted as it moves over the mountain range. The air rises and cools, forming clouds that typically precipitates upwind of the mountain ridge. Particularly prominent mountains, oriented across the wind gradient, receive the heaviest precipitation. This causes major variations in precipitation loads, even within small distances.

6.2 Detected changes in historical climate and hydrology

The historical temperature, precipitation and runoff in the for the 20^th century are examined in this section.

6.2.1 Air temperature

As pictured in Figure 6.1, air temperature gauged at Florida has increased for all seasons, but with the greatest tendency for the spring and summer season. It needs to be noted that the rise in temperature during winter appears as low due to the extreme event in 2010 strongly affecting the trend. However, its distinct nature compared to the warm years in 2011 and 2014, emphasizes the uniqueness and severity of the event.

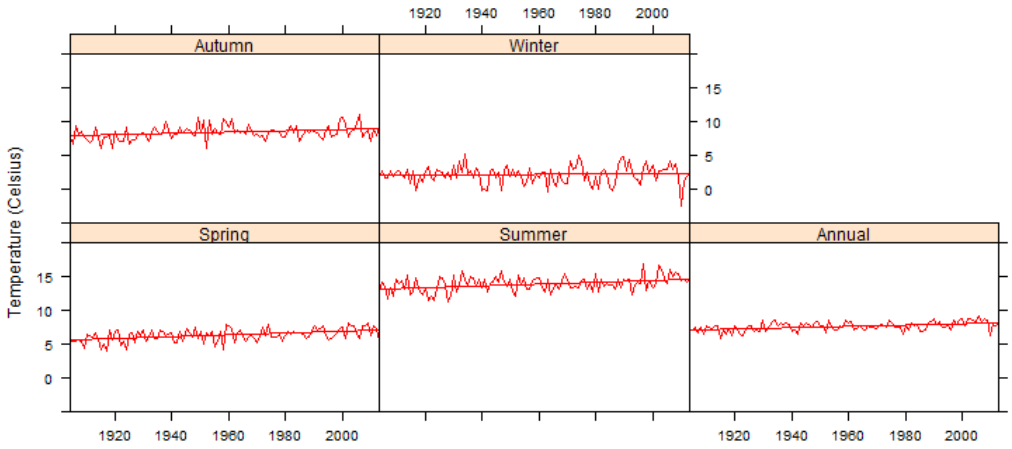

Figure 6.1: Annual and seasonal temperature at Florida (1904-2013). The trend is positive for all seasons; autumn (1.08 °C); winter (0.23 °C); spring (1.41 °C); summer (1.36 °C); and annual (1.02 °C).

6.2.2 Precipitation and runoff

Both precipitation and runoff have an increasing annual trend of around twenty percent for the historical period. However, the seasonal distribution is more pronounced for observed runoff than for observed precipitation. While precipitation has increased by 27.1 % for summer, runoff has decreased by 0.01 %. Temperature rise in winter and spring leads to an earlier snow melt, at the same time

as a higher evapotranspiration during summer reduces the hydrological recharge considerably, leading to periods with particularly low flow for this season. Even though precipitation has increased more for autumn than for winter, the air temperature rise during winter causes less precipitation stored as snow and an inflow rise of nearly fifty percent. By studying this trend isolated, it seems implausible that the 2010-event could have taken place at the end of this trend.

Long winters of air temperatures below the freezing point are likely to reoccur in Bergen, even though a clear climate change has taken place in the region during the period of 1934-2013. However, the risk for disturbance on the water resource availability is likely to be more affected by low flows during summer, than during winter.

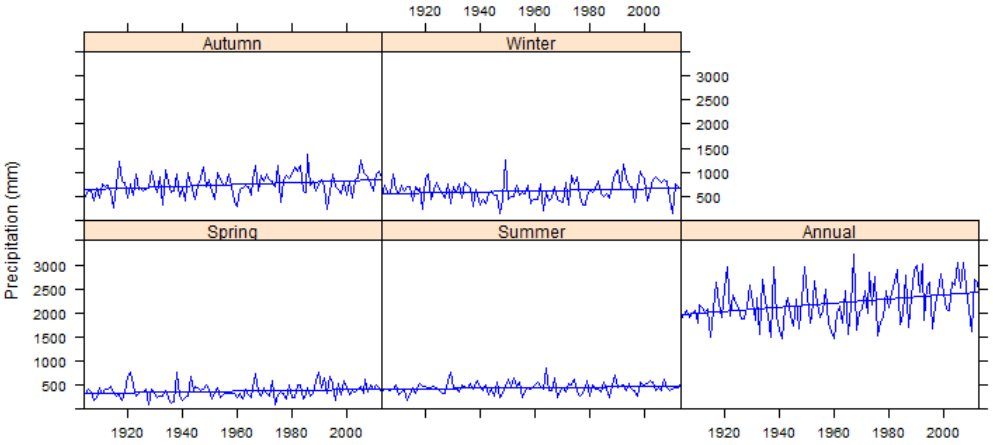

Figure 6.2: Annual and seasonal precipitation at Florida (1904-2013). The trend is positive for all seasons; autumn(31.2 %); winter (20.0 %); spring (27.1 %); summer (13.3 %); and annual (23.6 %).

Figure 6.4 a) and b) illustrate the daily FDCs for three periods of similar length in the historical data records. The curves show a clear upward shift from the first period (1934-1960) to the third (1988-2013). The increase is larger for the higher percentiles than for the lower. Moreover, the greatest change is found for the last period. Accordingly, the weather today has become wetter.

6.3 Extreme drought analysis

In this section Bergen region's vulnerability to drought events is studied. Extreme drought analysis is conducted on the basis of historical data from Røykenes, determining annual maximum duration d_{max}, and annual maximum deficit volume

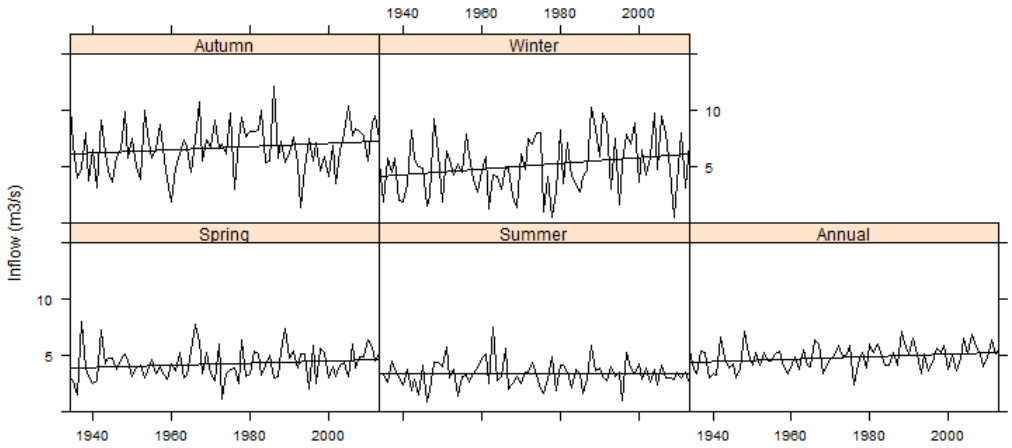

Figure 6.3: Annual and seasonal inflow for Røykenes (1934-2013). The trend line shows respectively; autumn (17.5 %); winter (47.4 %); spring (20.9 %); summer (-0.01 %); annual (21.9 %).

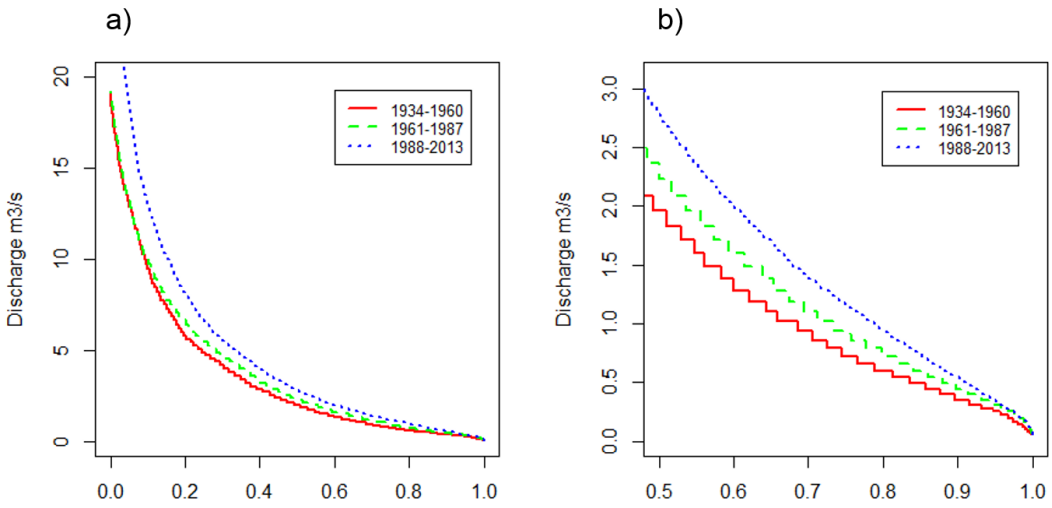

Figure 6.4: Daily FDCs for Røykenes, extracted from the three periods; 1934-1960, 1961-1986, and 1987-2013. In a), the whole data set is displayed, whereas in b), a zoomed version depicts the changes for the flows occurring less than 50 % of the time.

w_{max} by the threshold level method. Drought seasons are chosen based on the temperature regime and the flow regime for Røykenes, as pictured in Figure 6.5. Clearly, the inflow peaks in spring and late autumn divide the year into two periods of lower flows. The tendency is supported by the 70 percentile temperature regime for Røykenes, which splits the year into two, one period of temperatures above and below zero. The seasons to represent summer and winter in drought analysis are thereby, 15 April - 30 November and 1 Dec - 14 April, respectively.

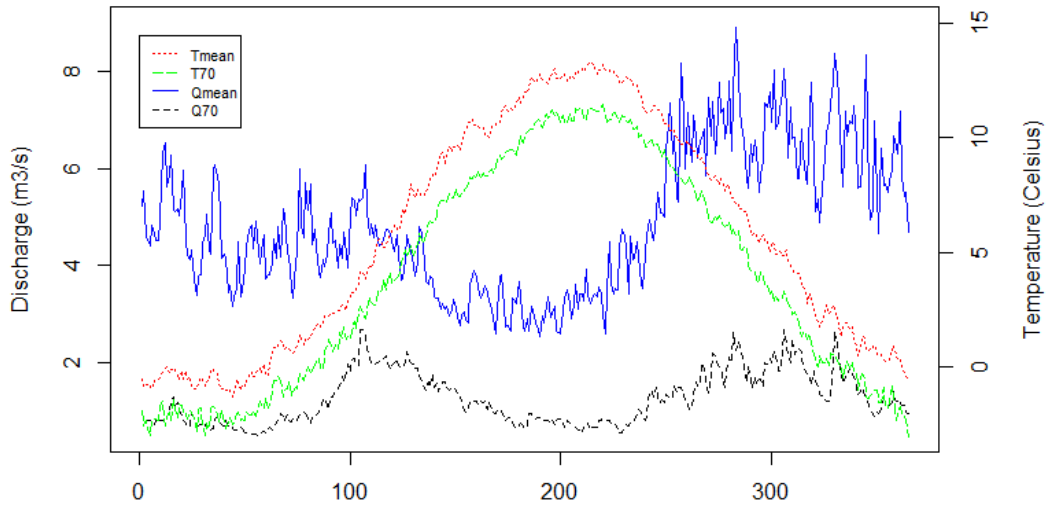

Figure 6.5: Averages and 70^{th} percentiles for daily air temperature and flow at Røykenes (1 January to 31 December). Temperature is scaled from Florida to Røykenes by using a dry adiabatic coefficient of 0.6 °C/100 m.

Threshold levels are chosen on basis of the FDC for each season. Figure 6.6 shows the discharges corresponding to the duration between the 50^{th} and the 90^{th} percentile for summer and winter drought seasons (1934-2013). Evidently, the winter discharge is beneath the summer discharge for all exceedance levels. In order to include the major drought event in 2010 as a whole sequence, while avoiding zero-drought years, Q70 is selected for the further drought analysis of the historical period 1934-2013.

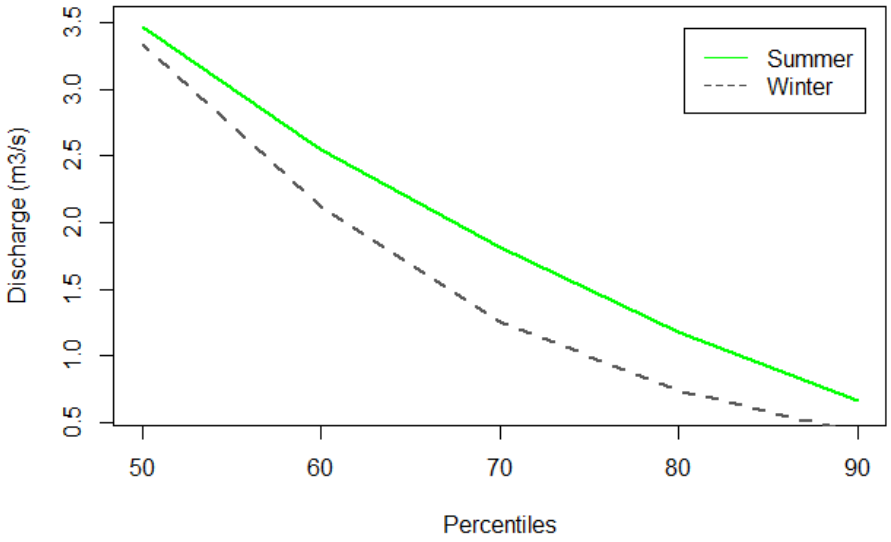

Figure 6.6: Daily discharge duration percentiles for summer and winter drought seasons (1934-2013).

6.3.1 Trends

The extreme drought event trend is examined to determine eventual changes in climate over time during the preceding century. Figure 6.7 displays the drought events in terms of d_{max} (days) and w_{max} (mill. m3) from 1934 to 2013, with corresponding trend lines. As shown in the diagrams, the most severe summer drought events occurred in 1936, 1982 and 1997 in terms of duration, whereas 1936, 1947, 1968, 1982, 1996 and 1997 stand out for deficit volume. Years with long lasting winter droughts are recorded in 1937, 1942, 1947, 1951, 1979 and later in 2010 (longest). In the form of deficit volume, the most critical winter droughts took place in 1936, 1942, 1947, 1962, 1979 and 2010. Note that some years of winter and summer droughts are connected; 1936/1937, 1947, 1996/1997 and 2005/2006. These are either caused by dry winters followed by dry summers, or dry summers followed by autumns where temperatures fall below the freezing point at an early stage. The trends in both winter and summer droughts (Fig. 6.7) are declining, and at a higher rate for winter than for summer, even though the 2010-event comes late in this particular time slice. Figure 6.8 displays drought events (1934-2013) in terms of histograms. Not surprisingly, the plots are left-skewed, indicating the rarity of extreme droughts in Bergen, especially for the winter season.

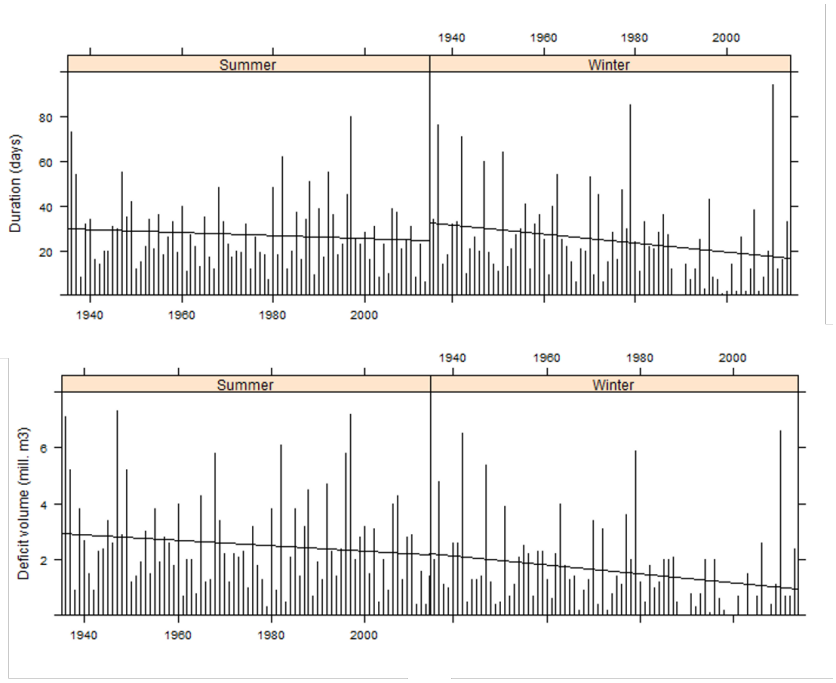

Figure 6.7: Annual maximum drought duration (d_{max}) and deficit volume (w_{max}) for summer and winter season (1934-2013) with truncation level Q70.

6.3.2 Return periods and levels

Return periods for d_{max} (days) and w_{max} (mill. m3), are estimated for each season by means of frequency analysis using GEV (Tab. 6.1). In Appendix C the model fit to each drought characteristics are visualized. The analysis is based on a data series of 80 years, which means that return levels exceeding two times the length of the series, i.e. 160 years, should be treated with carefulness. The return periods displayed in Table 6.1 range from 10 to 1000 years.

The return levels appearing in Table 6.1 indicate that in a historical perspective, summer droughts are shorter than winter droughts for all return periods. However, summer droughts generally cause higher deficits for the shorter return periods, but is bypassed by winter droughts for the return period of 200 years an higher. From this model approach, the 2010-drought is estimated to a 90-year event, whereas the same duration for the summer season is a 200-year event.

The results obtained in this brief analysis on historical climate in Bergen, emphasize the need to research possible climate change in the future.

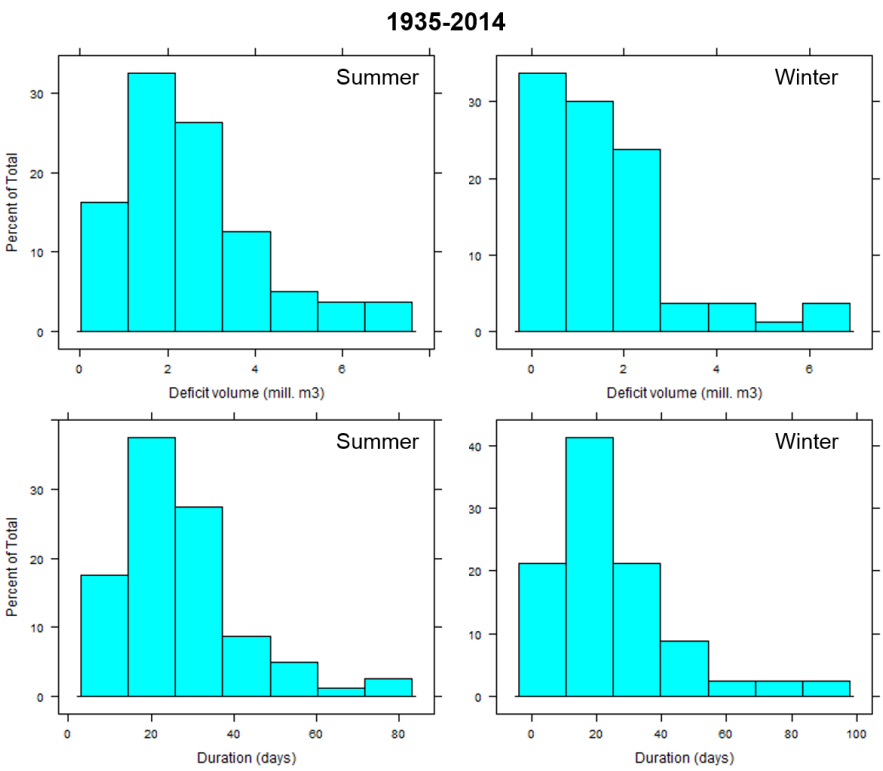

Figure 6.8: Histograms of annual maximum drought duration (d_{max}) and deficit volume (w_{max}) for summer and winter season, with truncation level Q70 (1934-2013)

Return period	**Duration**		**Deficit volume**	
(years)	Summer (days)	Winter (days)	Summer (mill. m3)	Winter (mill. m3)
1000	124	188	14.5	18.0
500	110	155	12.6	14.5
300	100	136	11.3	12.3
200	93	123	10.4	10.5
150	88	114	9.8	9.6
100	81	102	8.9	8.3
50	62	84	7.5	6.5
20	56	63	5.8	4.6
10	47	49	4.7	3.4

Table 6.1: Drought return periods in terms of annual maximum duration and deficit volume. Based on frequency analysis on historical observed data (1934-2013) by the GEV distribution model.

Chapter 7

Results and evaluation

This chapter constitutes the results and evaluation of hydrological modeling, downscaling and climate change impact studies conducted in accordance with the methodology presented in Chapter 4 and the data assessed in Chapter 5.

7.1 Hydrological modeling

In this section the results from the hydrological modeling procedure to achieve a complete inflow series to BW is presented. HBV calibration for Røykenes is accomplished, followed by a reservoir routing approach to determine the best way to scale the model inflow simulations.

7.1.1 Reservoir inflow analysis

In the following, results from inflow analysis of Røykenes, Haukåselva and Svartediket catchment are presented.

Inflow series to Røykenes and Haukåselva

Measured inflow series to Røykenes and Haukåselva have been compared for the time-span 2007-2015. Both inflow records are adjusted for average inflow, Q_m. By this adjustment, scaled record series are left dimensionless, and uninfluenced by the size of the catchment area. Figure 7.1 presents parts of the investigated series. The figure is an indicator for the overall trend found in the complete series, and it effectively shows the correspondence between the two inflow-patterns. Both catchments seem to share a similar variation over the year, in terms of response time and rate, and recession after flow-peaks. Inconsistency between the catchments is found for periods of low-flow and flow-peaks. Generally, some inconsistency is expected due to diverging soil characteristics in the catchments, and the large local

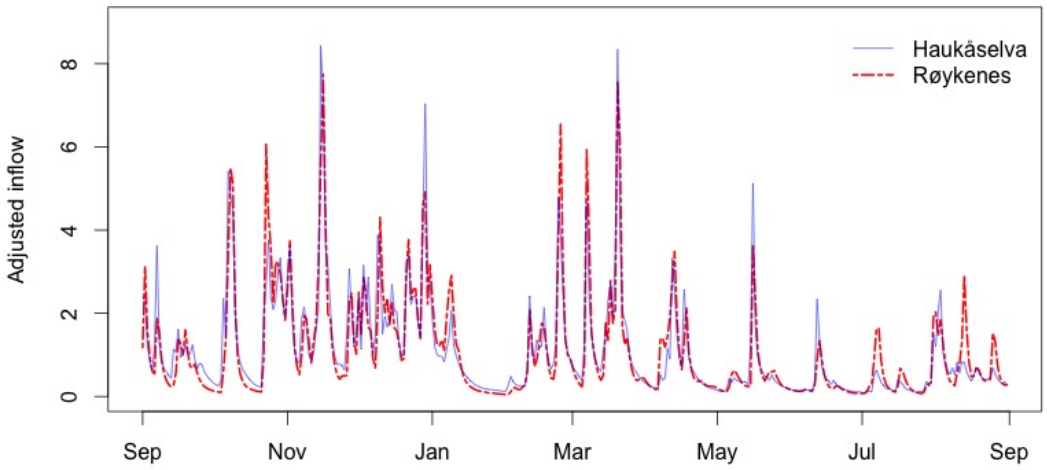

Figure 7.1: Relative inflow series for Røykenes and Haukåselva Sep. 2013 - Sep. 2014. Inflow series are scaled with average runoff, Q_m, and are thus dimensionless.

variations characteristic for Bergen. Haukåselva and Røykenes are located north and south of Bergen, respectively, and the convincing correspondence is thus supporting the assumption that variations in inflow is closely related across catchment borders.

Inflow series to Svartediket

Calculated runoff series to Svartediket are compared to a scaled runoff series from Røykenes in order to evaluate how realistic the results are. Initial calculations of the water balance of Svartediket over the time-span of available data, 2010-2014, did not yield satisfactory correlation with Røykenes and there was a significant amount of negative runoff values. Thus, initial calculations were rejected by a simple visual inspection. There were however periods of more reasonable results, and it was decided to continue assessment on the period of the presumably best results, namely the hydrological year 2013-2014. Figure 7.2 shows the obtained runoff to Svartediket and scaled runoff to Røykenes for the initial calculations. Calculations for Svartediket are able to predict the major variations detected in the Røykenes series, but the runoff is consequently overestimated. Additionally, the model efficiency coefficient, R^2, (Tab. 7.1) does not support this calculation method, as a negative value of -0.661 indicates that the model is not able to

Water level	**R^2**
Initial	-0.661
minus 5cm	0.419
minus 6cm	0.502
minus 7cm	0.553
minus 8cm	0.576
minus 9cm	0.577
minus 10cm	0.560

Table 7.1: Model efficiency criterion for different adjustments of the water level series, Svartediket.

satisfactorily predict inflow. Additionally, there are still incidents of negative inflow values.

Based on the aforementioned remarks, and experience pointing towards a measuring error on the water level gauge, calculations with different modifications of the water level data were conducted. Previous observations have revealed that the gauging equipment may measure with a systematic error, yielding a measured record value for the water level that is higher than the true value. Therefore, calculations have been carried out for inflow where the original water level is lowered between five and ten centimeters. Table 7.1 demonstrates the effect these adjustments had on the balance's ability to predict inflow to Svartediket. R^2 is altered from a negative value of -0.661 to a positive; 0.577 at the highest. The highest R^2 value corresponds to a lowering of the water level of 9 cm. The increased R^2 value, and the coinciding graphs visualized in Figure 7.3, are both evidence of a positive correlation between calculated values and scales series from a proxy catchment. They also reveal the clear shortcoming of the water level measuring device, and underpin the importance of accuracy in measuring devices when records are requisite for modelling purpose.

Although lowering of the water level improves results of inflow calculations, occurrences of negative runoff values are still present. Figure 7.4 summarizes the magnitude of the negative values and the timing of their appearance for all experiments with lowered water level. Mostly, the graphs are coinciding, meaning the negative values are not affected by the lowering, but there are still some cases where a tendency of increasing error occurs when water level is decreased. As indicated in the figure, these values correspond to dates where the original water level were above 77 m.a.s.l., the threshold for the activation of the weir in Svartediket. This behaviour is logic in terms of the water balance; a decreasing water level yields a decreasing amount of outgoing flow, which in turns have a reducing

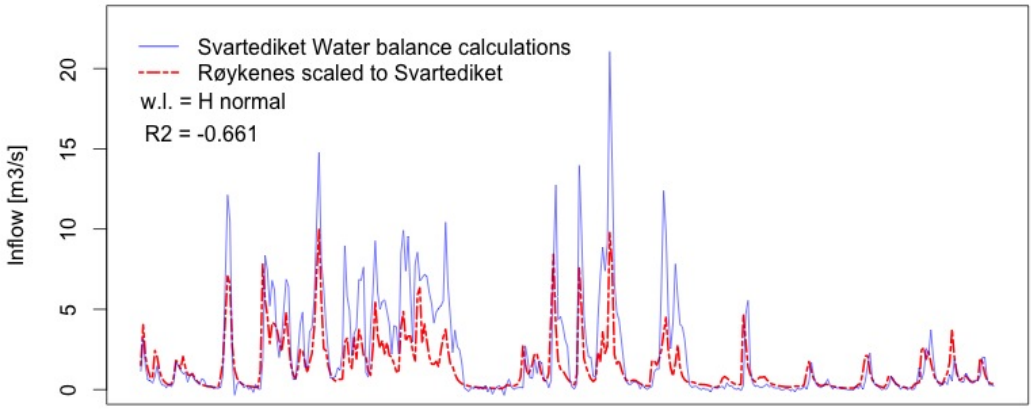

Figure 7.2: Calculated inflow to Svartediket and scaled runoff series from Røykenes for the hydrological years 2013-2014.

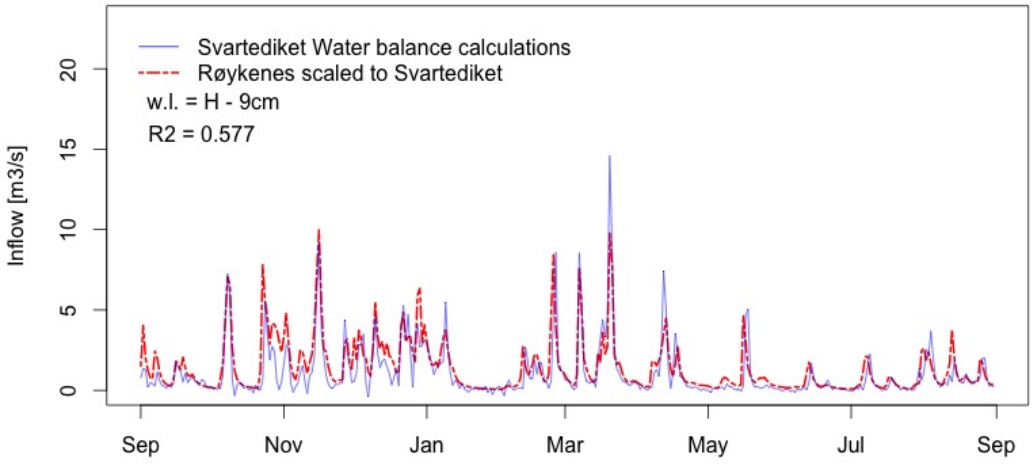

Figure 7.3: Calculated inflow to Svartediket and scaled runoff series from Røykenes for the hydrological years 2013-2014, when water level is lowered 9cm.

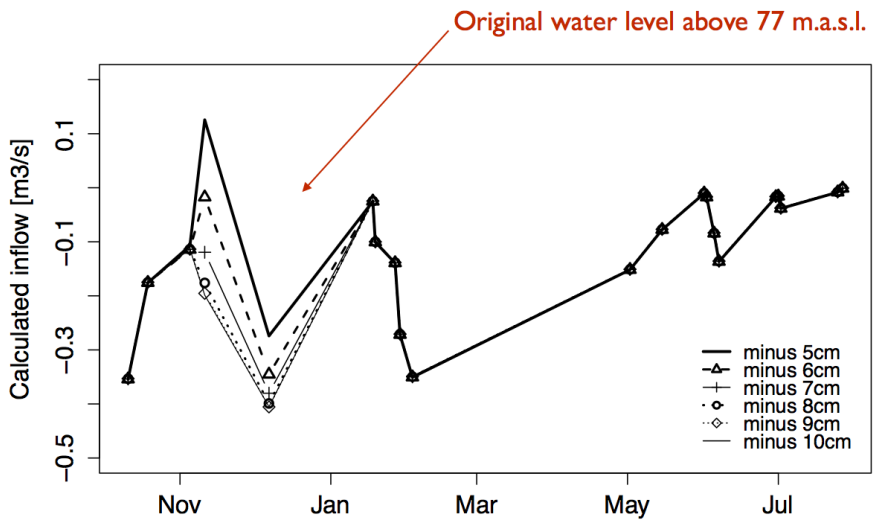

Figure 7.4: Negative inflow values for each lowering of the water level. A total of 18-21 occurrences within the time-frame November 2013 to August 2014

impact on the calculated inflow.

However, the majority of the errors seem unaffected by the water level adjustment. Although it is suspected, it is not evident that they are caused by the inaccuracy of the water level gauge. Consequently, time-series are plotted, and timing of negative values indicated for all components of the balance (Fig. 7.5) in order to discover an interrelationship between the appearance of negative values and one of the components. From the Figure 7.5 it is perceptible that there is no clear connection between any of the flow components and the negative values. There is however, remarkably many occurrences of negatives in times of decreasing water level in the reservoir.

7.1.2 HBV calibration

HBV-modeling is conducted to explore the changes in reservoir inflow to BW in the future, on the basis of recent historical data from 1980-2009 (hydrological years).

As indicated in Table 7.3, the precipitation stations were weighted 0.6 for Florida and 0.4 for Eikanger Myr, providing a better model fit when only using Florida. The flow regimes for simulated and observed inflow to Røykenes are displayed in Figure 7.6, whereas the computed HBV summary is captured in Table 7.2. The model is concluded to have good ability to reproduce runoff, though it overestimates the lowest flows during summer and winter to some extent, and

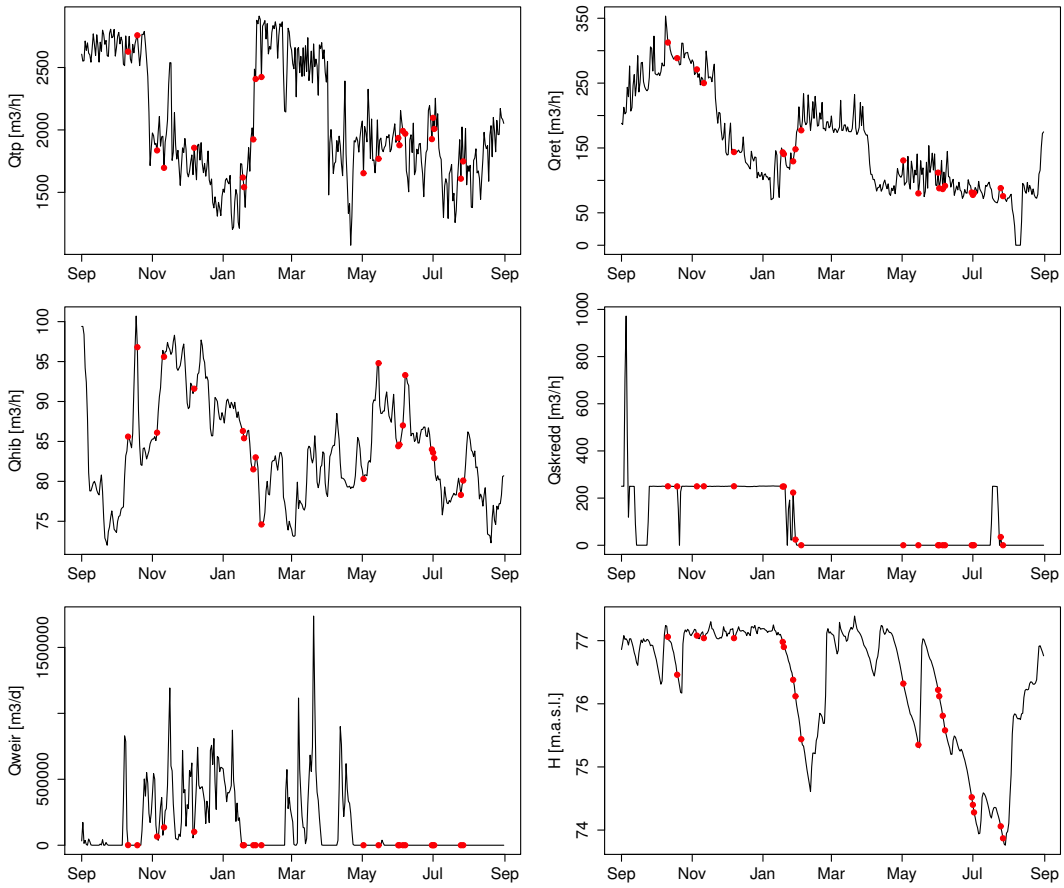

Figure 7.5: Error analysis: records of the components comprising the Svartediket water balance (time-series) and timing of negative inflow values (red dots) in water balance calculations.

HBV summary	
R^2	0.801
Q_obs	5.162
Q_sim	5.162
% deviation	-0.001
R^2 (corr)	0.801

Table 7.2: Summary from calibration of Røykenes catchment in HBV-Excel (01.09.1980-31.08.2009)

underestimates the highest peaks. This tendency is also captured by the higher percentiles illustrated for simulated and observed inflow during summer and winter (drought seasons) in Figure 7.7. However, the impact of climate change is a relative analysis where the expected change is of interest rather than exact values.

Element	Parameter	Value	Units
PREC	PKORR	1.09	
	SKORR	1.10	
	HPKORR	11.6	% per 100 m
SNOW	CX	3.00	mm/°C/day
	TS	-0.68	°C
	TX	0.88	°C
	PRO (CFR)	10.00	% of normal melt
	CPRO (SW)	4.7	% of dry snow
SOIL	FC	167	mm
	BETA	2.40	
	LP	82.0	%
UPPER	KUZ2	0.50	1/day
	KUZ1	0.14	1/day
	UZ1	14.7	mm
	PERC	0.42	mm/day
LOWER	KLZ	0.07	mm/day
Temperature lapse rate	TPGRAD	-0.58	°C/100 m
	TCGRAD	-0.91	°C/100 m
Initial states	Soil water	87.0	% of FC
	Upper zone	18.5	mm
	Lower zone	9.6	mm
Rain gauges	Florida	0.6	
	Eikanger	0.4	

Table 7.3: Parameter set obtained from calibration of Røykenes catchment in HBV-Excel (1980-2009)

7.1.3 Inflow transferring

The calibrated HBV model for Røykenes yields two outputs; a simulated inflow series of 30 years, and a parameter set that fits the observed inflow series of the catchment. The inflow analysis in Section 7.1.1 supports Røykenes as directly scalable to Svartediket and Haukåselva. It is further tested whether a direct scaling process by the traditional method, or a scaling of the HBV-parameters to each catchment, gives the most appropriate inflow regime of the ungauged catchments of BW. The two procedures are described in Chapter 4.

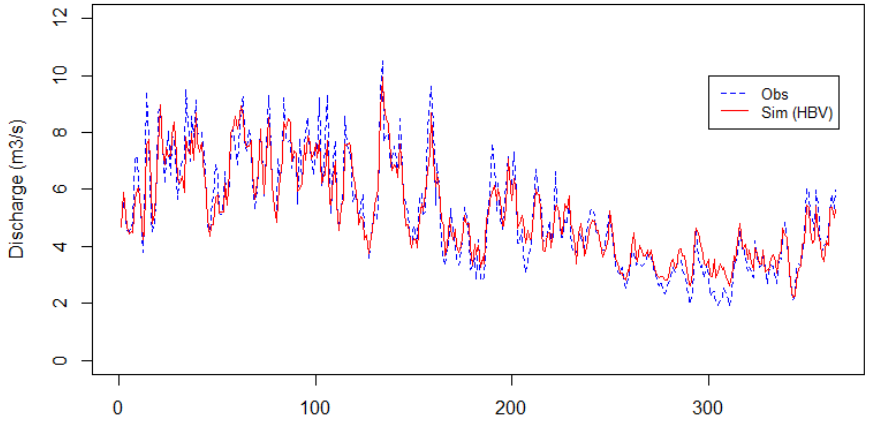

Figure 7.6: Average daily flow regime for simulated and observed inflow to Røykenes (1 September to 31 August) for the calibration period 1980-2009.

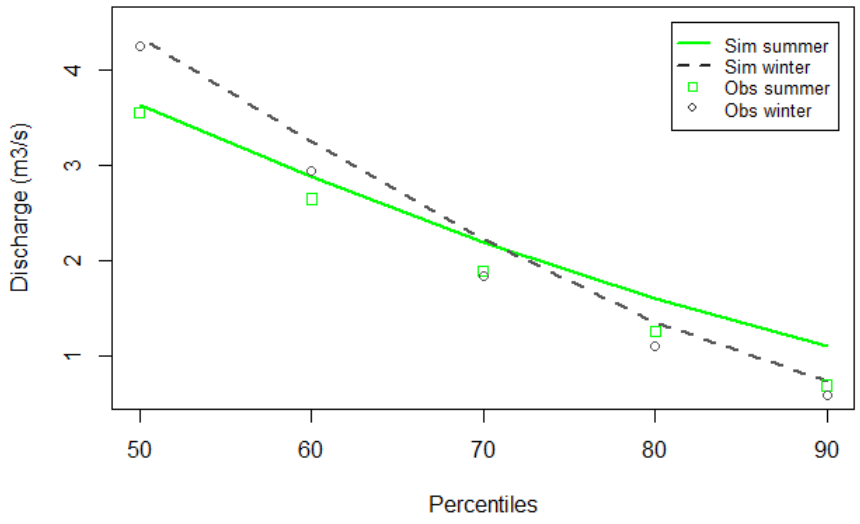

Figure 7.7: Derived percentiles of observed and simulated discharge for summer and winter drought seasons. The deviation can reduce the representation of droughts.

Comparison of scaled inflow series

Primarily, the inflow series generated by the traditional scaling method and the scaling of parameters method are compared. Figure 7.8 a) presents the monthly average inflow regime generated from the individual HBV model for each catchment. The inflows are scaled to Røykenes to allow for direct comparison. The graph shows the local differences in inflow. By average, the flow regimes are characterized by moderate flow during winter, a marked low-flow season from April to September, and a high-flow season in autumn from October to the end of December. Jordalsvatnet, Svartediket and Sædalen have the most similar inflow trend relative to Røykenes. For easier interpretation, the elevation distributions of the catchments are illustrated in Figure 7.8 b). Not surprisingly, the hypsographic curves for Svartediket and Jordalsvatnet are very close to the curve for Røykenes. Kismul is the catchment of the lowest altitude distribution, causing the average winter flow to become nearly as high as the flow during autumn, whereas the low-flow season is more distinct during summer compared to the other catchments (the latter is also the case for Jordalsvatnet). Espeland has the highest elevation distribution of the catchments. This is reflected in the seasonal distribution of flow, where the lowest flows occur during winter due to precipitation being stored as snow, and the highest flows occur in spring, at the time of snowmelt from March until late June. An additional finding is that inflow scaled from Røykenes is close to the mean of the BW catchments' inflows. Similarly, the catchments within BW cover approximately the same elevations as Røykenes alone.

Consequently, Figures 7.8 a) and b) show that a direct scaling from Røykenes by the traditional method fails to capture inflow variability, induced by the catchment's hypsographic curve.

Hydrological routing

An additional comparison of the inflow scaling methods is executed using a hydrological storage routing procedure. The inflow series are processed in a simple reservoir simulation model, producing output in terms of daily storage volume associated with each treatment plant. In Table 7.4 the correlation between the simulated storage and observed storage is presented for the two methods respectively. For all catchments the scaling of parameters method yields a higher R2-value than traditional scaling. It captures the variation in storage better for Svartediket, and Svartavatnet with R2-values of 0.59 and 0.65, respectively. For Jordalsvatnet the difference is smaller. As BW does not provide adequate water level data for Sædalen, this treatment plant is not considered. For Kismul, both R2-values obtained are relatively low compared to the other catchments, with R2-value of 0.32 for the scaling of parameters, and 0.30 for the traditional method. The overall results

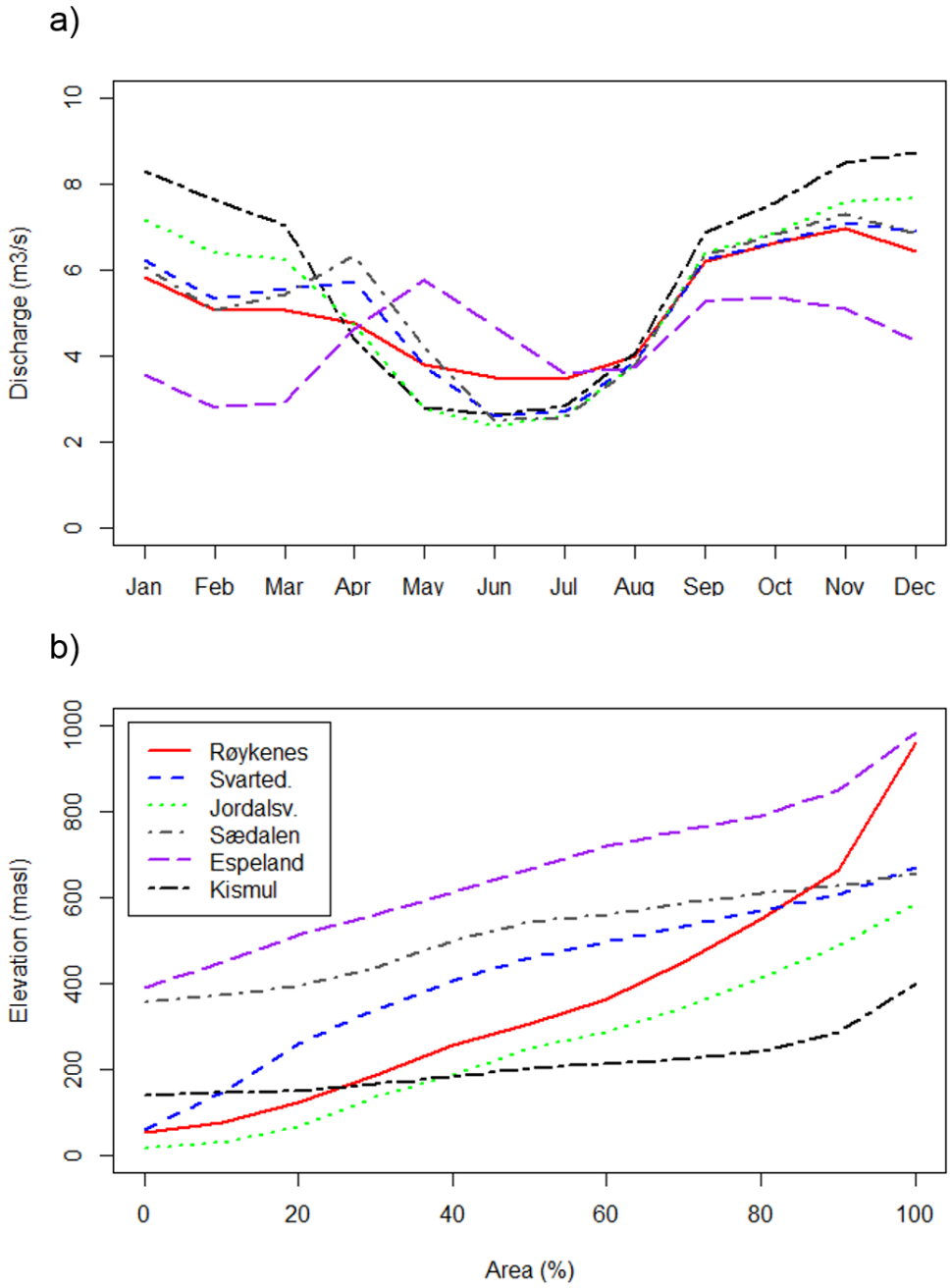

Figure 7.8: Characteristics of Røykenes and BW catchments in terms of a); mean monthly flow regime from individual HBV simulations (1980-2009), and b); hypsographic curves.

obtained in the reservoir storage routing support the usage of the scaling of parameters method, namely the employment of individual HBV models to simulate inflow series for ungauged catchments in Bergen region.

Reservoir	**Period**	**Scaled parameters**		**Traditional scaling**	
		R2	Dev.	R2	Dev
Svartediket	12.06.2007-31.08.2014	0.59	2 %	0.42	3 %
Jordalsvatnet	11.05.2006-31.08.2014	0.59	3 %	0.56	3%
Nedre Gløvrevatn	-	-	-	-	-
Svartavatnet	11.11.2002-09.04.2012	0.65	2 %	0.41	5 %
Ulvvatnet	01.01.2009-31.08.2014	0.32	1 %	0.30	1 %

Table 7.4: Correlation between routing simulated and observed storage, in terms of Nash-Sutcliffe coefficients, calculated for inflow inputs from traditional scaling and transferring of HBV parameters.

7.2 Downscaling

Results from downscaling of three GCM models (CNRM-CM5, MPI-ESM-MR and NorESM1-M) are presented and evaluated in the following section. The GCMs are downscaled for the scenarios RCP2.6, RCP4.5, and RCP8.5. The model skill of the GCMs are evaluated based on their simulation of present climate (Fig. 7.9), the distribution of the outputs (Fig.7.10) and their ability to preserve variance (Fig. 7.11). Since model experiments for predictions start 01-2006, downscaling results are evaluated with respect to the climatology of the normal period 1975-2005. Results from the NorESM1-M model is further utilized in the subsequent modeling of discharge and drought analysis.

7.2.1 Downscaled GCM output

Figure 7.9 presents results from the downscaling of historical temperature and precipitation for the different GCMs. For comparison, the corresponding observations are plotted in the same figures. Both observed and simulated values represent present climate, i.e. values are averaged over the normal period 1975-2005. Although the fit between observed and simulated values is not perfect, the variations seem to follow the same patterns. CNRM-CM5 has the lowest performance according to these plots, while NorESM1-M is the model which best reproduce the historical conditions.

Future emission scenarios for the same GCMs are downscaled and visualized in box-plots (Fig. 7.10), where projected scenarios are presented on a seasonal basis.

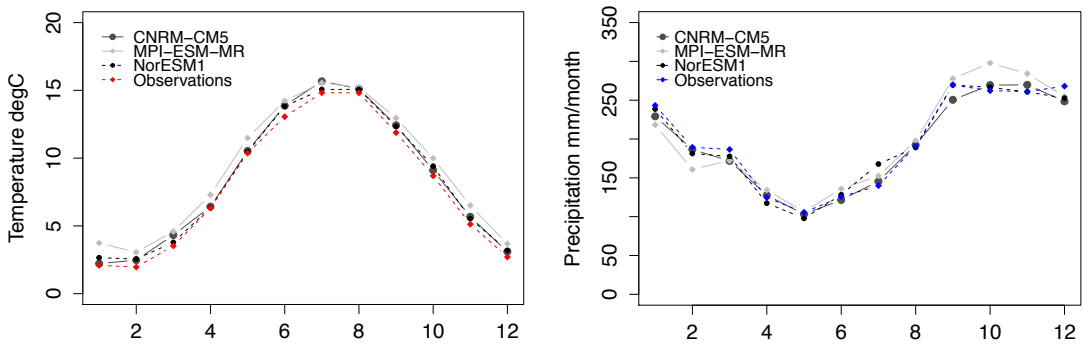

(a) (b)

Figure 7.9: GCM simulated mean monthly temperature (7.9a) and historical monthly precipitation (7.9b) for 1975-2005 compared to observations.

A steady increase of the median over the years can be observed for temperature. There are small differences between winter, spring summer and fall. However, the temperature change is remarkably higher at the end of the century than for the first decades. On average, the different scenarios and GCMs predict a temperature change of 2°C by the end of the 21st century. Downscaled precipitation does not show any clear trends; neither on seasonal or decadal basis. Only slight changes, both positive and negative, can be observed. Common for both temperature and precipitation is the wide spread, and apparently, not very skew data. Presumably, the wide spread data are a result of inconsistency in GCM output for the different models. Thus, the box-plot reveals the distribution of the data, but does not give an idea of which GCM is the most reliable for prediction of future climate conditions. They do however, exemplify how contradictory projections of the future may be and how decisive the choice of GCM model is for further impact analalysis.

Relative standard deviation (RSD) for downscaled precipitation is presented in the upper part of figure 7.11. RSD yields the standard deviation relative to the mean and is calculated for the whole scenario-period (2005-2100) on a monthly basis. For comparison, RSD for historical observations for a time-span of equal length (1910-2005) is plotted in the same figure. RSD of simulated precipitation is consistently lower than observed; evidence of the models' lack of ability to preserve variability of precipitation. Since temperature is not on ratio scale, RSD can not be utilized to evaluate the variety. Instead *standard deviation* (SD) is calculated and presented in the lower part of figure 7.11. SD for temperature yield good correlation between simulated variance and historical variance. These findings indicate a general trend in results of the downscaling. All models tend to conserve variance in temperature, but they are not equally successful for precipitation.

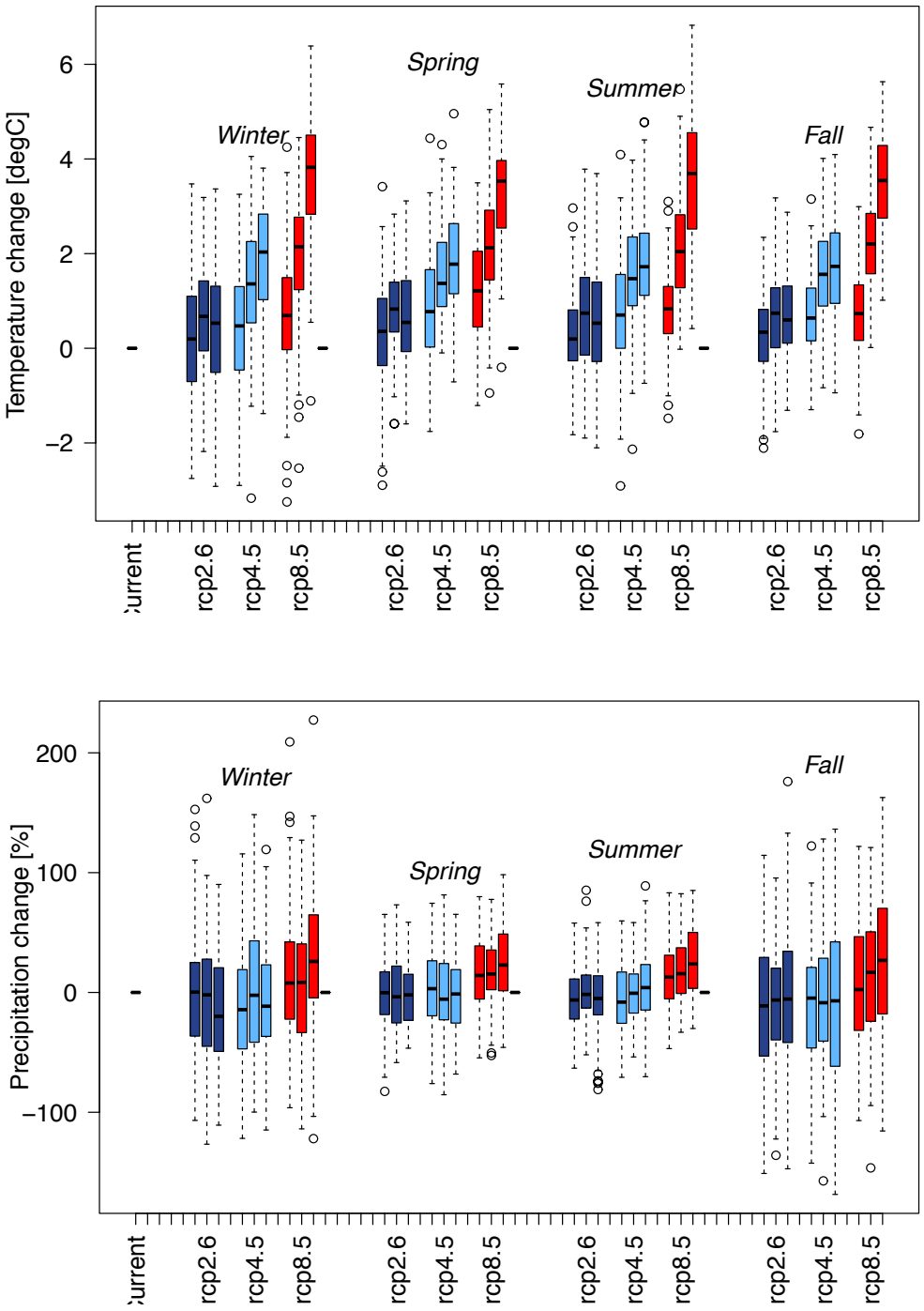

Figure 7.10: Seasonal change in temperature (upper) and precipitation (lower) with respect to 1975 - 2005. For all seasons, three boxes are plotted. They represent the three reference periods 2011-2040, 2041-2070, and 2071-2100. The box and whiskers show IQR and full range, respectively, while the median is represented by the line. Finally, extremes are marked as dots.

This is likely due to the choice of predictor, but it may also be caused from a non-optimized choice of GCM.

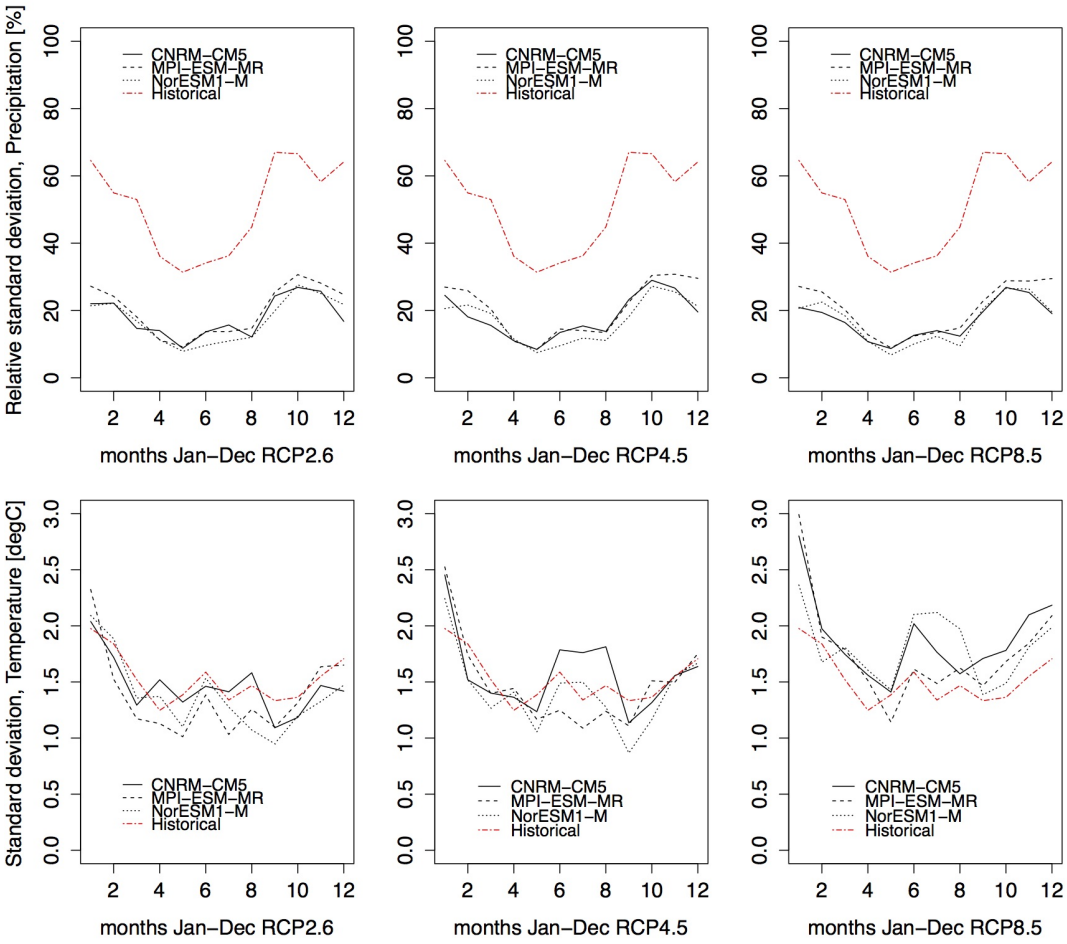

Figure 7.11: Relative standard deviation [%] for precipitation (upper) and standard deviation [degC] for temperature (lower) of GCM simulations 2005-2100; compared to historical observations 1910-2005.

7.2.2 Downscaled NorESM1-M output

Based on the results evaluated in the previous section, the NorESM1-M model is further evaluated. NorESM1-M is the most successful model in simulation of historical temperature and precipitation of the Florida weather station, and is assumed to have some benefits being developed on the basis of the regional model

for Bergen, Bergen Climate Model (Sec. 5.2). Complete time-series of predicted temperature and precipitation anomalies are presented in Appendix D for each of the evaluated RCPs. The anomalies are calculated with respect to 1975-2005 climatology (Tab. 5.3, Cha. 5). Furthermore, monthly delta change factors have been calculated for both variables, temperature and precipitation, each RCP, and each of the projection periods; first-decades (2011-2041), mid-decades (2041-2070), and late-decades (2071-2100). Calculated values are rendered in Appendix D, and visualized in Figure 7.12. As expected, temperature changes reflect a steady increase over each projection period and RCP, while changes in precipitation vary significantly over the years for each RCP, and between projection periods. The major trend for precipitation with RCP2.6, is a decrease in winter and summer-months, while spring will be wetter. For RCP4.5 and RCP8.5 the results are more consistent, both yielding patterns of increased precipitation.

An additional quality control of downscaled precipitation is displayed in Figure 7.13. As discussed in section 5.2.3, GCM simulations for future scenarios starts in 2005, yielding a short time-window to explore the different scenarios' likelihood to match today's climate. The figure illustrates the intricacy of downscaling precipitation. Simulations manage very roughly to catch the major trends for some periods, but fails to reproduce maximums and minimums. The higher the RCP, the more true these observations seem to be. The failing of reproducing maximums and minimums is connected to the inability of conserving variance (fig. 7.11).

7.3 Climate change impacts on water resources

In this section the projected changes that result from hydrological modeling with downscaled climate data for future scenarios are presented. Impacts are first studied for inflow, followed by drought characteristics, as an attempt to describe the possible directions, towards which the hydrological behavior is moving for the different scenarios. Finally, projected changes in water supply capacity are studied.

7.3.1 Projected changes in inflow

Inflow series are generated based on delta changes in temperature, precipitation and evapotranspiration. Figure 7.14 illustrates the seasonal changes induced by each scenario in each projection period for Røykenes, and all BW catchments seen as an entirety. The results show that increases in average annual runoff are moderate, whereas the changes in seasonal runoff are more distinct. For RCP2.6, the major seasonal change is related to spring and summer, resulting in a negative annual change of –5 to –10 %. RCP4.5 replicates slight increases in runoff for autumn and winter, and decreases in spring and summer. Annually, these changes

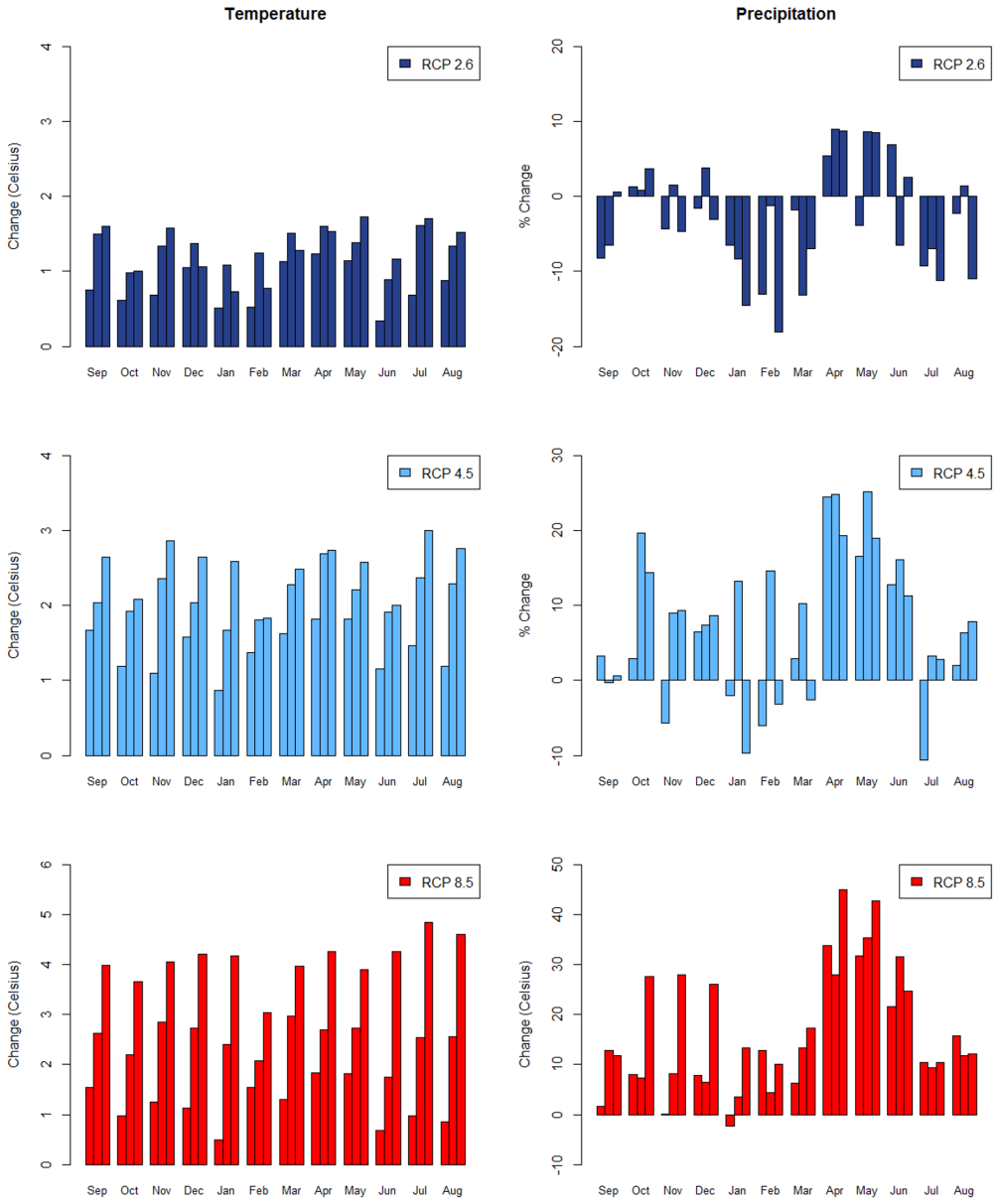

Figure 7.12: Delta change factors for NorESM-M downscaling of temperature and precipitation. There are three columns for each month, representing each of the three periods 2011-2040, 2041-2070, and 2071-2100.

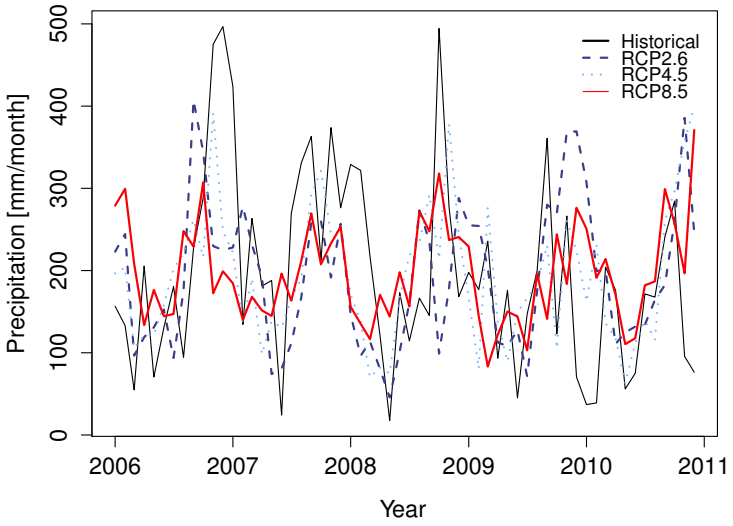

Figure 7.13: NorESM1-M: Ability to reproduce the years 2006-2010 with RCP2.6, RCP4.5 and RCP8.5, compared to historical observations.

practically eliminate each other. Finally, RCP8.5 predict major increases in runoff during autumn and winter, which results in an annual increase of 10-20 %. Changes in inflow to Røykenes and BW show an unmistakably similar pattern, despite for the spring season.

In order to understand the nature of this "summary", Figure 7.15 is included, displaying a more detailed representation of the projection changes taking place at each catchment on a monthly basis. It emerges from the diagrams that catchments situated at similar altitudes tend to have similar response. Higher temperatures during winter will cause alterations in snow conditions, leading to more precipitation occurring as rain and an earlier snow melt. Winter runoff is consequently increased and spring runoff reduced. Catchments that are not affected by snow will experience changes that correlates more to precipitation changes.

7.3.2 Projected changes in drought characteristics

Drought characteristics are retrieved from simulated inflow for control and future scenarios. Consequently, d_{max} (days) and w_{max} (mill. m3) are extracted for summer and winter drought seasons. The computed climate change impact on drought characteristics for each projection period and scenarios are summarized in terms of box-plots in Figure 7.16.

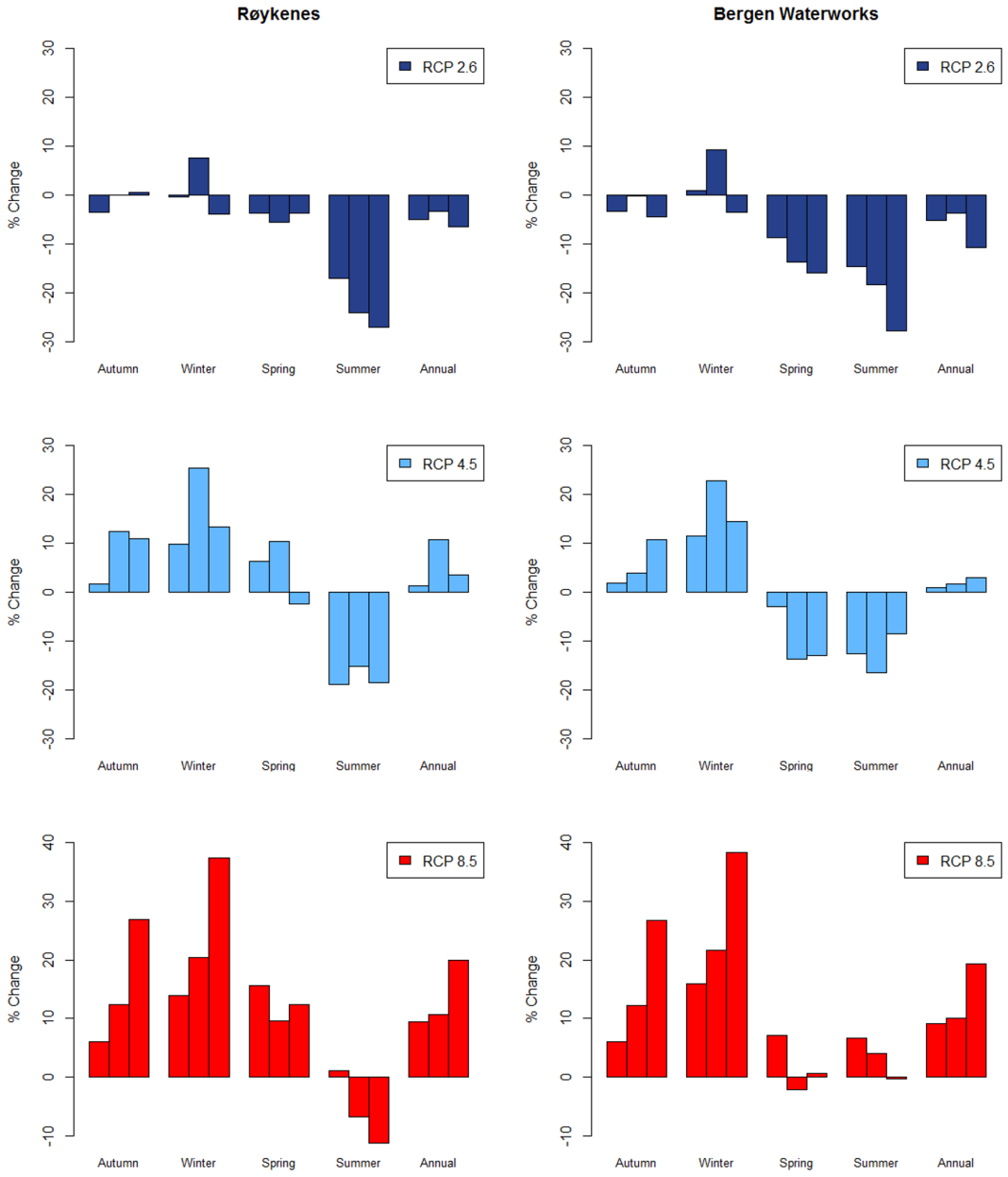

Figure 7.14: Projected changes in seasonal inflow to Røykenes and BW catchments, presented as percentages relative to the control period. The three bars signify the three projection periods: 2011-2040, 2041-2070, 2071-2100.

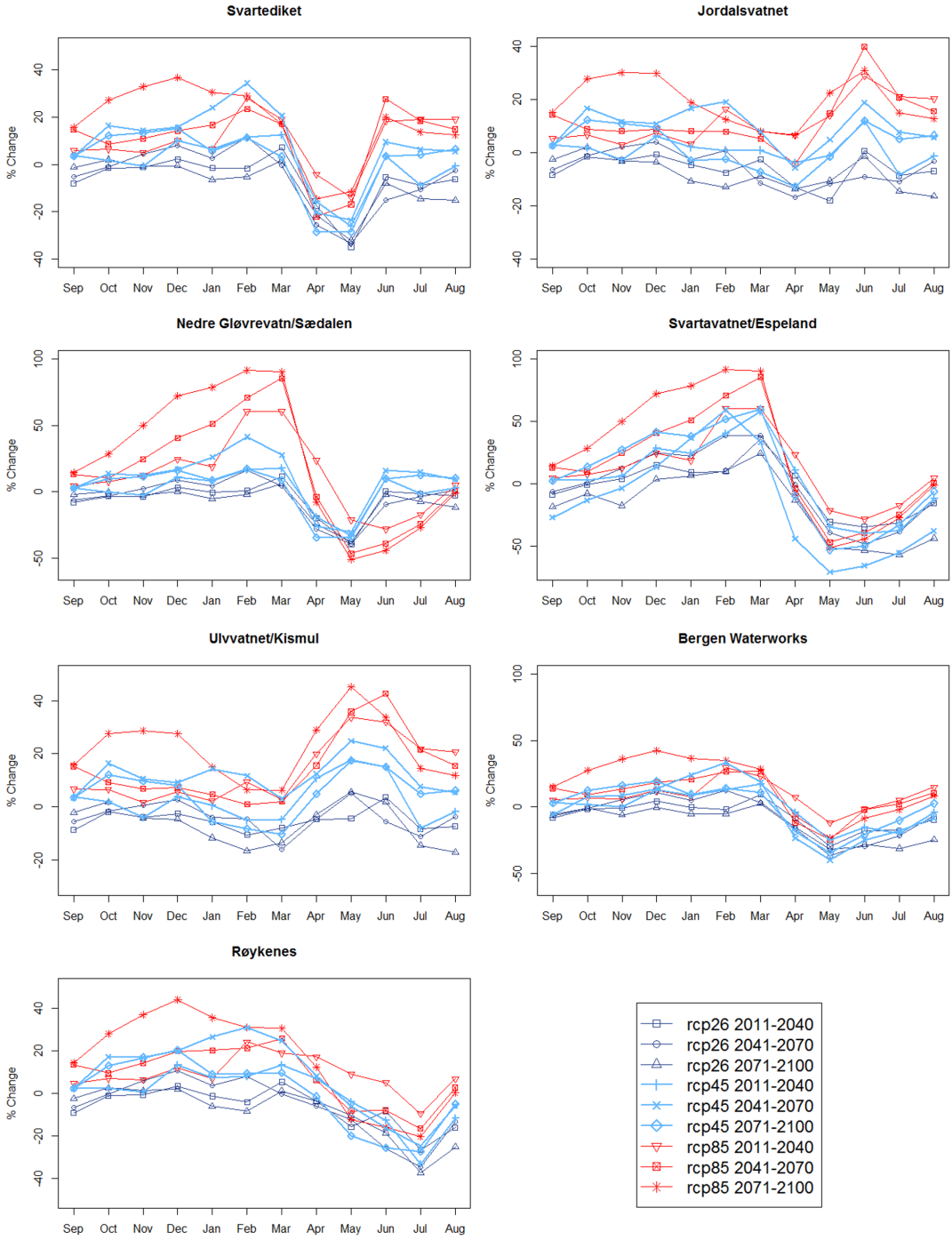

Figure 7.15: Mean monthly inflow changes in percentage for all catchments, on the basis of downscaled climate data for projection periods 2011-2040, 2041-2070, and 2071-2100, with scenarios RCP2.6, RCP4.5 and RCP8.5.

Accordingly, winter droughts are expected to maintain the average duration for all scenarios, however with a decreasing trend in deficit volume. The changes are most significant for the extreme values, where both durations and deficit volumes are expected to decrease for all scenarios, except RCP2.6. This scenario implies decrease in precipitation for winter months, resulting in drought extremes similar to the control period.

Projected summer drought characteristics resemble a clear ascending trend for both averages and extremes. The full range exceeds the most for RCP2.6 from the mid-decades. This can be explained by the reduction in precipitation during summer and autumn. Comparably, RCP4.5 and RCP8.5 indicate higher extremes for all projection periods. More precipitation can to some extent compensate for the increased evapotranspiration related to these scenarios. However, natural climatic variability can cause serious stress in water availability.

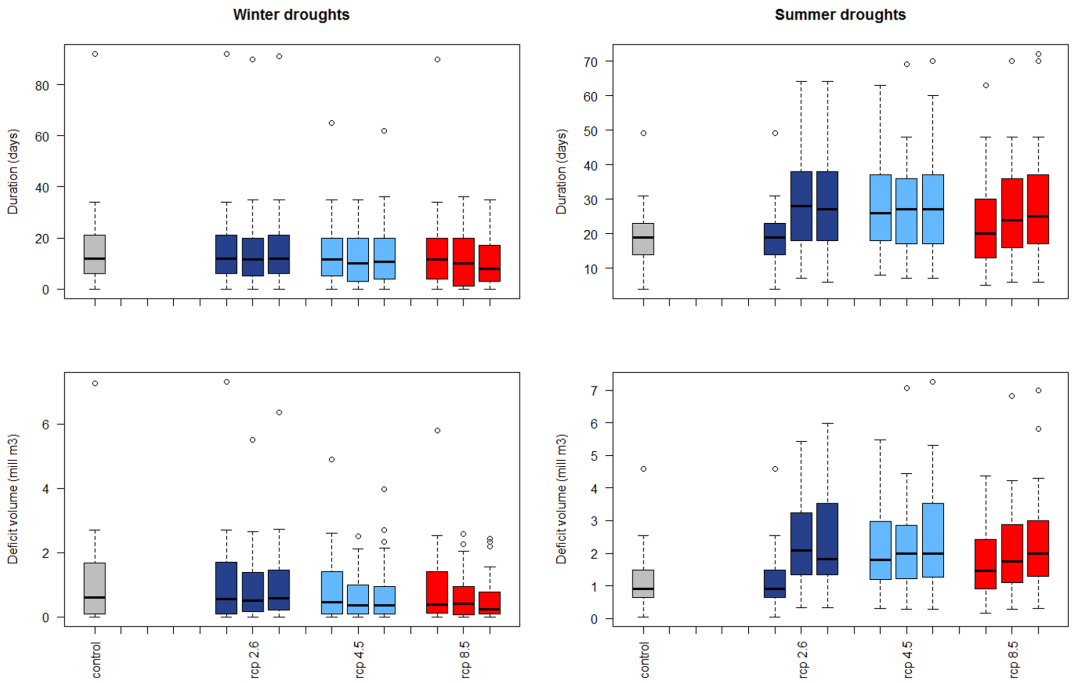

Figure 7.16: Projected change in drought characteristics for summer and winter seasons respectively. The box and whiskers show IQR and full range, respectively, while the median is represented by the line. Finally, extremes are marked as dots.

7.3.3 Projected changes in drinking water demand

Population growth in Bergen is projected by combining the two models of SSB, BEFINN (national) and BEFREG (regional) in accordance with the method explained in Chapter 4. Estimations of population growth is presented in Figure 7.17.

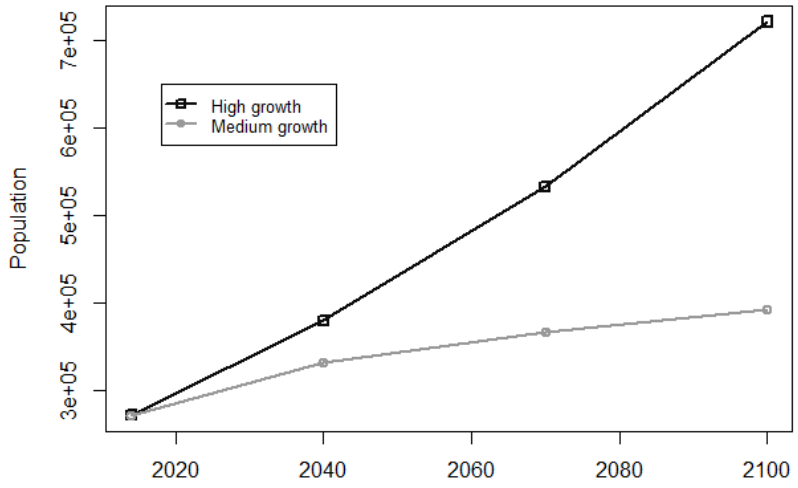

Figure 7.17: Estimated projections of population in 2040, 2070 and 2100 for Bergen municipality based on national and regional projections [SSB, 2014].

7.3.4 Projected changes in supply capacity

A one-reservoir simulation model is constructed to evaluate the climate change impacts on the supply capacity. Consequently, the maximum discharge that can be withdrawn from the system without any incidents of storage falling below the limit (50 days) is determined. In addition, the model takes into account the required minimum flow at Espeland. The minimum reserve volume is computed as 5.5 mill. m^3, and remains constant for all projection periods.

The relation between projected maximum supply capacity and projected demand is pictured in Figure 7.18. Evidently, climate change impact on water supply is negative for all scenarios. Note that the gradient between the periods is varying. The largest decline in maximum capacity is linked to RCP2.6, closely followed by RCP4.5, before 2100.

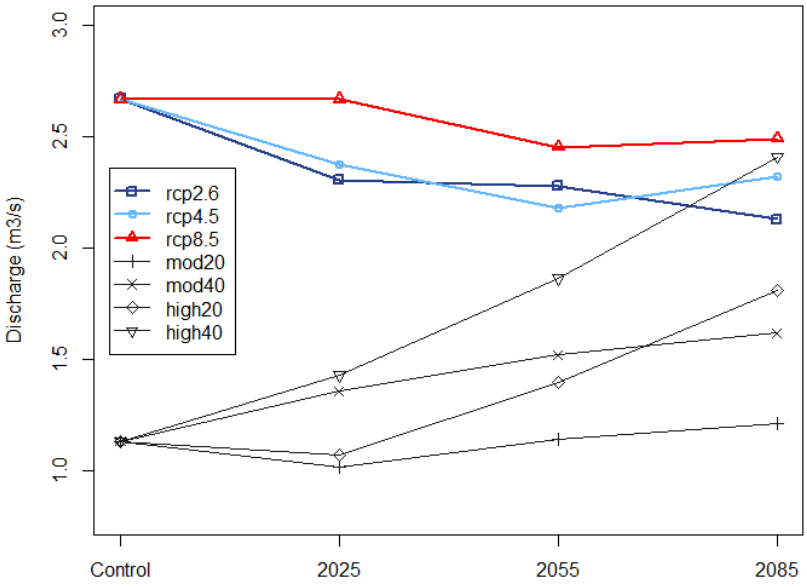

Figure 7.18: Projected changes in maximum supply capacity at BW for emissions scenarios RCP2.6, RCP4.5 and RCP8.5 and projected demand based induced by scenarios of moderate and high population growth and 20% and 40 % leakage in the system. The projection stages are depicted in terms of the middle year in each period, corresponding to 2025, 2055 and 2085.

Drinking water demand has a corresponding opposite behavior, though at a higher rate than the maximum capacity. The only demand scenario threatening the supply capacity throughout the period in study, is HIGH40, which crosses both RCP2.6 and RCP4.5 during the transition 2055-2085. As illustrated in Figure 7.18, MOD40 approaches 2025 with 50 % higher demand than HIGH20. This stresses that in the short run, leakage percentage contributes more to the demand than population growth. After 2025, population growth is more influential than the leakage percentage.

Chapter 8

Conclusion and discussion

8.1 Discussion

The results obtained in this thesis involve many uncertainties that need to be accounted for when evaluated. Hereunder, we discuss the major uncertainties related to our results, and the methods utilized in the chosen research approach.

Reservoir inflow analysis The calculation of inflow series to Svartediket based on measured water balance components was conducted and designated semi-successful. The calculated inflow series were validated through comparison with a scaled runoff series from Røykenes, and an obtained value of the Nash-Sutcliffe model criterion of 0.577. Nevertheless, an unresolved issue with the water level component of the balance led to the rejection of this approach for further analysis.

Calculations revealed that the model performance tends to be poor in times of recession. It may look like the catchment is behaving differently to rising runoff than to falling runoff. According to O'Kane and Flynn [2007], residual errors in hydrological prediction frequently show high serial correlation, especially during periods of flow recession between storms. This behavior indicates presence of non-local memory in the model, and is sometimes regarded as evidence of hysteresis.

The hysteresis effect underpins the fact that the relation between stage and runoff is not a one-to-one mapping. It suggests a dependency between the runoff at one instant of time and the runoff in a past stage. In catchment-scale hydrology this may be explained by the fact that a rising flood receives less hindrance in propagation than in a falling flood [Bhattacharya and Solomatine, 2005]. This effect is not embedded in the reservoir balance, thus the calculations fail in times of recession because the calculations at one time step does not "know" if the flow is increasing or decreasing.

The hysteresis effect is discussed as a theoretical explanation of the observed

behaviour of the results, but it does not yield compelling evidence or an unambiguous conclusion of the error genesis. VA-etaten has been involved in investigating the equipment and gathering information from the equipment supplier, but no physical cause to the errors have been found. VA-etaten is planning a new arrangement for the measuring of water level in Svartediket, which hopefully will provide more accurate measurements in future studies.

Nevertheless, for the purpose of the modeling in this study, transferred inflow series to Røykenes has been utilized in further analysis. The inflow series is compared directly to Hauskåselva observations, and indirectly to measurements made in Svartediket. The observations in Haukåselva and Svartediket are completely different systems, and independent of each other. Thus, comparisons where Røykenes shows good correspondence to both of the other catchments, is strong evidence of Røykenes' ability to reflect other catchments in the region.

Hydrological modeling The obtained R^2 at 0.801 for 30 years of data, is considered a remarkable conformity for runoff simulation. Arguably, a sensitivity analysis would have complemented the results, through quantifying parameter instability an non-uniqueness, as recommended by Wilby [2005]. Such analyses are not completed herein. However, comprehensive trial and error sequences of manual and automatic calibration were entailed to reach the result, and even if not systematically, the procedure endeavoured towards improved parameter combinations.

Kismul catchment is constructed by several minor catchments patched together to represent the watershed of the main reservoir, Ulvvatnet. This simplified coarse procedure can lead to wrongful representation of the catchment, and further incorrect simulations of inflow. From the reservoir routing procedure it is difficult to verify the assumption made for the catchment representation, due to the low correlation coefficients for transferring methods. Whether it can be explained by erroneous data records, or faults in the assumptions is difficult to conclude. Consequently, the inflow to the catchment should be treated with caution.

It was found, when comparing the inflows with the two different transfer methods, that the average inflow to Røykenes is remarkably similar to the average of the inflows to BW catchments. This discovery may question the benefits of using transfer of calibrated parameters, when the aim was to retrieve the impact on the system as a whole. However, it has been valuable to be able to convey the flow regime at catchment scale, and to understand the hydrological impacts of climate change at catchments of different characteristics.

The uncertainty from the hydrological modeling is considered small relative to the uncertainty due to the projected meteorological data from the climate model [Arnell, 2004; Wilby, 2005]. The first assumption is that the same set of parameters

is valid for both present and future climate. Hence, it is necessary to similarly assume that characteristics within the watersheds remain unchanged in the future. The other important assumption for the hydrological model is the presence of identical model errors during both time periods (control and scenario period). There is no guarantee that the same relation between observed and simulated inflow is always present. However, this assumption is decisive for interpreting the difference in the modeled climate as believable estimates of change in climate.

Drought analysis The threshold level to be chosen in drought analysis, depends on the hydrological regime in question. The choice fell on Q70 for historical climate drought analysis, and Q80 for the climate impact study. Røykenes is a fairly large catchment, therefore the difference between Q70, Q80 and Q90 is quite small. Nevertheless, the choice of truncation level is found to have profound interference on the yielded d_{max} and w_{max}. For example, Q80 retrieved for the period (1934-2013) is too low to capture the whole drought event of 2010, splitting the 93 day period into two drought periods of 43 and 31 days, separated by a gap of 7 days. However, it is clear that this short rise in inflow was insufficient to call off the drought. Since the events are already pooled with the MA-method, it was found unreasonable to merge the events. In comparison, Q80 for the HBV-simulated inflow (1980-2009) and Q70 for observed inflow (1934-2013) hold to include the period of a total 92 days. This relation confirms the flow regime change that have taken place during the preceding 80 years, where the 80^{th} percentile flow have become larger.

When the whole year is divided into two seasons, this also allows for analyzing incidents of winter droughts continuing into summer droughts, or vice-versa, as discussed by Hisdal et al. [2001] and Van Loon et al. [2010]. This, however, is not studied here. Since expected temperature increases in the winter months will hinder precipitation of being stored as snow, climate change is likely to gradually eliminate occurrences of winter droughts in the future. In future drought studies winter droughts may be given the same nature as summer droughts, which allows for extending the season to represent the whole year. Inevitably, climate change is likely to cause summer season to consume parts, if not all, of the winter season. In this study the seasons are kept fixed to allow for temporal comparison in drought characteristics, and at the same time avoid the risk of a false conclusion that increased summer droughts are a result of a longer summer season, as was discussed by Wong et al. [2011].

Downscaling Downscaling of temperature is considered successful. Historical conditions are satisfactorily reconstructed, variation preserved and the three selected GCMs yield consistent results. Additionally, the downscaled temperature

corresponds to the generally accepted prediction of a warmer climate. Precipitation varies more than temperature on a local-scale, and is generally considered more difficult to downscale. A predictor with a strong physical relation to the predictor, such as large and local-scale temperature, is not as easy to obtain. In this thesis we have made an attempt on keeping a physically inspired downscaling model by choosing large-scale precipitation as the predictor. Despite the uncertainties, historical reconstruction of 1975-2005 climatology was executed, and results are considered reasonable for all GCMs. Projections for the future, however, reveal an inability to conserve variance within the variable. In terms of preserving variance, a different statistical approach, such as the analog method discussed in Chapter 3.1.6, may be better suited for downscaling of precipitation [Imbert, 2003]. Nevertheless, the statistical method's inability to preserve variance is the main reason for continuing the delta-change approach, as the historical records, to which the change factors are applied, account for variation at the local station in question.

Another challenge with the precipitation downscaling was inconsistency in downscaled variables of the different GCMs. The NorESM1-M model was selected for further analysis because it was superior to the others in reconstructing historical climatology, and because of the model's connection to the Bergen region. However, the skillfulness is determined comparing only three GCMs, while state-of-the-art practice is to compare a greater amount of models. Although it would require additional and more comprehensive data acquisition and processing, further analysis where more models are included would be of great significance for the reliability of the results. Undoubtedly, it would secure a stronger basis for model selection, and offer additional support in model acceptance or rejection.

Downscaling is essentially about finding a link between the large-scale predictor and the local-scale predictand, and historical records are utilized for finding the relationship between the two. Furthermore, we assume that the link we find during historical conditions, yields for future scenarios. Nevertheless, we do not have an assurance for this stationarity. We are not able to predict all impacts of climate change, or if those impacts could cause alterations in either atmosphere, geosphere, biosphere or hydrosphere, such that the assumed relationship is disturbed.

8.2 Conclusion

Based on hydrological modeling and a storage routing simulation with outputs from NOR-ESM1-M, we have quantified the effects of climate change on a water works situated in Bergen. Indicated results involve changes in the seasonal distribution of inflow, with increases in winter and autumn, and decreases in spring and summer. The forcings are seasonal changes in precipitation and temperature

increases, leading to major alterations in snow conditions and increased evapotranspiration. The most important finding is that the higher-emissions scenario, RCP8.5, provides the least impact on the water supply capacity, while the lower-emissions-scenario, RCP2.6, provides the greatest.

We have successfully devised a sequence of procedures constituting a model for predicting future water supply capacity. With regards to previous discussion, we are confident that the major uncertainties of the approach are uncovered, and that the model results may be beneficial and valuable to VA-etaten, and other stakeholders in Bergen.

Answers to research questions

RQ1 Is it feasible to conduct a hydrological assessment incorporating climate change impacts for VA-etaten?

As concluded above, a system of modeling procedures for climate change impact studies has been devised and tested, it is thus feasible to conduct such a system. However, the work in this thesis has revealed that hydrological modeling based on data records from BW is not currently possible, due to insufficient length of record series, and unidentified errors in the measurements. Hydrological assessment has therefore been based on transferred inflow series from Røykenes. The chosen approach is well-documented and justified in this thesis, although on-site measurements from the catchment being modeled would be beneficial.

RQ2 What are the expected impacts of climatic change on runoff and drought in Bergen, with respect to historical inflow pattern and drought incidents, such as the one in 2010?

The results obtained show that Bergen region will experience higher inflow during winter and autumn and lower inflow during spring and summer. Given the "business as usual"-scenarios, the severity in winter drought extremes will be more than halved, and given the best case-scenario it will remain as today. Either development in emissions will cause a clear increase in summer drought extremes by 30 to 50 % in duration and 30 to 60 % in deficit volume.

RQ3 Is there sufficient supply capacity to account for climate change, population growth, and altered leakage conditions in the supply network?

Comparing projected supply with projected demand estimations substantiate that BW has sufficient supply capacity, provided a leakage reduction to less than 40 %, by no later than 2070. If leakage is reduced to 20 %, then, whatever the population growth rate, water availability is considered adequate for the citizens of Bergen within the time frame of our analyses.

RQ4 Which precautionary measures can be made to withstand significant impacts on water resources, and ensure reliable drinking water supply?

VA-etaten can influence the impacts on the supply capacity by reducing leakage. Leakage reduction is found to be the main contributor to drinking water demand, above population growth, until 2070. Therefore, we utterly support VA-etaten's Master Plan aim at detecting and reducing leakages to 20 % within 2040.

8.3 Further work

This thesis has been conducted with the awareness of the BINGO project's commencement summer 2015. We have thus aimed to convey a work that is easily adaptable, and valuable for ensuring a quick ramp-up of the ensuing project. With regards to this, and the research questions answered in the previous section, we suggest the following venues for further work:

- In reply to the first question, lack of reliable measurements in BW reservoir is considered a drawback for hydrological modeling. We recommend VA-etaten to benefit from the completed hydrological assessment of this thesis, and until proper data is at hand, we suggest the water utility to use the HBV-model in its current form, with Røykenes as reference catchment. On the longer term, we encourage VA-etaten to improve their routines of data recording and quality control, such that data series from internal catchments may be used to verify the model and allow for further improvement.

- Although the aspired model is considered successfully devised, implementation of an additional step for a more methodical evaluation of GCMs is recommended. Being able to thoroughly investigate GCM performance in comparison to each other, will reduce pronounced uncertainty in the downscaling step.

- The quantitative answers to research question two and three are answered with results from thesis-specific analyses. In order to follow and predict, water availability for other time-spans and scenarios than those evaluated herein, extension of the model to function as operative, with updating and forecasting possibilities, would be of considerable value.

- In answer to the fourth question of this thesis, we have argued that leakage reduction is the major precautionary act for minimizing impacts of reduced water availability. We have established a one-reservoir model for transferring projected inflow patterns for the future, into quantitative effects on the maximum capacity and the water resource availability in Bergen. No

consideration of distributed tapping for the individual catchments has been undertaken. This is a possible improvement of the analysis that ought to be regarded in further research, in order to investigate if other factors, such as strategic operation of the reservoirs, could influence the resulting impact of occasional dry spells.

Appendix A

Evapotranspiration

Actual evapotranspiration is calculated within the HBV-model as a function of soil moisture deficit from estimates of potential evapotranspiration (PET) [Killingtveit and Sælthun, 1995]. PET is a semi-confined parameter, and may thus be determined on the basis of experience and knowledge about the catchment area.

Methods for calculating PET range from single-variable (temperature) such as the one introduced by Thornthwaite [1948], to more data-demanding (temperature, humidity, radiation and wind speed) approaches, like the Penman-Monteith PET [Monteith, 1981]. Several studies on climate change impacts have favoured the simpler model, due to its independence to other variables than temperature [Chernet et al., 2013; Kay and Davies, 2008]. The Thornthwaite approach will be used in this thesis, since it allows for easy derivation of PET for future situation based on downscaled temperature data. Equation A.1 renders how PET is calculated in this approach:

$$PET = 16\left(10\frac{t}{I}\right)^{a} \tag{A.1}$$

In this equation, t represent monthly average temperature, while I is a heat index, given by the sum of 12 monthly indexes.

$$I = \sum_{j=1}^{12} i_j \tag{A.2}$$

Where

$$i = \left(\frac{t}{5}\right)^{1.514} \tag{A.3}$$

Finally, the exponential, a, is derived from I by the following formula:

$$a = 6.75 \cdot 10^{-7} I^3 - 7.71 \cdot 10^{-5} I^2 + 1.79 \cdot 10^{-2} I + 0.49 \tag{A.4}$$

Appendix B

Generalized Extreme Value Distribution

The statistical distribution chosen for the frequency analysis of extreme drought events is the Generalized Extreme Value Distribution (GEV). Hereunder, a detailed description of the procedure is explained, in coherence with Taylor et al. [2012]. The cumulative distribution function of the GEV is defined as:

$$G(z;\theta) = \exp\left\{-\left[1+\xi\left(\frac{z-\mu}{\sigma}\right)\right]^{\frac{-1}{\xi}}\right\}, \tag{B.1}$$

where z denotes the data measure of interest, in this case the annual maximum drought duration or deficit volume. Further, $\theta = [\mu, \sigma, \xi]$ and $[1+\xi(\frac{z-\mu}{\sigma})] \geq 0]$. The location parameter, μ, is the value of which the distribution is centered. Further, the scale parameter, $\sigma > 0$ is the spread of the distribution, and the shape parameter ξ indicates the behavior of the distribution's upper tail [Coles et al., 2001]. The value of the shape parameter leads to three types of tail behaviors; exponential decrease ($\xi = 0$), polynomial decrease ($\xi > 0$) and a finite value of the tail $z = \mu - \frac{\sigma}{\xi}$ ($\xi < 0$), also known as the Gumbel, Fréchet and Weibull. Parameters are estimated using the Maximum Log-Likelihood Estimation (MLE). The Log-likelihood (llh) equation is defined as:

$$llh(\theta) = \sum_{i=1}^{N} log\ g(z_i;\theta) \tag{B.2}$$

For evaluation of goodness of fit, the probabilistic quantiles of the GEV are analyzed. Quantiles, $z_{(1-p)}$ are obtained by inverting Equation B.1:

$$z_(1-p) = \begin{cases} \mu - \frac{\sigma}{\xi}[1-(-log\ (1-p))^{-\xi}], & \text{for } \xi \neq 0, \\ \mu - \sigma log(-log\ (1-p)), & \text{for } \xi \neq 0, \end{cases} \tag{B.3}$$

with $0 < p < 1$. Namely, the probability of exceeding $z_{(1-p)}$ is $p = 1$. As a consequence, $z_{(1-p)}$ corresponds to the return level, which is expected to be exceeded on average once every $1/p$ years.

Appendix C

GEV model fit

This appendix gives the obtained fit for the GEV modeling of droughts included in this thesis. The procedure is conducted in R, with the functions offered by the package, 'fExtremes'. Figure C.1 to C.4 give the summary plots provided by R, and Table C.1, the estimated parameters for BM of duration (d_{max}) and deficit volume (w_{max}) for summer and winter respectively.

Parameters	**Winter**		**Summer**	
	d_{max} (days)	w_{max} (mill. m3)	d_{max} (days)	w_{max} (mill. m3)
xi	0.187	0.279	0.101	0.138
mu	16.06	0.950	20.45	1.772
beta	11.80	0.791	10.37	1.108

Table C.1: GEV parameter estimation from MLE in fExtremes.

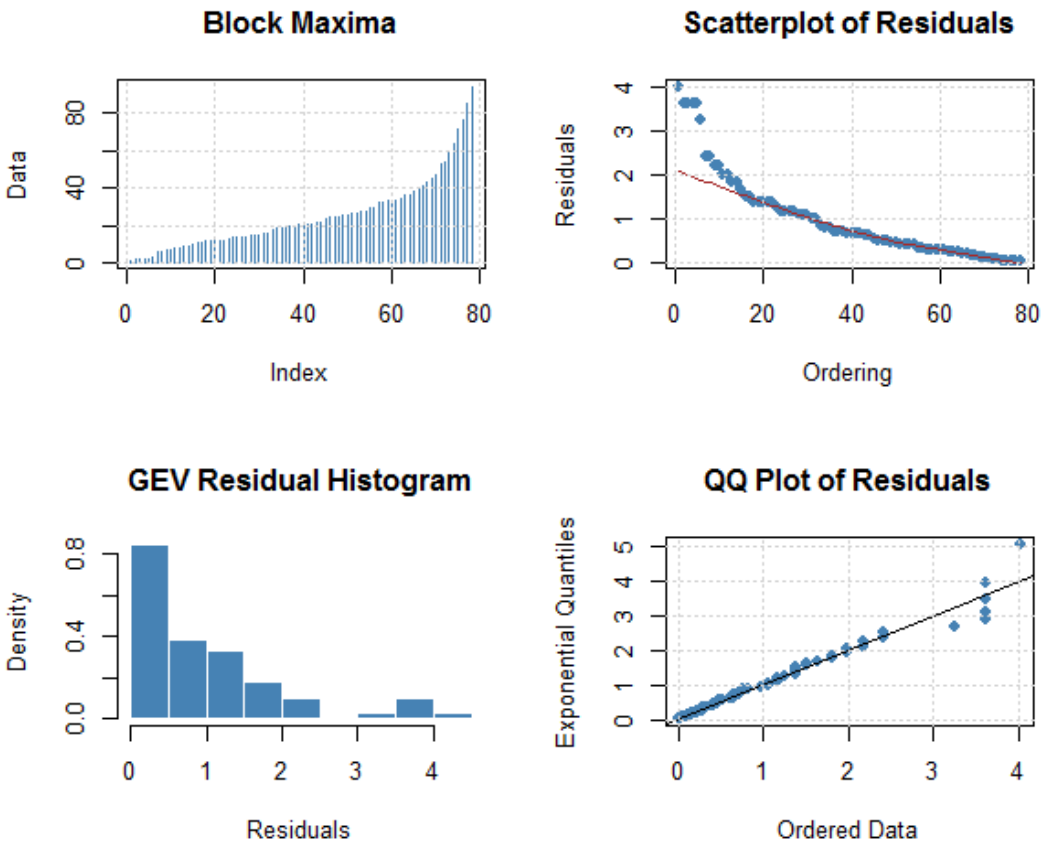

Figure C.1: Summary of GEV fit for winter drought duration provided from fExtremes.

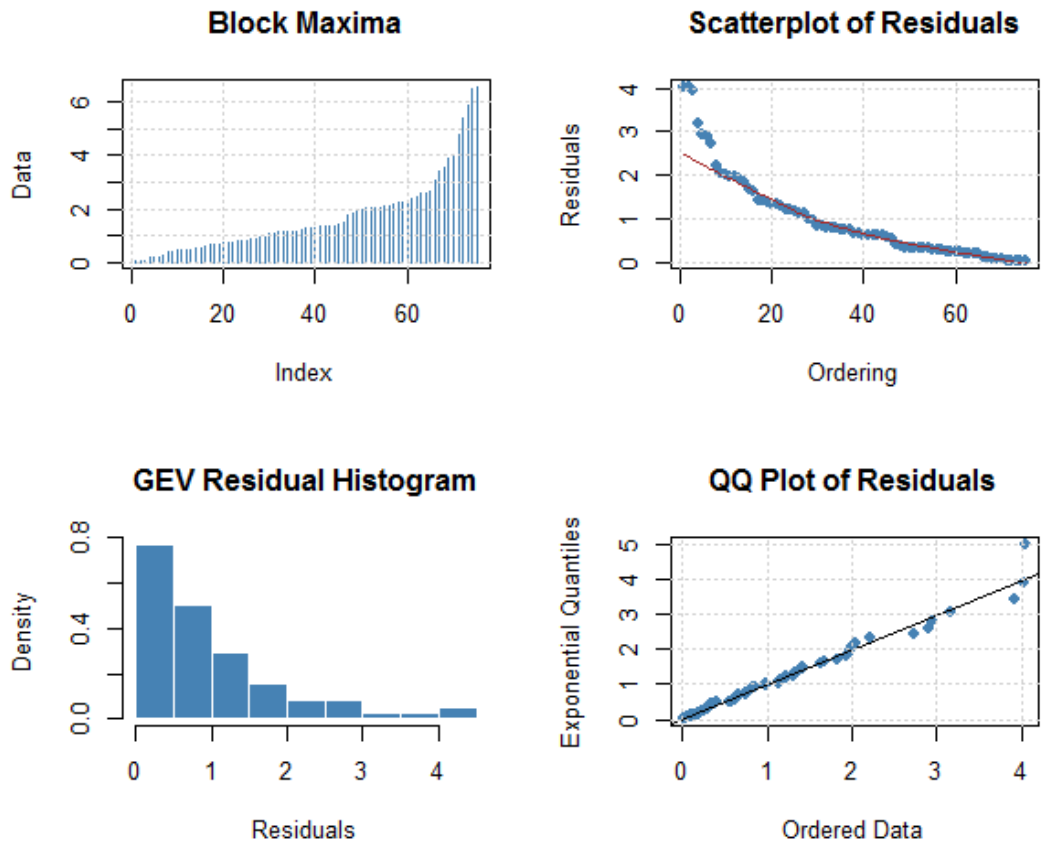

Figure C.2: Summary of GEV fit for winter drought deficit volume provided from fExtremes.

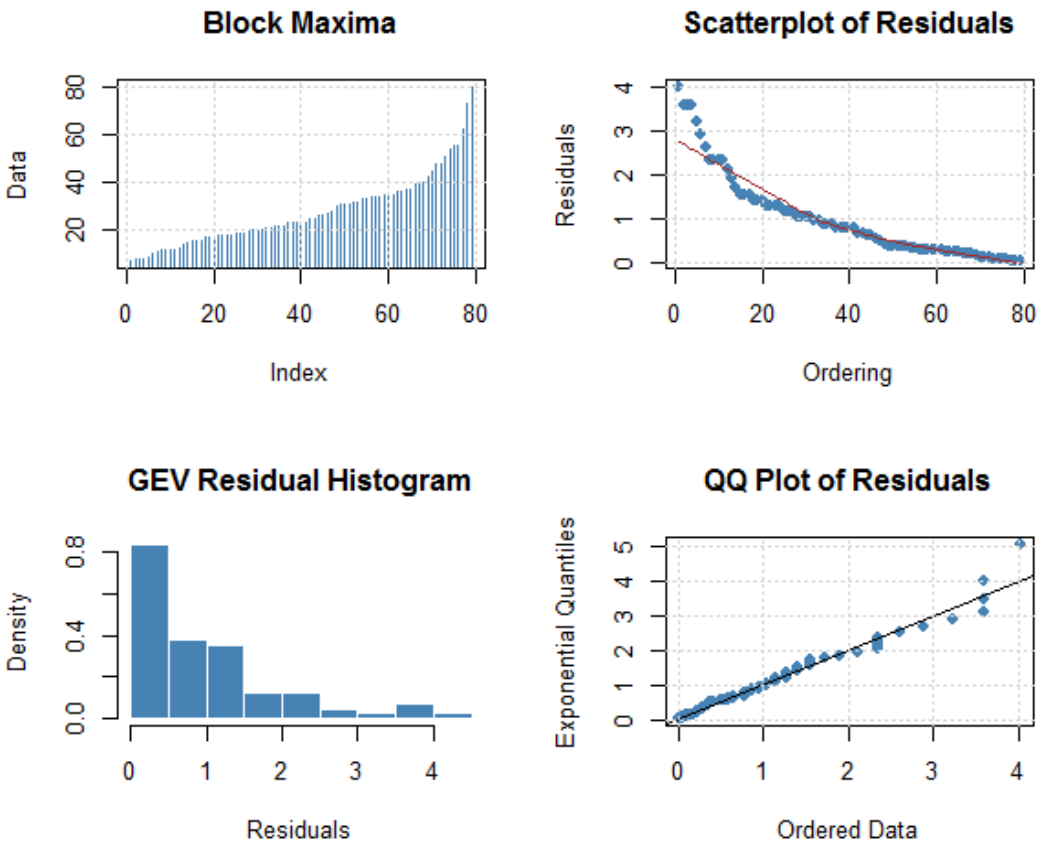

Figure C.3: Summary of GEV fit for summer drought duration provided from fExtremes.

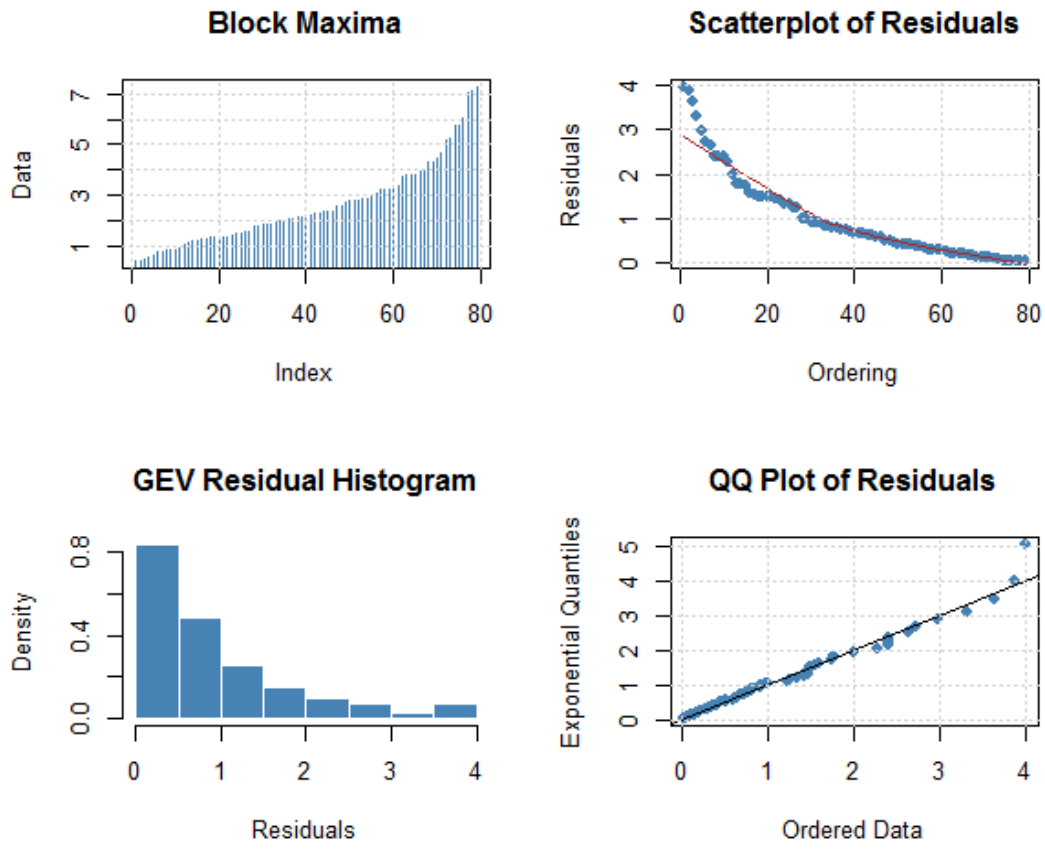

Figure C.4: Summary of GEV fit for summer drought deficit volume provided from fExtremes.

Appendix D

Results from downscaling

Sc.	Jan	Feb	Mar	Apr	May	Jun	Jul	Aug	Sep	Oct	Nov	Dec	
2011-2040 (RCP2.6)		-6.5	-13	-1.7	5.5	-3.9	7.0	-9.3	-2.2	-8.2	1.3	-4.3	-1.6
2041-2070 (RCP2.6)		-8.3	-1.2	-13.2	9.0	8.6	-6.4	-6.9	1.4	-6.5	0.8	1.5	3.8
2071-2100 (RCP2.6)		-14.5	-18.1	-7.0	8.8	8.5	2.5	-11.3	-11.0	0.6	3.7	-4.6	-3.1
2011-2040 (RCP4.5)		-2.0	-6.0	3.0	24.5	16.6	12.8	-10.6	2.0	3.3	2.9	-5.7	6.4
2041-2070 (RCP4.5)		13.2	14.6	10.3	24.9	25.2	16.1	3.3	6.4	-0.3	19.7	9.0	7.4
2071-2100 (RCP4.5)		-9.7	-3.2	-2.6	19.4	19.0	11.3	2.9	7.9	0.7	14.4	9.4	8.7
2011-2040 (RCP8.5)		-2.3	12.8	6.3	33.9	31.8	21.5	10.4	15.7	1.6	8.1	0.1	7.9
2041-2070 (RCP8.5)		3.5	4.3	13.3	28.0	35.4	31.6	9.3	11.9	12.8	7.4	8.1	6.4
2071-2100 (RCP8.5)		13.4	10.1	17.3	45.1	42.8	24.6	10.4	12.1	11.9	27.7	28.0	26.0

Table D.1: Monthly change in precipitation [%] averaged over the three reference periods; 2011-2041, 2041-2070, 2071-2100; for RCP2.6, RCP4.5, and RCP8.5

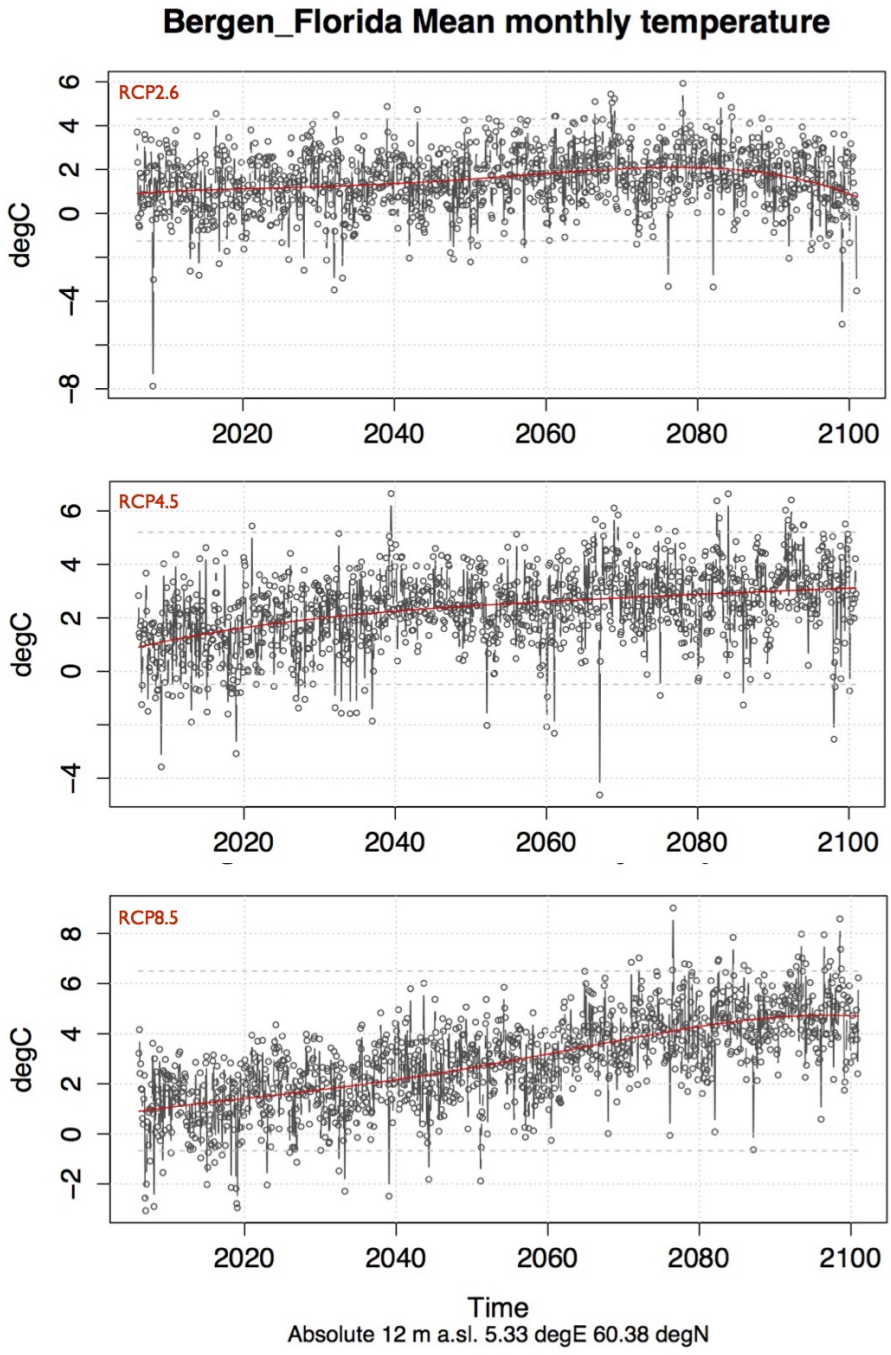

Figure D.1: Downscaled temperature anomalies with respect to 1975-2005, for RCP2.6, RCP4.5 and RCP8.5, and 5th order polynomial trend line (red line).

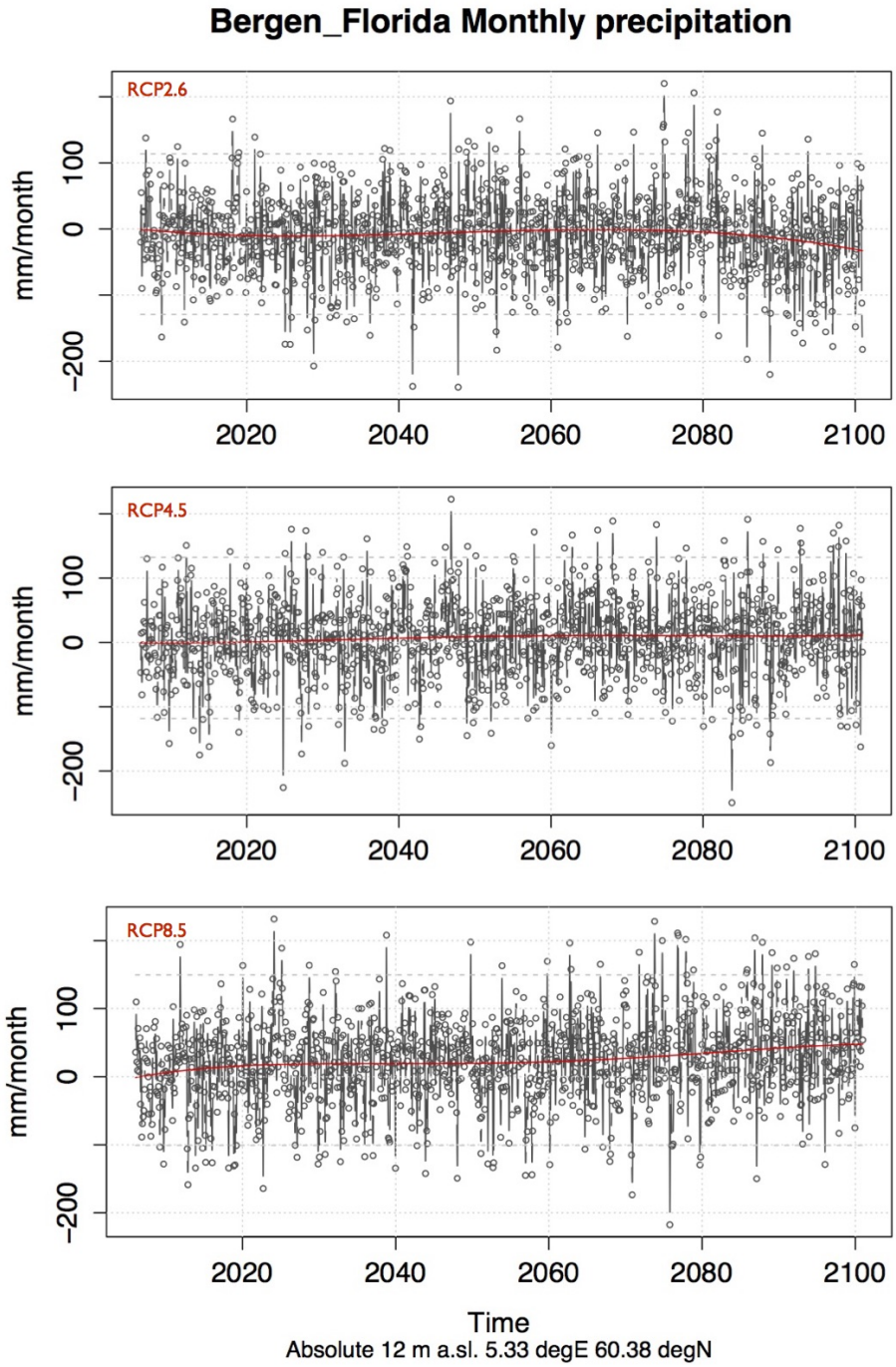

Figure D.2: Downscaled precipitation anomalies with respect to 1975-2005, for RCP2.6, RCP4.5 and RCP8.5, and 5th order Polynomial trend line (red line).

Sc.	Jan	Feb	Mar	Apr	May	Jun	Jul	Aug	Sep	Oct	Nov	Dec
2011-2040 (RCP2.6)	0.5	0.5	1.1	1.2	1.1	0.3	0.7	0.9	0.8	0.6	0.7	1.1
2041-2070 (RCP2.6)	1.1	1.3	1.5	1.6	1.4	0.9	1.6	1.3	1.5	1.0	1.3	1.4
2071-2100 (RCP2.6)	0.7	0.8	1.3	1.5	1.7	1.2	1.7	1.5	1.6	1.0	1.6	1.1
2011-2040 (RCP4.5)	0.9	1.4	1.6	1.8	1.8	1.2	1.5	1.2	1.7	1.2	1.1	1.6
2041-2070 (RCP4.5)	1.7	1.8	2.3	2.7	2.2	1.9	2.4	2.3	2.0	1.9	2.4	2.0
2071-2100 (RCP4.5)	2.6	1.8	2.5	2.7	2.6	2.0	3.0	2.8	2.7	2.1	2.9	2.6
2011-2040 (RCP8.5)	0.5	1.5	1.3	1.8	1.8	0.7	1.0	0.9	1.5	1.0	1.3	1.1
2041-2070 (RCP8.5)	2.4	2.1	3.0	2.7	2.7	1.7	2.5	2.6	2.6	2.2	2.8	2.7
2071-2100 (RCP8.5)	4.2	3.0	4.0	4.3	3.9	4.3	4.8	4.6	4.0	3.7	4.1	4.2

Table D.2: Monthly change in temperature [^{o}C] averaged over the three reference periods; 2011-2041, 2041-2070, 2071-2100; for RCP2.6, RCP4.5, and RCP8.5

Appendix E

ESD procedure

In the following appendix we wish to elaborate the procedure for ESD, based on our experiences as beginners to downscaling techniques and the software utilized to employ them, R. Our aim is to uncover some maneuvers to come around avoidable and (circumstantially) tedious technicalities. This appendix is not a deep dive into the theoretical aspects of ESD, but an attempt to address some time-saving information. A summary of useful links are found in Table E.1, followed by a visualized technical description in Figure E.1.

- 'clim.pact' has not been updated for a while, due to the development of a new substituting package, 'esd', and is therefore only compatible with R version 2.15.3. This version is still available and easily accessed from the Internet by a quick Google search. The 'clim.pact' package may be downloaded from R Cran (Tab.E.1). The scripts utilized for downscaling in this thesis, given in Appendix (F) and (G), are based on functions from the 'clim.pact' package.

- The 'ds_.R' script requires three types of input files; point-observations, gridded observations, and GCM simulations. These inputs may be downloaded from indicated suppliers of data (fig. E.1). One drawback of the 'clim.pact' package is that it does not read the file-format netcdf4, which is the standard format for AR5 GCM simulations. Most gridded observations have also been compressed to this format. In this thesis, we surpassed this problem by decompression from netcdf4 to netcdf3 with the 'nccopy' tool from the NetCDF software from the Unidata Program Center.

- The NetCDF software offer other tools valuable when working with climate data. For example, it may be beneficial to control that units of GCM output and gridded data series are the same, before running the downsclaing script. CDO is another supplier of tools necessary to retrieve basic information of data stored in netcdf-format.

- The point-observations need to be on the form of a station object when fed into the 'ds_m.R' script. In a station object, observations are stored on a monthly basis in a data frame where columns represent the months of the year, and the rows represent the years covering the sample. Additionally, a station object includes information about the station such as name, station number, locataion (longitude and latitude), etc. In the script 'statobj.R' observations of precipitation or temperature is transformed from daily time series to monthly time series. The 'statobj.R'- script works with a folder containing two Excel files, one for each of the observation records (temperature and precipitation). Both files should include two columns with headers; 'Date' and 'pr'/'tas'. Dates should be given on the form yyyy-mm-dd. Additionally, 'tas' should be included in the filename of the file containing the temperature records, and "pr" in the filename for the precipitation file.

- As mentioned, three types of input are required of the 'ds_.R'- script. The script works with the indicated folder structure in Figure E.1. The main folder, 'Folder', contains one file for each of the observations, and another folder, 'IPCC_AR5'. GCM output for all wanted GCMs, and respective simulations, are stored in the 'GCMs' folder within 'IPCC_AR5'. In lines 11-22 of the script, various parameters are fixed before downscaling starts. Parameters include, the variable to be downscaled (ele=601 for precipitation and ele=101 for temperature), the months to be downscaled (cmons), which scenario to be downscaled (scen), etc. Gridded observations are retrieved in lines 62-75, by the retrieve.nc function, and file-name of the gridded observations may be adjusted there. The same applies to point-observations, lines 81-96. The downscaling function is called in line 175.

Link	**Description**
http://cran.r-project.org	R homepage. For downloading of R and 'clim.pact'
http://rcg.gvc.gu.se/edu/esd.pdf	Free compendium on ESD by Benestad, Hanssen-Bauer and Chen
https://www.unidata.ucar.edu/software/netcdf/docs/guide_nccopy.html	Description of the 'nccopy' utility
https://code.zmaw.de/projects/cdo	Information on Climate Data Operators (CDO)

Table E.1: Useful links to technical information on software and downscaling

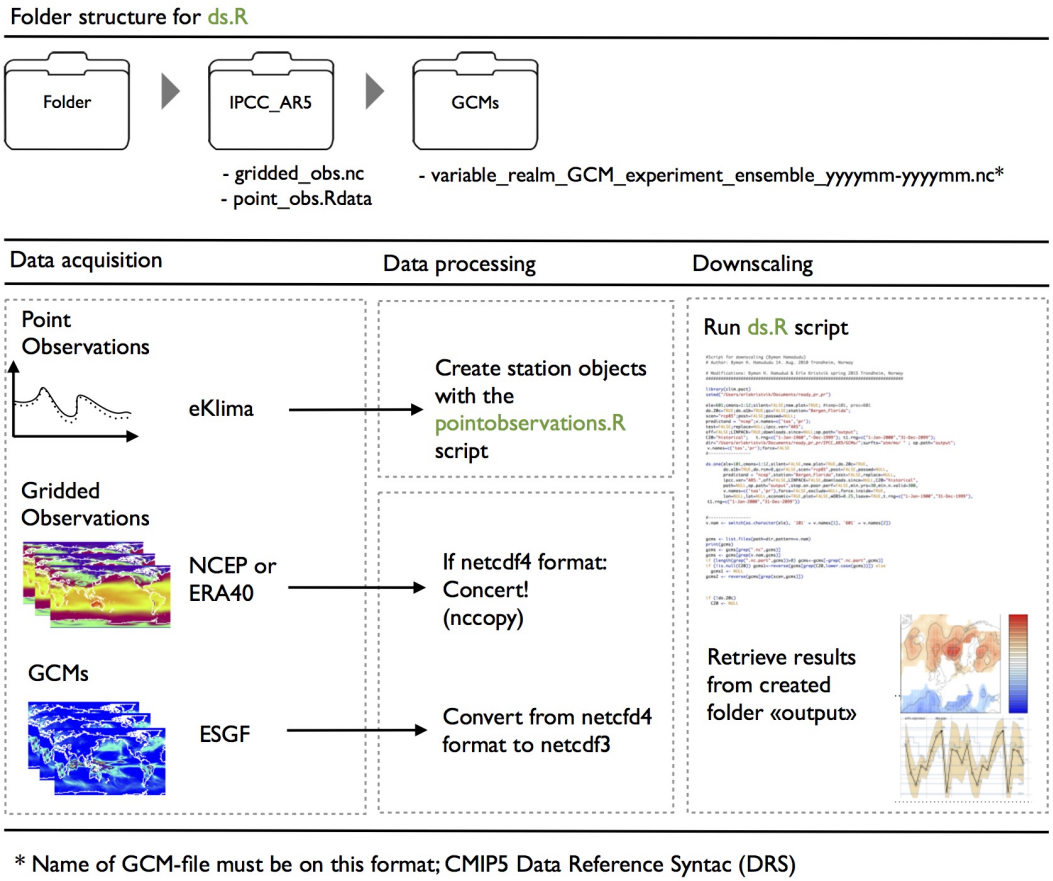

Figure E.1: Technical description of the downscaling procedure, covering data acquisition and processing, and visualizing the requisite folder structure and content for running the 'ds_.R'-script.

Appendix F

Script for creating station objects 'statobj.R'

```
#Script for creating station objects
#Author: Byman H. Hamadudu
#Modifications: Erle Kristvik, Spring 2015 Trondheim, Norway

library(reshape2);library(hydroTSM);library(xlsx);
library(zoo);library(clim.pact)

setwd("path2files")

# create list of all files with "pr" in the filename
files <- list.files(pattern = "pr")

# read the first file of the list "files"
dat<-read.xlsx(files[1],header=TRUE,1)

# create zoo object
ppt.z <- zoo(dat$RR,as.Date(paste(dat$Date),"%Y-%m-%d"))

#create a monthly time series
ppt.zm<-daily2monthly(ppt.z,FUN="sum")
assign(files[1],ppt.zm)


#for Temperature reading ------------------------------------

tfiles <- list.files(pattern = "tas")
tdat<-read.xlsx(tfiles[1], header=TRUE,1)
tmp.z <- zoo(tdat$TAM,as.Date(paste(tdat$Dato),"%Y-%m-%d"))

#create a monthly time series
    tmp.zm<-daily2monthly(tmp.z,FUN="mean")
```

```
    assign(tfiles[1],tmp.zm)

#If there is need to plot the data ---------------------------
# Plotting the monthly values
# plot(tmp.zm, xlab="Time",ylab="Prec (mm)")
# Plotting the annual moving average in station 'x'
#lines(ma(tmp.zm, win.len=20), col="blue")
#lmm <- lm(coredata(ppt.zm) ~ index(ppt.zm)-1)
#plot(lmm,col="red")

#write the dat to files
write.zoo(tas_florida.xlsx, file = "florida_tas.csv",
  index.name = "Index", row.names = FALSE, col.names = NULL)
write.zoo(pr_florida.xlsx, file = "florida_pr.csv",
  index.name = "Index", row.names = FALSE, col.names = NULL)

# reshape
myObjects <- NULL
myObjects[[1]] <-pr_florida.xlsx
myObjects[[2]] <-tas_florida.xlsx

names(myObjects) <- c("florida_pr","florida_tas")

for(i in 1:length(myObjects)){
df<-data.frame(
year=substr(index(myObjects[[i]]),1,4),
mons=substr(index(myObjects[[i]]),6,7),
dat=coredata(myObjects[[i]]))

dfr<-reshape(df, idvar="year",timevar="mons",direction = "wide
   ")
write.csv(dfr,file = paste(names(myObjects)[i],".csv",sep=""),
          row.names = FALSE, col.names = TRUE)
}

temper <- read.csv(file="florida_tas.csv", header=TRUE, sep=",
   ")
precip <- read.csv(file="florida_pr.csv", header=TRUE, sep=","
   )

# Create station object for precipitation

  names(precip) <- c("year", month.abb)
  val <- as.matrix(precip[,2:13])
  yy <- precip[,1]
  station <- 50540
  lat <- 60.3830
  lon <- 5.3327
  alt <- 12
```

```
  xyx <- NULL
  xyy <- NULL
  location <- "Bergen_Florida"
  wmo.no <- 50540
  start <- 1904
  yy0 <- 1900
  ele <- 601
  obs.name <- "Monthly precipitation"
  unit <- "mm/month"
  country <- "Norway"
ref <- "eklima.no/met.no"

bf_p <- station.obj(val, yy = yy, station = station,
        lat = lat, lon = lon, alt = alt,
        location = location, wmo.no = wmo.no, start = start,
        yy0 = NULL, ele = ele, obs.name = obs.name,
        unit = unit, country = country,  ref = ref)
save(bf_p, file ="Bergen_Florida_pr.Rdata")

# Create station object for temperature

names(temper) <- c("year", month.abb)
val <- as.matrix(temper[,2:13])
yy <- temper[,1]
station <- 50540
lat <- 60.3830
lon <- 5.3327
alt <- 12
xyx <- NULL
xyy <- NULL
location <- "Bergen_Florida"
wmo.no <- 50540
start <- 1904
yy0 <- 1900
ele <- 101
obs.name <- "Mean monthly temperature"
unit <- "degC"
country <- "Norway"
ref <- "eklima.no/met.no"


bf_t <- station.obj(val, yy = yy, station = station,
        lat = lat, lon = lon, alt = alt,
        location = location, wmo.no = wmo.no, start = start,
        yy0 = NULL, ele = ele, obs.name = obs.name,
        unit = unit, country = country,  ref = ref)
save(bf_t, file ="Bergen_Florida_tas.Rdata")
```

Appendix G

Downscaling script 'ds_m.R'

```
#Script for downscaling (Byman Hamadudu)
#Author: Byman H. Hamududu 14. Aug. 2010 Trondheim, Norway

#Modifications:
#Byman H. Hamududu & Erle Kristvik, Spring 2015 Trondheim,
    Norway


library(clim.pact)
setwd("/Users/erlekristvik/Documents/test")

ele=601;cmons=1:12;silent=FALSE;new.plot=TRUE;
do.20c=TRUE;qc=FALSE;station="Bergen_Florida";
scen="rcp45";post=FALSE;passwd=NULL;
predictand = "florida";v.names=c('tas','pr');
test=FALSE;replace=NULL;ipcc.ver="AR5";
off=FALSE;LINPACK=TRUE;downloads.since=NULL;
op.path="output";C20="historical";
t.rng=c("1-Jan-1960","-Dec-1999");
t1.rng=c("1-Jan-2000","31-Dec-2099");
dir="/Users/erlekristvik/Documents/test/IPCC_AR5/GCMs/";
surfts="atm/mo/␣";op.path="output";v.names=c('tas','pr');
force=FALSE

#-----------------

#ds.one(ele=601,cmons=1:12,silent=FALSE,new.plot=TRUE,
    #do.20c=TRUE, do.rcm=0,qc=FALSE,scen="rcp85",post=FALSE,
    #passwd=NULL,predictand = "ncep",station="Bergen_Florida",
    #test=FALSE,replace=NULL,ipcc.ver="AR5.",off=FALSE,
    #LINPACK=FALSE,downloads.since=NULL,C20="historical",
    #path=NULL,op.path="output",stop.on.poor.perf=FALSE,
    #min.yrs=30,min.n.valid=300, v.names=c('tas','pr'),
```

```
    #force=FALSE,exclude=NULL,force.inside=TRUE,lon=NULL,
    #lat=NULL,economic=TRUE,plot=FALSE,wOBS=0.25,lsave=TRUE,
    #t.rng=c("1-Jan-1900","31-Dec-1999"),
    #t1.rng=c("1-Jan-2000","31-Dec-2099"))
#-----------------
v.nam<-switch(as.character(ele),`101`=v.names[1],`601`=v.names
    [2])

gcms <- list.files(path=dir,pattern=v.nam)
print(gcms)
gcms <- gcms[grep(".nc",gcms)]
gcms <- gcms[grep(v.nam,gcms)]

if(length(grep(".nc.part",gcms))>0)gcms<-gcms[-grep(".nc.part"
    ,gcms)]

if (!is.null(C20)) {
  gcms1<-reverse(gcms[grep(C20,lower.case(gcms))])
} else {
  gcms1 <- NULL
}
gcms2 <- reverse(gcms[grep(scen,gcms)])

if (!do.20c)
  C20 <- NULL

if ( (op.path!="./") & !exists(op.path) ) {
  print(paste("Create new directory (1):",op.path))
  dir.create(op.path )
}

print("Get gridded observations")
if (ele==101) {

  ncep<- retrieve.nc("gridded_obs.nc", v.nam="tas",
            x.rng=c(-30,40),y.rng=c(40,75))

} else if (ele==601) {

ncep<- retrieve.nc("prate.sfc.mon.mean.nc", v.nam="pr",
                    x.rng=c(-30,40),y.rng =c(40,75))

  ncep$dat <- ncep$dat*3600*24*30

}

if (!is.null(C20)) print(gcms1)
if (!silent) { print("GCMS:"); print(gcms2)}
if (class(station)[1]=="character") {
```

```
80
81    if (ele==101) {
82      load('point.obs.RData')
83      print(bf_t$location)
84      print(bf_t)
85
86      obs<-bf_t
87
88    } else if (ele==601){
89
90      load('Bergen_Florida_pr.Rdata')
91      print(bf_p$location)
92      print(bf_p)
93
94      obs<-bf_p
95
96    }
97
98  }
99
100 if (sum(is.na(obs$val))>0)
101   obs$val[length(obs$yy),] <- NA
102 x.rng <- c(max(c(obs$lon-20,-180)), min(c(obs$lon+20,180)))
103 y.rng <- c(max(c(obs$lat-20,-90)), min(c(obs$lat+15,90)))
104
105 print(x.rng); print(y.rng)
106
107 fname <- paste("ds_one_",ipcc.ver,"_",
108         strip(obs$location),"_",ele,sep="")
109 print(fname)
110
111 fname.png <- paste("ds_one_",ipcc.ver,"_",
112             strip(obs$location),"_",ele,
113           ".png",sep="")
114 filename=paste(getwd(),"/",fname.png,sep="")
115
116 plot(c(1900,2100),c(min(rowMeans(obs$val[,cmons]),na.rm=TRUE)
    -15,
117       max(rowMeans(obs$val[,cmons]),na.rm=TRUE)+20),type="n",
118       main=paste(substr(lower.case(attr(obs,"location")),1,5),
119       attr(obs,"country"),sep=",␣"),ylab=obs$obs.name,xlab="
    Years")
120 grid()
121
122
123 obs.ts <- plotStation(obs,what="t",add=TRUE,col="grey20",
124             type="p",pch=19,l.anom=FALSE,mon=cmons,
125                   trend=TRUE,std.lev=FALSE)
126
```

```
print(obs$location)
i.gcm <- 0
if (!is.null(C20)) {
  for (gcm in gcms1) {
    i.gcm <- i.gcm + 1
    print(gcm)
    dot <- instring(".",gcm)
    if (length(dot)>=3) {

      gcm.nm <- substr(gcm,dot[1]-40,dot[1]-37)

    } else {
      dash <- instring("_",gcm)
      gcm.nm <- substr(gcm,dash[2]+1,dash[3]-1)
    }

    slsh <- instring("/",obs$location)
    if (slsh[1] > 0) {
      obs$location <- substr(obs$location,1,slsh[1]-1)
    }

    subdir <- paste(strip(obs$location),ele,sep="_")
    fname <- paste(op.path,"/",subdir,"/ds_one_",ipcc.ver,"_",
                   strip(obs$location),"_",ele,
                   "_",gcm.nm,"_",C20,".",sep="")

    if (!file.exists(paste(op.path,"/",subdir,sep=""))) {
      if (!silent) print(paste("Creating
␣␣␣␣␣␣␣(2)",op.path,"/",subdir,sep=""))
      dir.create(paste(op.path,"/",subdir,sep="") )
    } else if (!silent) print(paste(op.path,"/",subdir,
    "exists...",sep=""))

    if (!silent) print(fname)
    if (!file.exists(paste(fname,"txt",sep=".")) &
          !file.exists(paste(fname,"Rdata",sep=".")) | (force)
   ) {

      GCM<-retrieve.nc(paste(dir,gcm,sep=""),
                x.rng=x.rng,y.rng=y.rng,v.nam=v.nam,
                silent=FALSE)

      class(GCM) <- c("field","monthly.field.object")

      GCM$attributes$time.unit<- "month"; GCM$dd[] <- 15
      attr(GCM$tim, "unit")<- "month";
      GCM$dat <- switch(as.character(ele),'101'=GCM$dat
   -273.15,
      '601'=GCM$dat*3600*24*30)
```

```
174
175       ds.station <- objDS(ncep,GCM,obs,mon=cmons,plot=TRUE,
176                direc="dsgraphicsoutput/",qualitycontrol=qc,
177                silent=silent,LINPACK=LINPACK)
178
179      x <- ds.station$station
180      print(paste("Saving␣in",fname))
181    save(file=paste(getwd(),"/",fname,"Rdata",sep=""),x,ds.
     station)
182
183   ds.scen <- data.frame(Year=x$yy,
184                     Jan=round(x$val[,1],2),Feb=round(x$val
     [,2],2),
185                     Mar=round(x$val[,3],2),Apr=round(x$val
     [,4],2),
186                     May=round(x$val[,5],2),Jun=round(x$val
     [,6],2),
187                     Jul=round(x$val[,7],2),Aug=round(x$val
     [,8],2),
188                     Sep=round(x$val[,9],2),Oct=round(x$val
     [,10],2),
189                     Nov=round(x$val[,11],2),Dec=round(x$val
     [,12],2)
190                       )
191
192       write.table(ds.scen,file=paste(fname,"txt",sep=""),
193                     row.names = FALSE,quote = FALSE, sep="\t␣")
194
195      } else {
196       load(paste(fname,"Rdata",sep="."))
197       print(paste(fname,"exists,␣reading␣from␣file."))
198      }
199
200      plotStation(x,what="t",add=TRUE,col="grey40",type="l",lwd
     =2,
201                  lty=1,l.anom=FALSE,mon=cmons,trend=TRUE,
202                  std.lev=FALSE)
203
204      plotStation(obs,what="t",add=TRUE,col="grey20",type="p",
     pch=19,
205                  l.anom=FALSE,mon=cmons,trend=TRUE,std.lev=
     FALSE)
206
207      plotStation(obs,what="t",add=TRUE,col="grey20",type="l",
208              lwd=1,lty=3,l.anom=FALSE,mon=cmons,
209              trend=FALSE,std.lev=FALSE)
210    }
211  }
212
```

```
213 print(paste("Scenarios␣&␣ipcc␣version:",ipcc.ver))
214 i.gcm <- 0
215 for (gcm in gcms2) {
216   i.gcm <- i.gcm + 1
217   print(gcm)
218   dot <- instring(".",gcm)
219   if (length(dot)>=3) {
220     gcm.nm <- substr(gcm,dot[1]-35,dot[1]-32)
221   } else {
222     dash <- instring("_",gcm)
223 
224     gcm.nm <- substr(gcm,dash[2]+1,dash[3]-1)
225   }
226 
227   slsh <- instring("/",obs$location)
228   subdir<-paste(strip(obs$location),ele,sep="_")
229   fname <- paste(op.path,"/",subdir,"/ds_one_",ipcc.ver,"_",
230                  strip(obs$location),"_",
231                  ele,"_",gcm.nm,"_",scen,".",sep="")
232 
233   if (!silent) print(fname)
234   if (!file.exists(paste(fname,"txt",sep="")) &
235         !file.exists(paste(fname,"Rdata",sep="")) | (force)) {
236 
237     GCM <- retrieve.nc(paste(dir,gcm,sep=""),
238                 x.rng=x.rng,y.rng=y.rng,v.nam=v.nam,
239                 silent=FALSE)
240     class(GCM) <- c("field","monthly.field.object")
241     GCM$attributes$time.unit<- "month"; GCM$dd[] <- 15
242     attr(GCM$tim, "unit")<- "month";
243     GCM$dat <- switch(as.character(ele),'101'=GCM$dat-273.15,
244     '601'=GCM$dat*3600*24*30)
245 
246     ds.station <- objDS(ncep,GCM,obs,mon=cmons,plot=TRUE,
247               direc="dsgraphicsoutput/",
248                         qualitycontrol=qc,silent=silent)
249     x <- ds.station$station
250     x$grade.pattern <- min(na.omit(
251       c(ds.station$Jan$grade.pattern,ds.station$Feb$grade.
    pattern,
252         ds.station$Mar$grade.pattern,ds.station$Apr$grade.
    pattern,
253         ds.station$May$grade.pattern,ds.station$Jun$grade.
    pattern,
254         ds.station$Jul$grade.pattern,ds.station$Aug$grade.
    pattern,
255         ds.station$Sep$grade.pattern,ds.station$Oct$grade.
    pattern,
```

```
256         ds.station$Nov$grade.pattern,ds.station$Dec$grade.
    pattern
257         )))
258     x$grade.trend <- min(na.omit(c(
259       ds.station$Jan$grade.trend,ds.station$Feb$grade.trend,
260       ds.station$Mar$grade.trend,ds.station$Apr$grade.trend,
261       ds.station$May$grade.trend,ds.station$Jun$grade.trend,
262       ds.station$Jul$grade.trend,ds.station$Aug$grade.trend,
263       ds.station$Sep$grade.trend,ds.station$Oct$grade.trend,
264       ds.station$Nov$grade.trend,ds.station$Dec$grade.trend
265       )))
266
267     x.ts <- plotStation(x,what="n",add=TRUE,col="steelblue",
268                         type="l",lwd=2,lty=1,l.anom=FALSE,
269                         mon=cmons,trend=TRUE,std.lev=FALSE)
270
271     if (!test) x$val <- x$val - x.ts$trend[1] +
272               obs.ts$trend[length(obs.ts$trend)]
273     print(paste("Saving␣in",fname))
274
275     if (!file.exists( paste(op.path,"/",subdir,sep="") )) {
276       if (!silent) print(paste("Creating␣(3)",op.path,"/",
277                                subdir,sep=""))
278       dir.create( paste(op.path,"/",subdir,sep="") )
279     } else if (!silent) print(paste(op.path,"/",subdir,
280                                     "␣exists...",sep=""))
281   save(file=paste(getwd(),"/",fname,"Rdata",sep="") ,x,ds.
    station)
282   ds.scen <- data.frame(Year=x$yy,
283                   Jan=round(x$val[,1],2),Feb=round(x$val
    [,2],2),
284                   Mar=round(x$val[,3],2),Apr=round(x$val
    [,4],2),
285                   May=round(x$val[,5],2),Jun=round(x$val
    [,6],2),
286                   Jul=round(x$val[,7],2),Aug=round(x$val
    [,8],2),
287                   Sep=round(x$val[,9],2),Oct=round(x$val
    [,10],2),
288                   Nov=round(x$val[,11],2),Dec=round(x$val
    [,12],2
289                     ))
290
291 write.table(ds.scen,file=paste(getwd(),"/",fname,"txt",sep="")
    ,
292               row.names = FALSE,quote = FALSE, sep="\t␣")
293   } else {
294     print(paste(fname,"exists,␣skipping␣ESD␣for␣this␣GCM."))
295     load(paste(fname,"Rdata",sep=""))
```

```
296   }
297 plotStation(x,what="t",add=TRUE,col="steelblue",type="l",lwd
      =2,
298        lty=1,l.anom=FALSE,mon=cmons,trend=TRUE,std.lev=FALSE)
299 }
300 print("Add␣observations...")
301 plotStation(obs,what="t",add=TRUE,col="grey20",type="p",pch
      =19,
302              l.anom=FALSE,mon=cmons,trend=TRUE,std.lev=FALSE)
303 print("Finished␣plotting")
304
305 dev.copy2eps(file=paste("ds_one_",
306           ipcc.ver,obs$location,obs$ele, ".eps",sep=""))
307
308 if (test) invisible(
309
310   x)
311 print("HERE")
```

Bibliography

Anderberg, M. (2014). *Cluster Analysis for Applications: Probability and Mathematical Statistics: A Series of Monographs and Textbooks*. Probability and mathematical statistics. Elsevier Science.

Archfield, S. and Vogel, R. (2010). Map correlation method: Selection of a reference streamgage to estimate daily streamflow at ungaged catchments. *Water Resources Research*, 46(10).

Arnell, N. W. (2004). Climate change and global water resources: Sres emissions and socio-economic scenarios. *Global environmental change*, 14(1):31–52.

Bárdossy, A. (2007). Calibration of hydrological model parameters for ungauged catchments. *Hydrology and Earth System Sciences Discussions*, 11(2):703–710.

Barnola et al. (1999). Historical co2 record from the vostok ice core in cdiac.

Beldring, S., Roald, L. A., and Voksø, A. (2002). Avrenningskart for norge, rapport 2. Technical report, NVE - Norges vassdrags- og energidirektorat.

Benestad, R. E. (2001). A comparison between two empirical downscaling strategies. *International Journal of Climatology*, 21(13):1645–1668.

Benestad, R. E., Hanssen-Bauer, I., and Chen, D. (2008). *Empirical-statistical downscaling*, volume 41. World Scientific.

Bentsen, M., Bethke, I., Debernard, J. B., Iversen, T., Kirkevåg, A., Seland, Ø., Drange, H., Roelandt, C., Seierstad, I. A., Hoose, C., and Kristjánsson, J. E. (2012). The norwegian earth system model, noresm1-m part 1: Description and basic evaluation. *Geoscientific Model Development Discussions*, 5(3):2843–2931.

Bergström, S. (2002). The HBV story in sweden. *Sweden, Norrköping, Swedish Meteorological and*.

Bergstrom, S. and Lindström, G. (2015). Interpretation of runoff processes in hydrological modelling–experience from the hbv approach. *Hydrological Processes*.

Beven, K. J. (2011). *Rainfall-runoff modelling: the primer*. John Wiley & Sons.

Bhattacharya, B. and Solomatine, D. P. (2005). Neural networks and m5 model trees in modelling water level–discharge relationship. *Neurocomputing*, 63:381–396.

Borga, M. (2001). Canonical correlation: a tutorial. *On line tutorial http://people. imt. liu. se/magnus/cca*, 4.

Bretherton, C. S., Smith, C., and Wallace, J. M. (1992). An intercomparison of methods for finding coupled patterns in climate data. *Journal of climate*, 5(6):541–560.

Chernet, H. H., Alfredsen, K., and Midttømme, G. H. (2013). Safety of hydropower dams in a changing climate. *Journal of Hydrologic Engineering*, 19(3):569–582.

Clarke, L., Edmonds, J., Jacoby, H., Pitcher, H., Reilly, J., and Richels, R. (2007). Ccsp synthesis and assessment product 2.1, part a: scenarios of greenhouse gas emissions and atmospheric concentrations. *US Government Printing Office, Washington DC*.

Coles, S., Bawa, J., Trenner, L., and Dorazio, P. (2001). *An introduction to statistical modeling of extreme values*, volume 208. Springer.

Dingman, S. L. (2015). *Physical hydrology*. Waveland press.

Doherty, J. et al. (1994). Pest: a unique computer program for model-independent parameter optimisation.

Field, C. B., Barros, V. R., Mach, K., and Mastrandrea, M. (2014). Climate change 2014: impacts, adaptation, and vulnerability. *Contribution of Working Group II to the Fifth Assessment Report of the Intergovernmental Panel on Climate Change*.

Fleig, A. K., Tallaksen, L. M., Hisdal, H., and Demuth, S. (2006). A global evaluation of streamflow drought characteristics. *Hydrology and Earth System Sciences*, 10(4):535–552.

Fujino, J., Nair, R., Kainuma, M., Masui, T., and Matsuoka, Y. (2006). Multi-gas mitigation analysis on stabilization scenarios using aim global model. *The Energy Journal*, pages 343–353.

Furevik, T., Bentsen, M., Drange, H., Kindem, I., Kvamstø, N. G., and Sorteberg, A. (2003). Description and evaluation of the bergen climate model: Arpege coupled with micom. *Climate Dynamics*, 21(1):27–51.

Giorgetta, M. A., Jungclaus, J., Reick, C. H., Legutke, S., Bader, J., Böttinger, M., Brovkin, V., Crueger, T., Esch, M., Fieg, K., et al. (2013). Climate and carbon cycle changes from 1850 to 2100 in mpi-esm simulations for the coupled model intercomparison project phase 5. *Journal of Advances in Modeling Earth Systems*, 5(3):572–597.

Graham, L. P., Andréasson, J., and Carlsson, B. (2007). Assessing climate change impacts on hydrology from an ensemble of regional climate models, model scales and linking methods–a case study on the lule river basin. *Climatic Change*, 81(1):293–307.

Hamududu, B. H. (2012). *Impacts of Climate Change on Water Resources and Hydropower Systems : in central and southern Africa*. PhD thesis, Norwegian University of Science and Technology, Department of Hydraulic and Environmental Engineering.

Hansen, J., Sato, M., and Ruedy, R. (1997). Radiative forcing and climate response. *Journal of Geophysical Research: Atmospheres (1984–2012)*, 102(D6):6831–6864.

Hanssen-Bauer, I. (2009). Climate in norway in 2100–background materials to nou climate adaptation. *preliminary issue in Norwegian*.

Härdle, W. K. and Simar, L. (2012). *Applied multivariate statistical analysis*. Springer Science & Business Media.

Hardoon, D., Szedmak, S., and Shawe-Taylor, J. (2004). Canonical correlation analysis: An overview with application to learning methods. *Neural computation*, 16(12):2639–2664.

HIJIOKA, Y., MATSUOKA, Y., NISHIMOTO, H., MASUI, T., and KAINUMA, M. (2008). Global ghg emission scenarios under ghg concentration stabilization targets. *Journal of Global Environment Engineering*, 13:97–108.

Hisdal, H., Stahl, K., Tallaksen, L. M., and Demuth, S. (2001). Have streamflow droughts in europe become more severe or frequent? *International Journal of Climatology*, 21(3):317–333.

Hisdal, H., Tallaksen, L., Peters, E., Stahl, K., and Zaidman, M. (2000). Drought event definition. *ARIDE Technical Rep*, 6.

Hisdal, H. and Tallaksen, L. M. (2003). Estimation of regional meteorological and hydrological drought characteristics: a case study for denmark. *Journal of Hydrology*, 281(3):230 – 247.

Hotelling, H. (1936). Relations between two sets of variates. *Biometrika*, pages 321–377.

Imbert, A. (2003). The analog method applied to downscaling of climate scenarios.

Imbert, A. and Benestad, R. (2005). An improvement of analog model strategy for more reliable local climate change scenarios. *Theoretical and Applied Climatology*, 82(3-4):245–255.

IPCC (2013). *Climate Change 2013: The Physical Science Basis. Contribution of Working Group I to the Fifth Assessment Report of the Intergovernmental Panel on Climate Change*. Cambridge University Press, Cambridge, United Kingdom and New York, NY, USA.

Iversen, T., Bentsen, M., Bethke, I., Debernard, J., Kirkevåg, A., Seland, Ø., Drange, H., Kristjánsson, J., Medhaug, I., Sand, M., et al. (2012). The norwegian earth system model, noresm1-m–part 2: Climate response and scenario projections. *Geosci. Model Dev. Discuss*, 5(3):2933–2998.

Jain, A. K., Mao, J., and Mohiuddin, K. (1996). Artificial neural networks: A tutorial. *Computer*, 29(3):31–44.

Kalnay, E., Kanamitsu, M., Kistler, R., Collins, W., Deaven, D., Gandin, L., Iredell, M., Saha, S., White, G., Woollen, J., et al. (1996). The ncep/ncar 40-year reanalysis project. *Bulletin of the American meteorological Society*, 77(3):437–471.

Kay, A. and Davies, H. (2008). Calculating potential evaporation from climate model data: a source of uncertainty for hydrological climate change impacts. *Journal of Hydrology*, 358(3):221–239.

Killingtveit, A. and Hamududu, B. (2012). Climate change effects on water supply system of oslo.

Killingtveit, Å. and Sælthun, N. (1995). Hydrology. hydropower development 7. *Norwegian Institute of technology, Trondheim*, 7.

Kuhn, M. and Johnson, K. (2013). *Applied predictive modeling*. Springer.

Lay, D. C. (2012). *Linear algebra and its applications*. Pearson.

Madsen, H., Rasmussen, P. F., and Rosbjerg, D. (1997). Comparison of annual maximum series and partial duration series methods for modeling extreme hydrologic events: 1. at-site modeling. *Water resources research*, 33(4):747–757.

Merz, R. and Blöschl, G. (2004). Regionalisation of catchment model parameters. *Journal of Hydrology*, 287(1):95–123.

Monteith, J. (1981). Evaporation and surface temperature. *Quarterly Journal of the Royal Meteorological Society*, 107(451):1–27.

Moss, R. H., Babiker, M., Brinkman, S., Calvo, E., Carter, T., Edmonds, J. A., Elgizouli, I., Emori, S., Lin, E., Hibbard, K., et al. (2008). Towards new scenarios for analysis of emissions, climate change, impacts, and response strategies.

Moss, R. H., Edmonds, J. A., Hibbard, K. A., Manning, M. R., Rose, S. K., Van Vuuren, D. P., Carter, T. R., Emori, S., Kainuma, M., Kram, T., et al. (2010). The next generation of scenarios for climate change research and assessment. *Nature*, 463(7282):747–756.

Mote, P. and O'Neill, A. (2000). *Numerical Modeling of the Global Atmosphere in the Climate System*. NATO ASI series. Springer.

Nakicenovic, N. and Swart, R. (2000). Special report on emissions scenarios. *Special Report on Emissions Scenarios, Edited by Nebojsa Nakicenovic and Robert Swart, pp. 612. ISBN 0521804930. Cambridge, UK: Cambridge University Press, July 2000.*, 1.

Nash, J. and Sutcliffe, J. V. (1970). River flow forecasting through conceptual models part i—a discussion of principles. *Journal of hydrology*, 10(3):282–290.

NMI (1999). Norwegian meterological institute, climate statistics - bergen, florida (hordaland).

Norwegian Mapping Authority (2014). Nationwide responsibility for geographical information.

NVE (2011). Intoduksjon til hydra ii - databasesystem for hydrologiske og meteorologiske data. Technical report, NVE - Norwegian Water Resources and Energy Directorate.

NVE Lavvann (2014). Map tool displaying thematic geodata.

O'Kane, J. P. and Flynn, D. (2007). Thresholds, switches and hysteresis in hydrology from the pedon to the catchment scale: a non-linear systems theory. *Hydrology and Earth System Sciences Discussions*, 11(1):443–459.

Petit, J.-R., Jouzel, J., Raynaud, D., Barkov, N. I., Barnola, J.-M., Basile, I., Bender, M., Chappellaz, J., Davis, M., Delaygue, G., et al. (1999). Climate and atmospheric history of the past 420,000 years from the vostok ice core, antarctica. *Nature*, 399(6735):429–436.

Riahi, K., Grübler, A., and Nakicenovic, N. (2007). Scenarios of long-term socio-economic and environmental development under climate stabilization. *Technological Forecasting and Social Change*, 74(7):887–935.

Schoof, J. T. and Pryor, S. (2001). Downscaling temperature and precipitation: A comparison of regression-based methods and artificial neural networks. *International Journal of Climatology*, 21(7):773–790.

Shlens (2014). A tutorial on principal component analysis.

Skog og Landskap (2014). Institute for research on forests, soils, outfields and the landscape.

Smith, S. J. and Wigley, T. (2006). Multi-gas forcing stabilization with minicam. *The Energy Journal*, pages 373–391.

Specialization project (2014). Tvm 4510, hydrological assessment of water resources in bergen, by birthe riisnes and erle kristvik.

SSB (2014). Population projections, 2014-2100.

Stahl, K., Hisdal, H., Tallaksen, L. M., van Lanen, H. A., Hannaford, J., and Sauquet, E. (2008). *Trends in low flows and streamflow droughts across Europe.* UNESCO Report, Paris.

Stanev, K. (2004). Application of the hbv model for assessment of climate change impacts on the elements of hydrological cycle for the struma river basin.

Tallaksen, L. M., Hisdal, H., and Lanen, H. A. V. (2009). Space–time modelling of catchment scale drought characteristics. *Journal of Hydrology*, 375(3–4):363 – 372.

Tallaksen, L. M., Madsen, H., and Clausen, B. (1997). On the definition and modelling of streamflow drought duration and deficit volume. *Hydrological Sciences Journal*, 42(1):15–33.

Tallaksen, L. M. and Van Lanen, H. A. (2004). *Hydrological drought: processes and estimation methods for streamflow and groundwater*, volume 48. Elsevier.

Tallaksen, L. M. and van Lanen, H. A. (2007). Key aspects of low flow and drought. *LOW FLOWS AND DROUGHTS*, page 13.

Taylor, K. E., Stouffer, R. J., and Meehl, G. A. (2012). An overview of cmip5 and the experiment design. *Bulletin of the American Meteorological Society*, 93(4):485–498.

Thornthwaite, C. W. (1948). An approach toward a rational classification of climate. *Geographical review*, pages 55–94.

VA-etaten (2014). Master plan for water supply 2014-2023.

Van Loon, A. F., Van Lanen, H. A., Hisdal, H., Tallaksen, L. M., Fendeková, M., Oosterwijk, J., Horvát, O., and Machlica, A. (2010). Understanding hydrological winter drought in europe. *Global Change: Facing Risks and Threats to Water Resources, edited by: Servat, E., Demuth, S., Dezetter, A., Daniell, T., Ferrari, E., Ijjaali, M., Jabrane, R., Van Lanen, H., and Huang Y., IAHS Publ*, 340:189–197.

van Vuuren, D. P., Den Elzen, M. G., Lucas, P. L., Eickhout, B., Strengers, B. J., van Ruijven, B., Wonink, S., and van Houdt, R. (2007). Stabilizing greenhouse gas concentrations at low levels: an assessment of reduction strategies and costs. *Climatic Change*, 81(2):119–159.

Van Vuuren, D. P., Edmonds, J., Kainuma, M., Riahi, K., Thomson, A., Hibbard, K., Hurtt, G. C., Kram, T., Krey, V., Lamarque, J.-F., et al. (2011). The representative concentration pathways: an overview. *Climatic Change*, 109:5–31.

van Vuuren, D. P., Weyant, J., and de la Chesnaye, F. (2006). Multi-gas scenarios to stabilize radiative forcing. *Energy Economics*, 28(1):102–120.

Voldoire, A., Sanchez-Gomez, E., y Mélia, D. S., Decharme, B., Cassou, C., Sénési, S., Valcke, S., Beau, I., Alias, A., Chevallier, M., et al. (2013). The cnrm-cm5. 1 global climate model: description and basic evaluation. *Climate Dynamics*, 40(9-10):2091–2121.

Wilby, R. L. (1997). Non-stationarity in daily precipitation series: implications for gcm down-scaling using atmospheric circulation indices. *International Journal of Climatology*, 17(4):439–454.

Wilby, R. L. (2005). Uncertainty in water resource model parameters used for climate change impact assessment. *Hydrological Processes*, 19(16):3201–3219.

Wilby, R. L., Dawson, C. W., and Barrow, E. M. (2002). Sdsm—a decision support tool for the assessment of regional climate change impacts. *Environmental Modelling & Software*, 17(2):145–157.

Wilks, D. S. (2005). *Statistical methods in the atmospheric sciences*, volume 100. Academic press.

Wise, M., Calvin, K., Thomson, A., Clarke, L., Bond-Lamberty, B., Sands, R., Smith, S. J., Janetos, A., and Edmonds, J. (2009). Implications of limiting co2 concentrations for land use and energy. *Science*, 324(5931):1183–1186.

Wong, W. K., Beldring, S., Engen-Skaugen, T., Haddeland, I., and Hisdal, H. (2011). Climate change effects on spatiotemporal patterns of hydroclimatological summer droughts in norway. *Journal of Hydrometeorology*, 12(6):1205–1220.

Zorita, E. and Von Storch, H. (1999). The analog method as a simple statistical downscaling technique: comparison with more complicated methods. *Journal of climate*, 12(8):2474–2489.